Hyperfine structure measurements in scandium for IR spectroscopy

Felix van Deelen

Lund Observatory
Lund University

2017-EXA113

Degree project of 60 higher education credits (for a degree of Master)
May 2017

Supervisors: Hampus Nilsson, Henrik Hartman

Lund Observatory
Box 43
SE-221 00 Lund
Sweden

To extend our reach to the stars above
James, Team Rocket

Abstract

Stellar abundances are important for understanding the chemical evolution of galaxies and provide us with constraints on stellar evolution and supernova nucleosynthesis. To determine stellar abundances accurately, atomic data is crucial. This data is incomplete for many elements, especially in the infrared region. In particular, hyperfine structure (hfs) data in the near-infrared region is lacking for neutral scandium. Incorrect scandium abundances are obtained when hfs is neglected in stellar abundance analysis, which has led to contradicting theories of the synthesis process of scandium. In this project, hfs constants for neutral scandium are derived by means of laboratory experiments. A spectrum was produced using a hollow cathode discharge lamp and the spectrum was recorded using a Fourier Transform Spectrometer. A model has been developed to produce synthetic spectra of hfs multiplets. Using the nonlinear least squares method, the model was fitted to observed transitions in order to find the best fit hfs constants. The hfs constants have been determined for 95 levels in neutral scandium. For 52 of these levels, the hfs constants were determined for the first time. An agreement with literature values was found. The behaviour of the developed program was probed given an offset in initial values, and various signal to noise ratios and widths of the structure. Additionally, oscillator strengths have been derived for 590 hfs transitions, using the Höln-Kronig intensity rule. The hfs data derived in this project will allow for more accurate analysis of scandium lines in stellar spectra. The transition in scandium from $3d4s(^3D)4p\ ^4D_{7/2}$ to $3d^2(^3F)4s\ ^4F_{7/2}$ in the spectrum of the star Alpha Boötis has been investigated in the light of the new hfs data and the new hfs constants were able to reproduce the observed line profile.

Popular summary

Everything is made up out of atoms. Not only trees, animals or the ink in these letters, but also astronomical objects such as stars and planets. Stars are basically extremely hot and dense clouds of atoms, emitting light in all directions. Astronomers are interested in which atoms build up stars, as this helps us understand how stars and galaxies evolve. Information about the composition of a star can be found from the light emitted by the star. The light emitted by a star consists out of many colours, or so-called *wavelengths.* To understand this, we should consider the processes that occur inside a star. The inner part of a star shines with a constant intensity at all wavelengths. Atoms in the outer part of a star absorb parts of the light that was emitted by the inner part. However, atoms only absorb light with specific wavelengths characteristic for the atom. For this reason, the intensity shows dips at certain wavelengths which are called *absorption lines.* Each element has its own unique set of absorption lines. In this way, the light emitted by a star is characterized by the atoms that are present in the star. Astronomers measure the light from stars using a method called *spectroscopy.* In spectroscopy, the spectrum of a star is recorded by measuring the intensity of the light at various wavelengths. By identifying the absorption lines in the recorded spectrum, one can infer which atoms are present in the star. Moreover, from the shape of an absorption line, the conditions in a star can be probed. For instance, from the depth of an absorption line one can determine the amount of a certain element that is present in a star. This is because the amount of light that is absorbed is related to the number of atoms. The shape of an absorption line can also tell us about the temperature and gravity in a star. Though, before all these parameters can be derived, the unique sets of absorption lines for different elements needs to be known. Luckily, the set of absorption lines characterizing an element can be measured in the lab. For some elements however, intrinsic processes influence the shape of the absorption lines, which complicates probing these stellar conditions. The element scandium for instance, shows very broad absorption lines. This is because the shape of scandium absorption lines in stellar spectra is not only affected by the stellar temperature, gravity and scandium abundance, but also by an intrinsic process called *hyperfine structure splitting.* In order to analyse scandium absorption lines in stellar spectra, it is necessary to know the influence that hyperfine structure splitting has on the shape of the absorption line. This can be described using so-called hyperfine structure constants. In this project, these constants have been measured for several scandium lines by means of laboratory experiments. This was done by recording a spectrum of pure scandium in the lab. A model was built to reproduce the shape of the recorded scandium lines using the hyperfine structure constants. The model was fit to the observed spectrum, which returned the hyperfine structure constants for several scandium lines. Using the constants determined in this thesis, we are better able to read the light from the stars and determine what is going on in the vast universe surrounding our small blue rock.

Populärvetenskaplig beskrivning

Allting är uppbyggt av atomer, inte bara träd, djur eller bläcket i dessa bokstäver, utan även astronomiska objekt så som stjärnor och planeter. Stjärnor är i princip extremt varma och kompakta moln av atomer, som skickar ut ljus i alla riktningar. Astronomer är intresserade av vilken sammansättning av atomer som bygger upp stjärnor eftersom detta hjälper dem att förstå hur stjärnor och galaxer bildas och utvecklas. Information om vilka ämnen en stjärna består av kan fås från ljuset de skickar ut. Ljuset som skickas ut från en stjärna innehåller olika färger, eller *våglängder*. För att förstå varför det är så behöver vi förstå vilka processer som sker i en stjärna. Den inre delen av en stjärna skickar ut kontinuerligt ljus i alla våglängder. Atomer i den yttre delen av stjärnan absorberar en del av det kontinuerliga ljuset. På grund av detta kommer intensiteten för vissa våglängder att minska, detta kallas *absorptionslinjer*. Varje grundämne har ett unikt set av absorptionslinjer. Det emitterade ljuset från en stjärna är karakteriserat av de atomer som finns stjärnan. Med *spektroskopi* studerar man spektrumet av en stjärna genom att mäta intensiteten som funktion av våglängd. Den kemiska sammansättningen av en stjärna kan således bestämmas genom att analysera spektrumet. Man kan även studera förhållande som råder i stjärnan genom att analysera formen av absorptionslinjerna. Till exempel kan man bestämma mängden av ett grundämne genom att mäta djupet på en absorptionslinje, eftersom mängden ljus som absorberas är ett mått på mängden atomer av grundämnet i stjärnan. Man kan även studera parametrar så som temperatur och gravitation med hjälp av absorptionslinjer. För att bestämma dessa stjärnparametrar måste de unika spektrallinjerna för de olika grundämnena vara kända från laboratoriemätningar. En del grundämnen har inneboende egenskaper som påverkar formen av spektrallinjerna och därför försvårar stjärnanalysen. Ett sådant ämne är scandium, som uppvisar breda spektrallinjer på grund av en inneboende effekt som kallas *hyperfinstruktur*. För att analysera scandiumlinjer i en stjärna är det nödvändigt att veta hur hyperfinstrukturen påverkar formen för varje linje. I detta arbete har hyperfinstrukturen mätts i laboratoriespektra för ett antal scandiumlinjer. En teoretiskmodell har utvecklades för att anpassa den experimentella datan och beskriva hyperfinstrukturen. Tack vare hyperfinstrukturerna som bestämts i detta arbete kan man få en bättre förståelse av ljuset som stjärnor skickar ut och vad som sker i det enorma universum som omger vår lilla blå planet.

Contents

List of Figures

List of Tables

Chapter 1

Introduction

The goal of astrophysics is to understand how the universe works. How are stars and galaxies born and how do they evolve? What are stars made of? And how do their lives end? Clues to answer these questions can be found within the radiation emitted by stars. Wollaston (1802) was the first to report absorption lines in the solar spectrum. A few years later, Fraunhofer invented the spectroscope, which allowed to measure the wavelengths of these solar absorption lines. Today, spectroscopy is one of the major observational techniques in astronomy. By measuring the intensity of radiation from a star at various wavelengths one can determine the chemical composition of the star and interstellar medium, and estimate the stars' temperature and mass (Prialnik, 2009). To analyse stellar spectra, accurate atomic data is essential. However, this data is unavailable or uncertain for many elements, especially in the infrared (IR) region (see e.g. Heiter *et al.*, 2015). This project aims to contribute to solving astrophysical questions by improving and extending atomic data, which will allow for more accurate analysis of stellar spectra. To be precise, hyperfine structure (hfs) constants will be determined for the element scandium. For elements with a net nuclear spin, the fine structure energy levels E_J can be split up into multiple hfs levels with energies E_F (see e.g. Kuhn, 1969). The hfs constants describe the energy shift of the energy levels relative to E_J due to interactions between the nucleus and electrons (Thorne *et al.*, 1999).

Hyperfine structure in stellar spectra

It is important to know stellar abundances, since this can tell us about the chemical evolution of galaxies and gives us constraints on stellar evolution and supernova nucleosynthesis (Matteucci, 2001). Stellar abundances can be derived by analysing the spectrum of a star (see e.g. Rutten, 2003). A commonly used method is to fit a synthetic spectrum to an observed stellar spectrum, see e.g. the Spectroscopy Made Easy (SME) model (Valenti and Piskunov, 1996). This model takes several stellar parameters and atomic data as input and then varies the elemental abundances and other parameters until the observed spectrum is fitted best. It is well known that neglecting hfs in the analysis of stellar spectra can result in errors in the elemental abundances. Wahlgren (2005) for instance investigated how the line profile of a holmium line in the spectrum of a star is affected by hfs. Wahlgren (2005) modelled a holmium line in the spectrum of a cool star with and without holmium given a range of holmium abundances, which is shown in Fig. 1.1 as a solid and dotted line respectively. The model that takes hfs into account produces asymmetrical lines and spreads out the intensity over a larger wavelength region compared to the model that neglects hfs. It can also be seen that for large holmium abundances the model with hfs predicts the largest equivalent width. This is because saturation effects are smaller for lines that are broadened by hfs (Prochaska *et al.*, 2000). Fitting a spectral line that was affected by hfs while neglecting hfs can return incorrect stellar parameters, as the width and equivalent width increase will be ascribed to the wrong stellar parameter. If for instance Doppler broadening is the dominant broadening mechanism in a star, the stellar temperature can be related to the width of spectral lines. However, when fitting spectral lines that are affected by hfs, the best fit solution for the temperature might have accounted for broadening due to hfs which would result in an overestimated temperature. In the same way, elemental abundances derived from fitting lines that are affected by hfs might be overestimated, because of desaturation of strong lines. Jofré *et al.* (2015) worked on quantifying the effect of hfs in measured stellar abundances, which is shown in Fig. 1.2. The scandium abundance in Arcturus (also known as Alpha Boötis/ Alpha Boo) was determined line by line using both methods that consider hfs structure and methods that neglect hfs. One can see that the scandium abundance can be either over- or underestimated when neglecting hfs. An underestimation in elemental abundance can be found when neglecting hfs, because the weakest components of a pattern might be too weak to be distinguished from the background signal (Wahlgren, 2005). Jofré *et al.* (2015) state that a slight offset was found in the final scandium abundances with and without hfs. It should be noted that it was possible to include hfs for the lines used in Jofré *et al.* (2015), as these lines are in the visible wavelength region. For these transitions, hfs data is available in contrast to many transitions in the IR region. On the other hand, hfs is of larger importance in the IR region, as the Doppler width becomes smaller at small wavelengths while broadening due to hfs splitting stays constant. An additional problem can arise from hfs when blended lines are observed in stellar spectra. If the hfs is not known, it will be difficult to verify whether such a line profile is created by hfs or by a line with an almost equal wavelength but originating from another element. If hfs constants are known for the levels involved in this transition, one could determine whether such a profile could be produced by hfs by calculating the wavelengths and intensities of all hfs transitions within the multiplet.

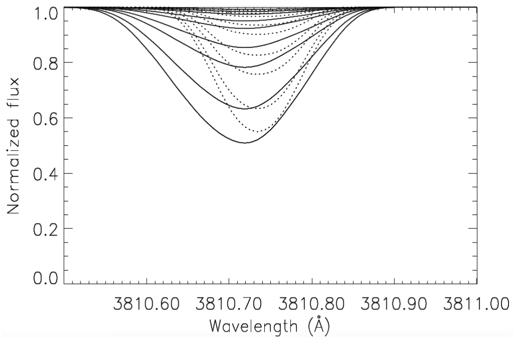

Figure 1.1: A model of a holmium line in a cool giant star for various holmium abundances. The solid lines show the model that included hfs, the dotted lines show the model that neglected hfs. The figure was taken from Wahlgren (2005).

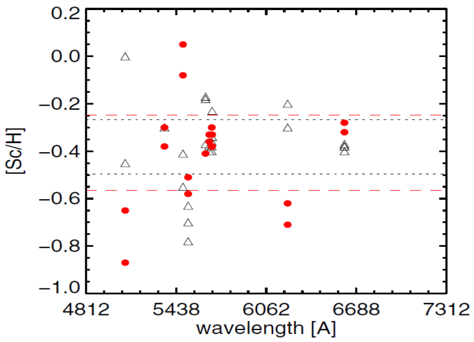

Figure 1.2: Line by line scandium abundance in Arcturus from a model including hfs structure (filled red circles)and neglecting hfs (open black triangles). The standard deviation with and without hfs is shown by the red and black lines respectively.

IR spectroscopy

As mentioned before, spectroscopy is one of the main observational techniques in astronomy and allows to determine stellar parameters such as chemical composition, temperature and mass (Prialnik, 2009). Astronomical IR spectroscopy is a fast-growing field. The advantage of spectroscopy in the IR region is that IR radiation can penetrate dusty regions (Schneider, 2015). It allows us for instance to look at newly formed stars and at the galactic centre of the Milky Way, which both are shrouded in dust. Moreover, about 75% of the stars in the solar neighbourhood radiate mainly in the IR region (Ledrew, 2001). Furthermore, most spectral lines of molecules lie in the IR region. Therefore, IR spectroscopy is an extremely useful tool in probing the abundances of molecules in space. The IR telescope ISO from the European Space Agency, has done many major discoveries through IR spectroscopy, for instance the detection of water in many regions of space (see e.g. Molster and Kemper, 2005). Additionally, ISO has discovered the formation of C_4H_2 and C_6H_2 molecules in protoplanetary nebula (Cernicharo *et al.*, 2001). These molecules are precursors of complex organic molecules. Atomic transitions are also prominent in the near-IR region (see e.g. Nicholls *et al.*, 2017). Examples of currently ongoing infrared spectroscopic surveys are APOGEE and VISTA.

In conclusion, IR spectroscopy is of great importance in astronomy. It is a new and growing field, but atomic data for this spectral region is lacking behind. For this reason, it is essential that atomic data is improved and extended for this spectral region.

The element scandium

Scandium is an iron-group element with atomic number $Z = 21$. It has a nuclear spin of $I = 7/2$ (Mills *et al.*, 1988) and a nuclear magnetic moment of $\mu = 4.756\mu_n$ (Ramsey, 1950), giving rise to hfs splitting in many spectral lines. It has only one stable isotope ^{45}Sc, and thus has no isotopic shift (Firestone *et al.*, 1999). The solar scandium abundance is $[Sc] = 3.16 \pm 0.04$ (Scott *et al.*, 2015). Scandium was first discovered in Sweden and owes its name to *Scandia*, the Latin name for Scandinavia. Astrophysically, the origin of scandium is not well understood (Zhang *et al.*, 2008) and the synthesis process and site of scandium are currently debated as is for instance underlined by Battistini and Bensby (2015).

Scandium in metal poor and metal rich stars

Nucleosynthesis models predict a sub-solar scandium abundance in metal poor stars (see e.g. Timmes *et al.*, 1995). This is in contradiction with observations (Nomoto *et al.*, 2013). The scandium abundance obtained from nucleosynthesis models depends on what synthesis process is used for scandium. Scandium might either be produced in supernovae type II (SN II), in which case scandium would behave like an alpha element (Arnett, 1978). Or it could be produced in supernovae type Ia, in which case scandium would be an iron peak element (Nomoto *et al.*, 1984). To determine whether scandium is an alpha or iron peak element, one can observe metal poor and metal rich stars. The metallicity of a star is defined as the number density ratio of iron over hydrogen. The metallicity of a star can be related to the time at which the star formed, since the interstellar medium (ISM) is enriched by metals gradually over time by supernovae (see e.g. Schneider, 2015). The timescale for SN II is smaller than the timescale for SN Ia (Tinsley, 1979), therefore the ISM is initially enriched in alpha elements. This can be used to investigate the synthesis process of scandium. If scandium is an alpha element, one would expect a metal poor star to be enhanced in scandium. On the other hand, if scandium is an iron peak element, one would expect metal poor stars to be underabundant in scandium. Investigations have been done in order to determine the origin of scandium, however contradicting results were published. A historical overview of several studies on the origin of scandium might illustrate the importance of including correct hfs treatment in stellar abundance analysis. Zhao and Magain (1990) investigated the chemical compositions of metal poor halo stars and found that these stars were enhanced in scandium, indicating scandium is an alpha element. In this study, hfs was included in the stellar abundance determination, but the hfs constants were not known accurately. One year later, Gratton and Sneden (1991) studied the abundance of scandium in metal poor stars as well, and found that [Sc/Fe] actually was solar, indicating that scandium is not an alpha element. In contradiction to Zhao and Magain (1990), Gratton and Sneden (1991) analysed scandium lines using hfs constants. Nissen *et al.* (2000) determined elemental abundances for stars of various metallicities and concluded that scandium behaves as an alpha element, since a trend was found where [Sc/Fe] decreases with increasing metallicity, as can be seen in Fig. 1.3. However, in the same year Prochaska *et al.* (2000) stated the trend found by Nissen *et al.* (2000) was due to the use of inaccurate hfs constants. Since the overestimation in elemental abundance increases with line strength, a spurious trend was observed (Prochaska *et al.*, 2000). Prochaska *et al.* (2000) determined scandium abundances by fitting all hfs components and find that the large majority of stars in the Nissen *et al.* (2000) sample show nearly solar [Sc/Fe]. The method used by Prochaska *et al.* (2000) requires hfs constants, which can be determined accurately in the lab. For lines that were analysed in Prochaska *et al.* (2000) hfs constants were available. In contrast to the visible region, this data lacks for many levels in scandium involved in transitions in the IR region.

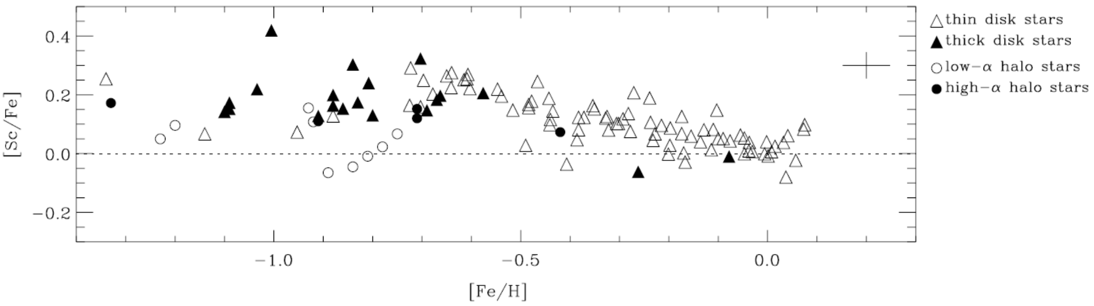

Figure 1.3: Abundance patterns of scandium for 4 types of stars, from Nissen *et al.* (2000). The scandium abundance seems to decrease with metallicity, indicating scandium is an alpha element. The uncertainties in the measurements are indicated by the cross in the top right of the plot.

Previous studies

For several levels in scandium hfs constants are available, see e.g. Zeiske *et al.* (1976); Ertmer and Hofer (1976); Krzykowski and Stefańska (2008); Singh *et al.* (1991); Aboussaïd *et al.* (1996); Fricke *et al.* (1959); Kopfermann and Rasmussen (1934); Childs (1971); Siefart (1977) and Başar *et al.* (2004). The three main methods used to record spectra are fluorescence spectroscopy (FS), Fourier Transform Spectroscopy and optogalvanic spectroscopy (OGS). It is worth noting that most of these studies did not look at transitions in the IR region. However, Aboussaïd *et al.* (1996) determined the hfs constants for 10 levels in neutral scandium from transitions in the IR wavelength region. There are also several theoretical studies, which employ models to determine the hfs constants. These models are not analytic, since it is not possible to solve the Schrödinger equation analytically for scandium. For multi-electron systems one needs to include Coulomb repulsion between electrons, resulting in a three (or more) body problem, which can not be solved analytically. Instead numerical simulations and perturbation theories are used, see for example Bieron *et al.* (2002) where the Dirac-Fock model is used to calculate hfs constants for scandium. The hfs constants calculated in these studies are often uncertain, because of the many approximations that are necessary.

Aim

In this project hfs constants for the element scandium were determined from transitions in the near-IR region. Atoms were excited using a Hollow Cathode Discharge Lamp (HCL) and spectra were recorded using the Fourier Transform Spectrometer in the Edlén Laboratory. A code was written to model synthetic spectra of hfs multiplets. To find the best fit hfs constants the model was fitted to observed lines using the nonlinear least squares method. Moreover, a code was written to derive oscillator strengths of hfs components given the fine structure oscillator strength. The main goal of this project is to present an evaluated set of transitions in the near-IR region for the element scandium including hfs data.

Chapter 2

Background theory

2.1 Atomic structure

In this section, basic theory of atomic structure is discussed following Thorne *et al.* (1999). The energy eigenvalues E of an atomic system can be found using the time-independent Schrödinger equation

$$H\Psi(\mathbf{r}_1, \mathbf{r}_2 ... \mathbf{r}_n) = E\Psi(\mathbf{r}_1, \mathbf{r}_2 ... \mathbf{r}_n) \tag{2.1}$$

Here Ψ is the eigenfunction or also called wave function and can be interpreted as a probability amplitude. $\mathbf{r}_i$ describes the position of electron i. H is the Hamiltonian energy operator and represents the total energy of the system. The aim of the following section is not to describe how to solve this equation, but to investigate what processes contribute to the Hamiltonian in an atomic system, since these processes determine the energy structure of the atom. First, the kinetic and potential energy of all electrons and the nucleus will be considered. The potential energy is influenced by electron-electron repulsion, which can be divided in a radial and tangential component. First, the radial component will be treated using the central field approximation. Secondly, two parts of tangential electron-electron repulsion are discussed. Next, spin-orbital interactions of the electrons giving rise to fine structure is considered. Finally, in more detail, two interactions causing hfs will be discussed.

2.1.1 The central field approximation

For many electron atoms the total energy of the system can be approximated as the sum of the kinetic and potential energy of all electrons and the nucleus. The Hamiltonian for many-electron atoms consists of two components. The first part of the Hamiltonian is the Coulomb attraction between the positively charged nucleus and the negatively charged electrons. The second part of the Hamiltonian is the repulsion between electrons. In the *central field approximation* the electron-electron repulsion is separated in a radial and tangential component, where the radial component is dominant. Considering only the radial component, the field created by the nucleus and the average effect of electron-electron repulsion is spherically symmetric or also called a central field. The non-central component can be treated as a perturbation, as this has a much smaller contribution to the Hamiltonian. The

Hamiltonian can now be written as

$$H = \sum_i [-\frac{\hbar^2}{2m}\nabla_i^2 + V(r_i)] \tag{2.2}$$

Here $\hbar$ is the reduced Planck constant, m is the mass of the electron and V_i is the potential energy of electron i. For this Hamiltonian Eq. (2.1) can be solved. Solutions can be found for the wave functions and their corresponding quantized energy levels. From these solutions one can see that the possible states of an atomic system can be described with a set of quantum numbers n, l, m_s and m_l. The energy level of an atomic system depends on the quantum numbers n and l of all its electrons. One can describe an energy eigenvalue of an atomic system using the electron configuration, which combines nl for all electrons. Spectroscopic notation is used to denote l, so for l=0,1,2,3,4,5, etc. s,p,d,f,g,h is used. An electron in subshell nl is $2(2l+1)$ degenerate. Two additional quantum numbers m_l and m_s are used to describe the state of an electron, where

$$m_l = -l, (-l+1), ..., (l-1), +l \tag{2.3}$$

and

$$m_s = \pm 1/2 \tag{2.4}$$

In spectroscopic notation, the number of electrons in a subshell is written as an exponent. The energy dependence on quantum numbers n and l can be explained by the fact that the inner electrons screen the nuclear charge for the outer electrons. Electrons with smaller n or l have a larger probability to be close to the nucleus and thus are more tightly bound and have a lower energy level.

2.1.2 LS coupling

In this section, two processes that have been neglected in the previous section are discussed. These processes are the non-central part of the electron-electron repulsion and the magnetic spin-orbit interactions of the electrons. If LS coupling is assumed the non-central electron-electron repulsion first splits up the energy states into terms, and next the spin-orbit interaction splits the terms into energy levels. LS coupling can be assumed, as scandium is a light atom in which case the contribution to the Hamiltonian from to spin-orbit interaction is much smaller than that from non-central electron-electron repulsion. An overview of the processes causing energy splitting and the order in which they occur are shown in Fig. 2.1 for a $3d4s(^3D)4p$ configuration of neutral scandium.

Non-central electrostatic repulsion

The non-central electrostatic repulsion splits a given configuration into terms. It can be divided up into two parts, i.e. exchange and direct splitting. The exchange splitting can be interpreted as the effect of exchanging two electrons. This can be quantified by the total electron spin angular momentum quantum number S, where $\boldsymbol{S} = \sum_i \boldsymbol{s_i}$. From the Pauli Exclusion Principle it is known that if the spin wave function is anti-symmetric ($S = 0$), the space wave function is forced to be symmetric, and vice versa. For symmetric wave functions the electrons are more separated on average, which causes less shielding from the nucleus (Leighton and

Furry, 1960). This makes the electrons more tightly bound, and therefore this state has a lower energy compared to a symmetric spin wave function (S=1). In general, the energy is lowest for the state with the highest quantum number S.
The direct non-central electrostatic repulsion energy splitting can be quantified by the total electron orbital angular moment quantum number L, where $\boldsymbol{L} = \sum_i \boldsymbol{l_i}$. If L is large, most electrons are orbiting in the same direction, and they will meet less often compared to having opposite orbital directions. In this case, the average separation of the electrons is large, which again means there will be less shielding of the nuclear attraction. In general, the energy is the lowest for the largest quantum number L, for a given S.

Spin-orbit interactions

The terms are further split into fine structure energy levels by the spin-orbit interaction. As the electron is a charged particle, it will give rise to a magnetic field due to its orbital motion and it will give rise to a magnetic moment due to its spin. The interaction between the magnetic moment and the magnetic field gives rise to a torque on the electron, which splits up the terms into fine structure energy levels. The total electron angular momentum $\boldsymbol{J}$ describes the spin-orbit interaction

$$\boldsymbol{J} = \boldsymbol{L} + \boldsymbol{S} \tag{2.5}$$

From vector addition the possible quantum numbers J can be found through

$$J = L + S, L + S - 1, ..., |L - S| \tag{2.6}$$

L, S and J can be combined into a term symbol as $^{2S+1}L_J$, with L=0,1,2,3, etc. for L=S, P, D, F. The term symbol in combination with the electron configuration of an atom describes the energy eigenvalue of the atom.

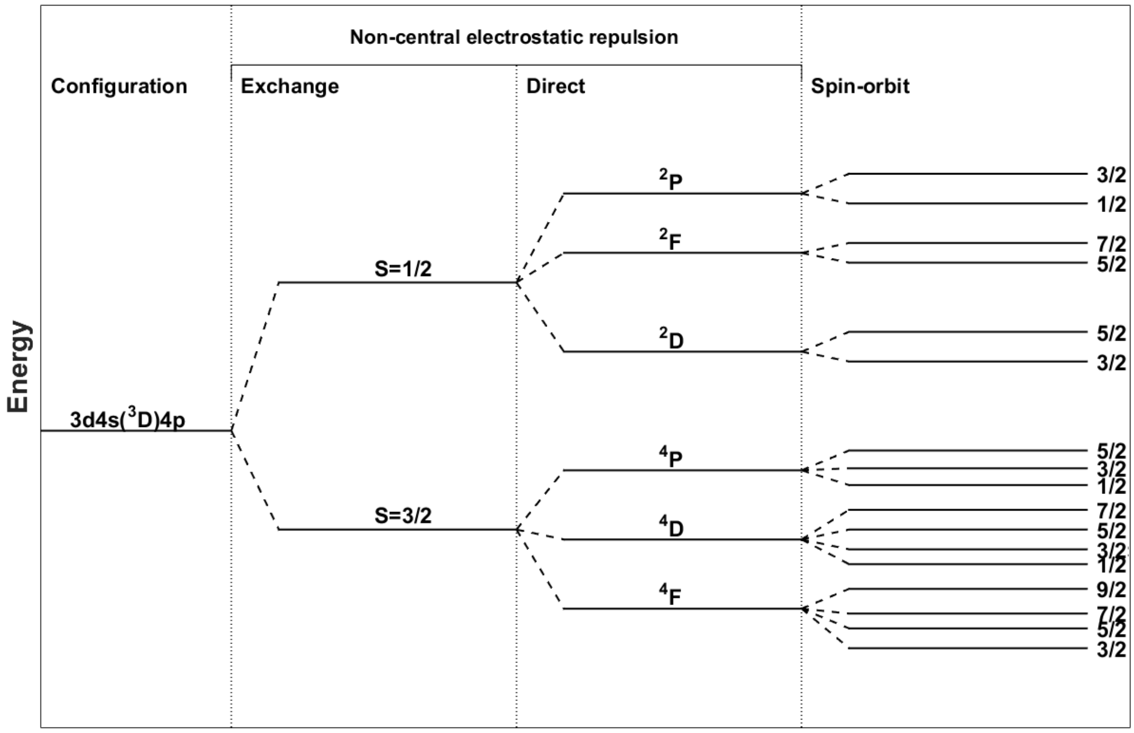

Figure 2.1: Energy splitting of a $3d4s(^3D)4p$ configuration in LS coupling. Values on the right denote the J value of the fine structure energy levels. The energy splitting is not to scale, the purpose of this image is to show the order in which configurations are split up into levels for LS coupling.

2.1.3 Energy structure in scandium

The energy level structure of neutral scandium is displayed in the energy level diagram in Fig. 2.2. Here the energy of levels relative to the ground level are shown on the y-axis. The ground level is defined as the level with an energy of 0 cm^{-1}. The energy levels of an atom can be sorted into parent terms, as is shown on the x-axis. Parent terms are the terms obtained from configurations where one electron is removed. The parent term is written in brackets inside the electron configuration. The first ionization limit is indicated at $E = 52922.0$ cm^{-1} (Sugar and Corliss, 1985). Above the ionization limit the free electron can have any kinetic energy. The electron configuration and term of the ground level of scandium is $1s^2 2s^2 2p^6 3s^2 3p^6 4s^2 3d$ $^2D_{3/2}$. There is only one electron outside a closed subshell in the ground configuration. This electron is outside the $4p^6$ subshell in a $3d$ subshell, thus scandium is a transition element.

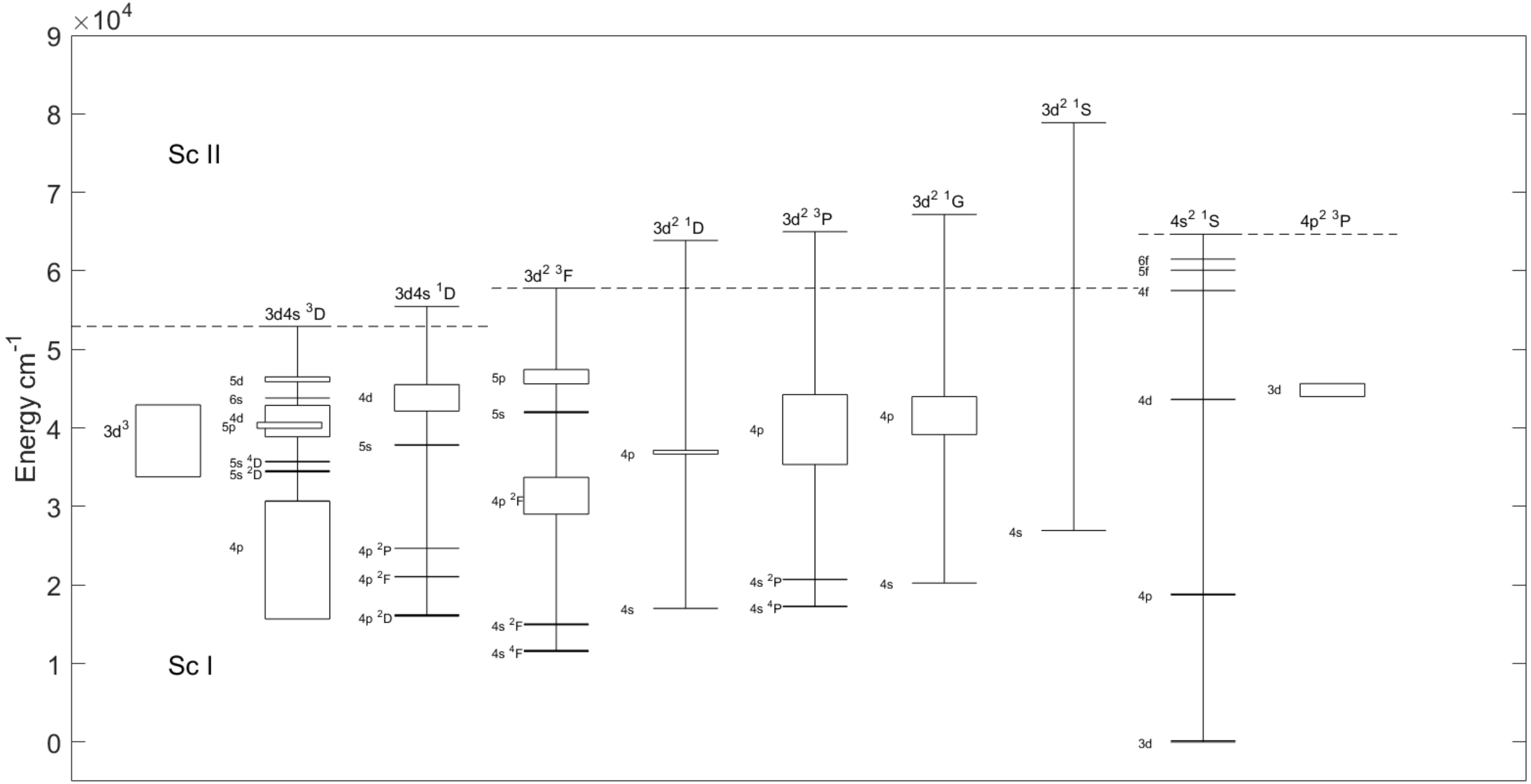

Figure 2.2: Energy level diagram for neutral scandium. The energy levels are grouped horizontally by their parent terms. Dashed lines denote an ionization limit. Solid lines indicate the energy of a fine structure level. A box indicates multiple levels belonging to the same configuration with roughly equal energies.

2.2 Transitions

When an atom undergoes a transition from a certain energy level to a lower energy level, a photon is send out with a frequency ν corresponding to the energy difference between the two levels ΔE (Thorne *et al.*, 1999). This is shown in Bohr's frequency condition

$$\Delta E = h\nu \tag{2.7}$$

Here h is Planck's constant. In this project wavenumber σ will be used instead of frequency ν, which is defined as

$$\sigma = \nu/c = 1/\lambda_{vac} \tag{2.8}$$

where c is the speed of light and λ_{vac} is the wavelength in vacuum. If the energy of a level is expressed in cm^{-1}, the wavenumber can be written as

$$\sigma = |E_l - E_u| \tag{2.9}$$

Throughout this thesis subscript letters l and u represent lower level and upper level respectively. All atoms have their own unique set of energy levels, and from to Eq. (2.7) one can expect all atoms to have unique spectrum as well. This is extremely useful, since this allows astronomers to identify spectral lines and to relate a stellar spectrum to the chemical composition of the star.

In a spectrum, a transition can be observed as a spectral line. In contrast to what this name suggests, a spectral line has a width, which is caused by broadening processes. For spectra produced using the HCL, one can assume that Doppler broadening is the dominant broadening process (Thorne *et al.*, 1999). Doppler broadening is caused by the Doppler effect: the wavenumber shifts because the source is moving towards or away from the observer. In the HCL the shift in wavenumber rises from thermal motions of emitting atoms. For Doppler broadening, a spectral line can be described using a Gaussian distribution with σ as mean and where the standard deviation is related to the Doppler width, $\Delta\sigma_D$. The Doppler width is defined as

$$\frac{\Delta\sigma_D}{\sigma} = 7.16 \cdot 10^{-7}\sqrt{T/M} \tag{2.10}$$

Where T is the temperature of the plasma containing the emitting atoms and M is the mass number of the element. As mentioned in the introduction, broadening by hfs is especially important when analysing spectra of small wavenumber regions. This can be explained using the equation above. An important property of the Doppler width is that it scales with the transition energy. The Doppler width will thus be small at small wavenumbers. As will be shown later, the broadening by hfs is not dependent on the wavenumber. Therefore, hfs broadening is more prominent and important for lines in the near-IR wavelength region compared to lines in the visible region.

2.2.1 Selection rules

A transition is only “allowed” when the selection rules are satisfied. The selection rules specify how the quantum numbers may change relative to their previous state. In this project, only electric dipole transitions (E1) are analysed, therefore only E1 transition rules are discussed.

The first selection rule can be obtained from conservation of angular momentum. A photon always carries parity, where parity is defined as $\sum l$ being even or odd. For emission, the atom sends out a photon, and thus l must change as

$$\Delta l = \pm 1 \tag{2.11}$$

A selection rule for J can also be derived

$$\Delta J = 0, \pm 1,\ \textit{J=0} \rightarrow \textit{0 is not allowed.} \tag{2.12}$$

There are selection rules for quantum numbers m_l and m_j

$$\Delta m_j = 0, \pm 1 \tag{2.13}$$

and

$$\Delta m_l = 0, \pm 1 \tag{2.14}$$

If LS coupling is valid, there are additional selection rules. The electron spin does not change during an electric dipole transition, so the following selection rule can be written for S

$$\Delta S = 0 \tag{2.15}$$

Combining the selection rules for J and S and recalling that $\boldsymbol{J} = \boldsymbol{L} + \boldsymbol{S}$, a selection rule for L can be derived

$$\Delta L = 0, \pm 1, \textit{L=0} \rightarrow \textit{0 is not allowed.} \tag{2.16}$$

2.2.2 Line strengths

The strength of a transition is related to the oscillator strength, f. The oscillator strength for an absorption line can be expressed as

$$f = \frac{g_u}{g_l}\frac{\varepsilon_0 m c^3}{2\pi e^2 \nu^2} A_{ul} \approx \frac{g_u}{g_l} 1.499 \cdot \lambda^2 A_{ul} \tag{2.17}$$

Here ν is the frequency of the transition, A_{ul} the transition probability in s^{-1}, ε_0 is the vacuum permittivity, e is the elementary charge and g is the statistical weight defined as $g = 2J + 1$. In astronomy the $\log gf$ values are often used instead of f. Here g is the statistical weight of the lower level. There exist methods to measure f values in the lab.

2.3 Hyperfine structure

Nuclear interactions can split up fine structure into hfs levels. There are two processes that can cause this. First, there is the magnetic moment arising from a net nuclear spin, which interacts with the magnetic field from electron spin and orbital motions. Secondly, for a non-spherical nucleus, an electric quadrupole moment rises, which interacts with the magnetic field from electron spin and orbital motion as well. These two processes are discussed in more detail below following Kuhn (1969).

2.3.1 Nuclear magnetic moment

hfs can occur if an atom has an odd mass number. In this case the intrinsic spins of neutrons and protons gives rise to a resultant nuclear angular momentum $\boldsymbol{I}$. Since the nucleus is charged, its resultant spin gives rise to a magnetic moment. The nuclear magnetic moment can be expressed as

$$\boldsymbol{\mu}_{nucleus} = \boldsymbol{I}\frac{\mu}{I\hbar} \tag{2.18}$$

Here μ is the magnitude of the nuclear magnetic moment, which is constant for a given isotope. The nuclear magnetic moment interacts with the magnetic field from electron spin and orbital motions, whose time average can be written as

$$\bar{\boldsymbol{H}} = \boldsymbol{J}\frac{\bar{H}}{J\hbar} \tag{2.19}$$

Here $\bar{H}$ is the magnitude of the magnetic field. The interaction of the magnetic field and magnetic moment gives rise to a torque between the nucleus and electrons and similar to electron spin-orbit interaction, this torque splits up the fine structure energy levels into hfs energy levels. The magnetic potential energy can be written as the dot product of a magnetic field and a magnetic dipole moment

$$E_{magn\_pot} = -\bar{\boldsymbol{H}} \cdot \boldsymbol{\mu}_{nucleus} = -\frac{\bar{H}\mu}{IJ\hbar^2}\boldsymbol{J} \cdot \boldsymbol{I} \tag{2.20}$$

Each hfs level is quantized by the total atomic angular momentum $\boldsymbol{F}$, which is defined by vector addition of $\boldsymbol{I}$ and $\boldsymbol{J}$

$$\boldsymbol{F} = \boldsymbol{I} + \boldsymbol{J} \tag{2.21}$$

therefore quantum number F can take values

$$F = I + J, I + J - 1, ..., |I - J| \tag{2.22}$$

The dot product of $\boldsymbol{I}$ and $\boldsymbol{J}$ can now be written as $\boldsymbol{J} \cdot \boldsymbol{I} = \frac{1}{2}(\boldsymbol{F}^2 - \boldsymbol{I}^2 - \boldsymbol{J}^2)$. By replacing the operators by functions representing their eigenvalues and substituting into Eq. (2.20), the magnetic potential energy can be written as

$$E_{magnpot} = \frac{A}{2}[F(F+1) - J(J+1) + I(I+1)] \tag{2.23}$$

Where A is the first hfs constant and is defined as

$$A = -\frac{\bar{H}\mu}{2IJ} \tag{2.24}$$

This formula is useful since it gives a physical interpretation to the first hfs constant. In practice however, A is not calculated using this formula, but is determined by means of laboratory measurements. A varies as $\bar{H}$, since the other terms are all constants for a given isotope and fine structure energy level. It can now be seen from Eq. (2.22) that when $I = 0$, F and J will be equal and no hfs occurs. Moreover, no hfs will occur if the nuclear magnetic moment is zero.

2.3.2 Electric quadrupole moment

If the nucleus is non-spherical, an electric quadrupole moment eQ will rise. Q basically describes the deviation from spherical symmetry: the nucleus is elongated if $Q > 0$ and flattened if $Q < 0$. The electric quadrupole moment interacts with the electrostatic potential V, giving rise to the second hfs energy perturbation. Similar as for the nuclear magnetic moment interaction, a second hfs constant B can be used to describe the energy perturbation due to the quadrupole moment interaction

$$E_Q = \frac{3C(C+1) - 4IJ(I+1)(J+1)}{8IJ(2IJ-1)(2J-1)} B \tag{2.25}$$

where

$$C = F(F+1) - I(I+1) - J(J+1) \tag{2.26}$$

and

$$B = \frac{1}{hc} eQ\bar{V_{JJ}} \tag{2.27}$$

Here $\bar{V_{JJ}}$ is the second derivative of the electrostatic potential in the direction of $\boldsymbol{J}$. Again, in practice B is determined by means of laboratory measurements. It should be noted that the energy perturbation from the quadrupole moment only occurs when I and J are both greater or equal than 1. For free atoms, the splitting caused by the electric quadrupole moment is generally small compared to splitting caused by the nuclear magnetic moment.

2.3.3 Hyperfine structure transitions

Combining the nuclear magnetic moment interaction and the electric quadrupole interaction by putting Eq. (2.23) and 2.25 together, gives an expression for the energy of a hfs level

$$E_F = E_J + \frac{A}{2}C + \frac{3C(C+1) - 4IJ(I+1)(J+1)}{8IJ(2IJ-1)(2J-1)} B \tag{2.28}$$

Or simply $E_F = E_J + 0.5A \cdot f(F, J, I) + B \cdot g(F, J, I)$. From this equation one can see that the energy of a hfs level can be calculated when the hfs constants A and B, the quantum numbers and the energy of a fine structure level are known. As will be shown in the methodology section, this formula forms the basis for creating synthetic spectra of hfs multiplets. As shown in Eq. (2.9) the wavenumber of a transition is determined by the energy difference between the upper and lower level. Combining this with Eq. (2.28), the wavenumber of a hfs transition can be expressed as

$$\begin{aligned} \sigma_F = E_{F_u} - E_{F_l} = \\ \sigma_J + \frac{A_u}{2} f(F_u, J_u, I) + B_u g(F_u, J_u, I) - \frac{A_l}{2} f(F_l, J_l, I) + B_l g(F_l, J_l, I) \end{aligned} \tag{2.29}$$

σ_J is often well known from laboratory measurements, so one can derive the wavenumbers of all hfs transitions if hfs constants are available.
A new selection rule is added for hfs transitions

$$\Delta F = 0, \pm 1, \textit{F=0} \rightarrow \textit{0 not allowed.} \tag{2.30}$$

Relative intensities

The relative intensities of hfs transitions within a multiplet can be calculated given the quantum numbers of the levels (Cowan, 1981). Consider a transition from an upper state with quantum numbers F_u, J_u, I to a lower state with quantum numbers F_l, J_l, I. For this transition the transitional probability $A(F_u \rightarrow F_l)$ can be expressed using the Höln-Kronig rule

$$A(F_u \rightarrow F_l) = (2F_l + 1)(2F_u + 1) \begin{Bmatrix} J_l & I & F_l \\ F_u & 1 & J_u \end{Bmatrix} A(J_u \rightarrow J_l) \tag{2.31}$$

Here $A(J_u \rightarrow J_l)$ is the transitional probability of the fine structure transition. This term is divided out when one is interested in the relative intensities within a hfs multiplet. The term within curly brackets is called a Wigner six-j symbol, which is defined as

$$\begin{Bmatrix} j_1 & j_2 & j_3 \\ l_1 & l_2 & l_3 \end{Bmatrix} = \sqrt{(\Delta(j_1, j_2, j_3)\Delta(j_1, l_2, l_3)\Delta(l_1, j_2, l_3)\Delta(l_1, l_2, j_3))} \cdot \sum_k \frac{(-1)^k (k+1)!}{f(k)} \tag{2.32}$$

where $\Delta(a, b, c)$ is the triangle coefficient, defined as

$$\Delta(a, b, c) = \frac{\Gamma(a + b - c)\Gamma(a - b + c)\Gamma(-a + b + c)}{\Gamma(a + b + c + 1)} \tag{2.33}$$

A built in Matlab function *gamma* exists to calculate $\Gamma(n)$, which executes the following equation

$$\Gamma(x) = \int_0^\infty e^{-t} t^{x-1} dt \tag{2.34}$$

The summation in Eq. (2.32) is over all integers k for which Γ has nonnegative arguments. Function $f(k)$ is defined as

$$\begin{split} f(k) = \Gamma(k - j_1 - j_2 - j_3)\Gamma(k - j_1 - l_2 - l_3)\Gamma(k - l_1 - j_2 - l_3) \\ \Gamma(k - l_1 - l_2 - j_3)\Gamma(j_1 + j_2 + l_1 + l_2 - k)\Gamma(j_2 + j_3 + l_2 + l_3 - k)\Gamma(j_3 + j_1 + l_3 + l_1 - k) \end{split} \tag{2.35}$$

Chapter 3

Methods

In this section, it is described how the hfs constants are measured. First, it is explained how a spectrum of scandium was recorded. The observed spectrum was fitted using the nonlinear least squares method, which returns the best fit hfs constants. It is described how the synthetic spectrum of a hfs multiplet can be modelled. Moreover, a method to determine the uncertainties on the hfs constants is described. Finally, a method for deriving oscillator strengths for hfs transitions is shown.

3.1 Experimental setup

To produce a spectrum of scandium, one needs a light source and a detector. In this section, it is first described how scandium atoms are excited. Next, it is explained how a spectrum can be recorded using interferometry.

3.1.1 The light source

Scandium atoms are excited by electron collisions using a double hollow cathode discharge lamp (HCL). Atoms are excited to various energy levels, so that many transitions can be observed in the resulting spectrum. A sketch of the HCL is show in Fig. 3.1. As can be seen it consists of two positively charged anodes at the edges and a negatively charged cathode in the middle, which are isolated by glass windows. Due to the charge difference, an electric field rises which causes free electrons to accelerate towards the anodes. Neon is used as a carrier gas and free electrons collide with neon atoms. When the free electrons collide, they exchange their kinetic energy and if the energy exchange is large enough neon is ionized

$$Ne + e^- \rightarrow Ne^+ + 2e^-$$

Neon can also be excited to a bound state, and send out a photon when de-exciting. Therefore, one can expect neon lines to show up in the spectrum. The positive neon ions will be accelerated towards the cathode by the electric field. A lump of scandium is placed inside the hollow cathode, where it is sputtered into the plasma by bombardment of the neon ions. Once scandium is sputtered into the plasma, it is excited through electron collisions. By spontaneous de-excitation it will return to a lower level and sends out a photon. A part of the photons will move in exactly the right direction to pass through a sapphire window and move towards the detector. As discussed in Sect. 2.2, the spectral lines will have a Doppler width depending on the temperature. To resolve hfs components, a small Doppler width is preferred. This can be achieved by running at low voltages. The downside of a low voltage is however that fewer atoms will be excited.

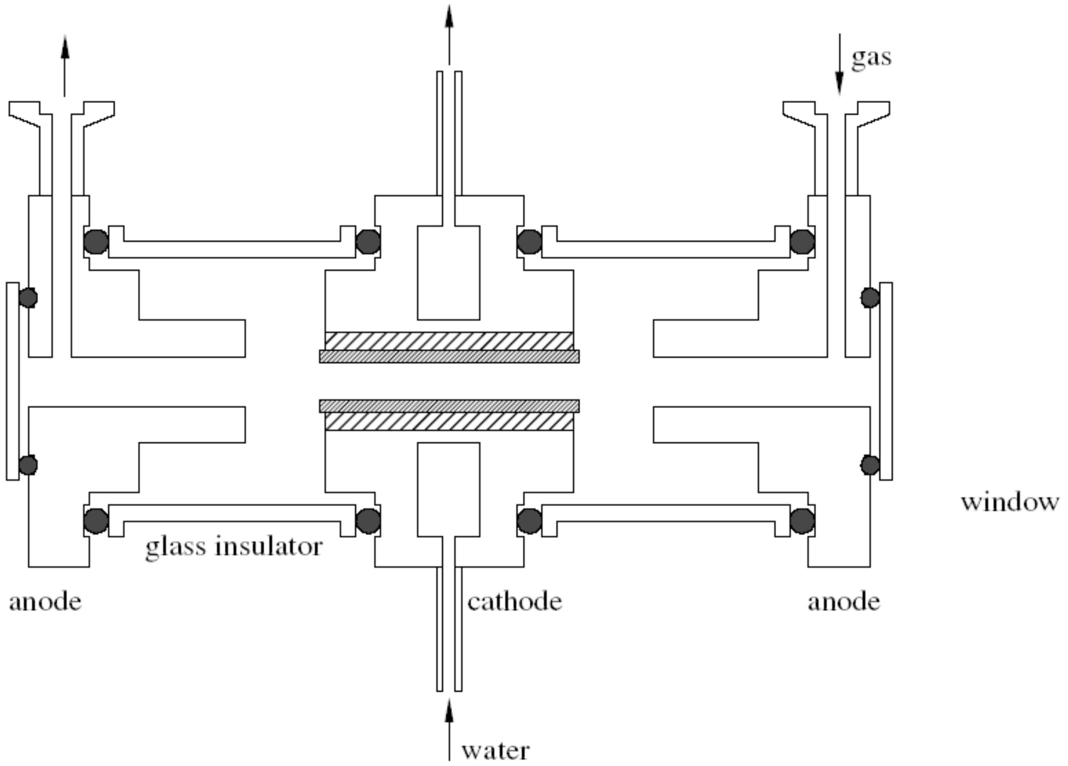

Figure 3.1: Sketch of the Hollow Cathode Discharge Lamp. Scandium is placed in the hollow cathode where it is sputtered into the plasma by colliding with neon ions. Photons can pass through the sapphire window on the right. Water is run through the HCL to reduce the Doppler width. By courtesy of Ulf Litzén.

3.1.2 The interferometer

The light beam send out by the HCL enters a mirror system. The mirror system leads the light beam into a Michelson interferometer, of which a sketch is shown in Fig. 3.2. To explain the concept of the Michelson interferometer it will now be assumed that the beam is monochromatic with wavelength λ, even though in reality the light beam consists of a set of photons having various wavelengths. Inside the Michelson interferometer the light beam will first encounter a beamsplitter. Here half of the light beam is reflected and send to mirror M_1 and the other half is transmitted and is send to another mirror, M_2. Both mirrors reflect the light beams back towards the beamsplitter, where the light beams are re-united and send to a detector. An important feature of the Michelson interferometer is that one of the mirrors can be moved while the other is fixed. A laser system can determine the position of the movable mirror very accurately. When one of the mirrors is moved, the detector will measure an intensity signal that is changing over time, because of constructive and destructive interference. The path difference can be defined as the length difference from the beamsplitter to mirror 1 relative to mirror 2

$$x = ||M_1B| - |M_2B|| \tag{3.1}$$

If for instance $x = 0$, one can expect a maximum intensity, because of constructive interference. If on the other hand $x = \lambda$, one can expect that the intensity signal will be zero, because of destructive interference. To quantify this, one can start by saying the amplitudes of both beams are a. The amplitude A of the beam after passing through the beamsplitter for the second time can be found from the law of cosines

$$A^2 = 2a^2(1 + \cos\delta) \tag{3.2}$$

Where δ is the phase difference between the two light beams. The phase difference can be related to the path difference x by considering the case where we have a path difference is equal to one wavelength. In this case the phase difference would be 2π, so one can write $\delta/2\pi = x/\lambda$, or $\delta = 2\pi\sigma x$. The intensity that will be registered by the detector will thus depend on σ and x

$$I = 2a^2(1 + \cos 2\pi\sigma x) \tag{3.3}$$

When the mirror moves at a constant speed v towards the beamsplitter, the path difference can be written as $x = vt$. Plugging this into the previous equation, one can expect that the detector will register a signal that varies as $\cos 2\pi vt$. The frequency of this signal is then σv, and since the frequency can easily be determined from the signal, this method allows to determine the wavenumber of the light beam.

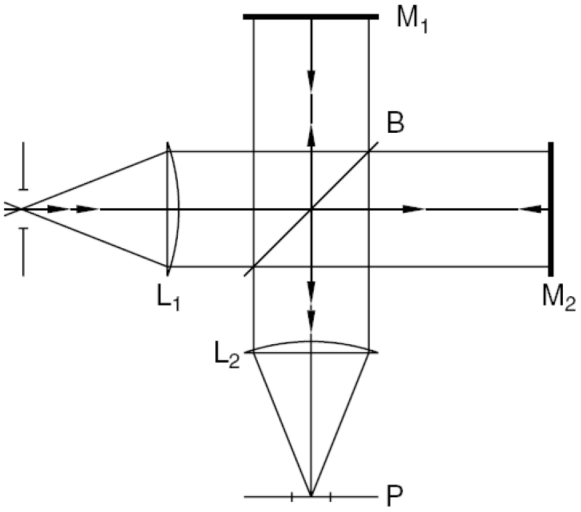

Figure 3.2: A sketch of an interferometer. L stands for lens, B is a beamsplitter, M represents the mirrors and P is the detector. One of the mirrors is movable.

3.1.3 The Fourier transform

In the above section, the light beam is treated as monochromatic, which does not represent the reality at all. Nevertheless, the same principle can be used for a light beam with multiple wavelengths. The intensity signal measured by the detector will be a sum of cosines with various frequencies and is called an interferogram. The light beam send out by the HCL will consist of many transitions, which all are Doppler broadened. The spectrum of the light beam can therefore be described using a spectral distribution $B(\sigma)$, which specifies the intensity at each wavenumber. The interferogram can be described as an integral over the wavenumber interval

$$I = I_0 + \int_{-\infty}^{\infty} B(\sigma)\cos 2\pi\sigma x \, d\sigma \tag{3.4}$$

It should be noted that $B(\sigma) = 0$ for $\sigma < 0$, since negative wavenumbers have no physical meaning. Nevertheless, these integral limits are kept this way, since these limits allow for inverse transformations. The interferogram I as expressed in Eq. (3.4) can now be recognized as the cosine transform of the spectrum $B(\sigma)$. From Fourier theory one can find the spectrum, given an interferogram by taking the inverse transform

$$B(\sigma) = \int_{-\infty}^{\infty} I(x) \cos 2\pi\sigma x \, dx \tag{3.5}$$

This allows to transform a measured interferogram to a spectrum. The interferogram as recorded by the FTS and the corresponding spectrum are shown in Fig 3.3 and 3.4 respectively. At $x = 0$ the interferogram has its maximum amplitudes, which is caused by constructive interference. From the spectrum one can see that many lines have been recorded in the wavenumber region from 2000 cm^{-1} to 20000 cm^{-1}. Spectral lines with wavenumbers above 20000 cm^{-1} were not recorded as the detector is not sensitive in this spectral region. Around 15000 cm^{-1} a strong line can be observed, which is partly negative. This line originates from the laser that determines the position of the mirror. A negative intensity is not physical, but can be explained by looking at the integral limits in Eq. (3.3). In practice, the mirror will move a few meter instead of to infinity. This causes unresolved lines such as the laser to show up in the spectrum with a *sinc* profile instead of a Gaussian.

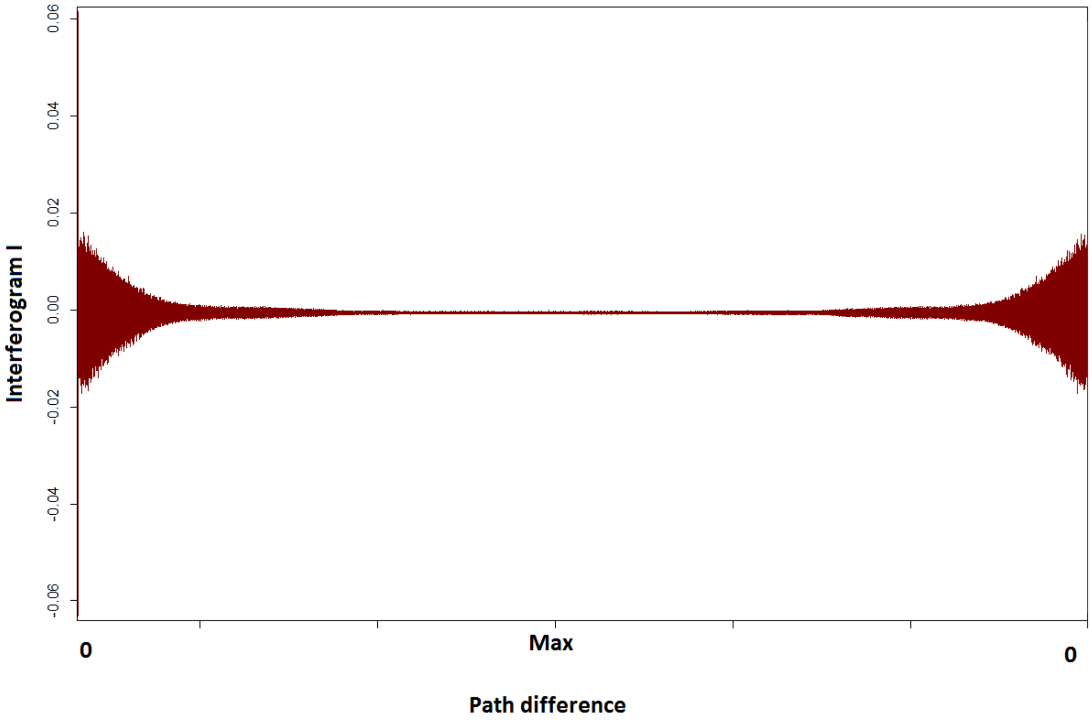

Figure 3.3: The interferogram as recorded by the FTS. The mirror moves from $x = 0$ to the maximum path difference and again back to $x = 0$.

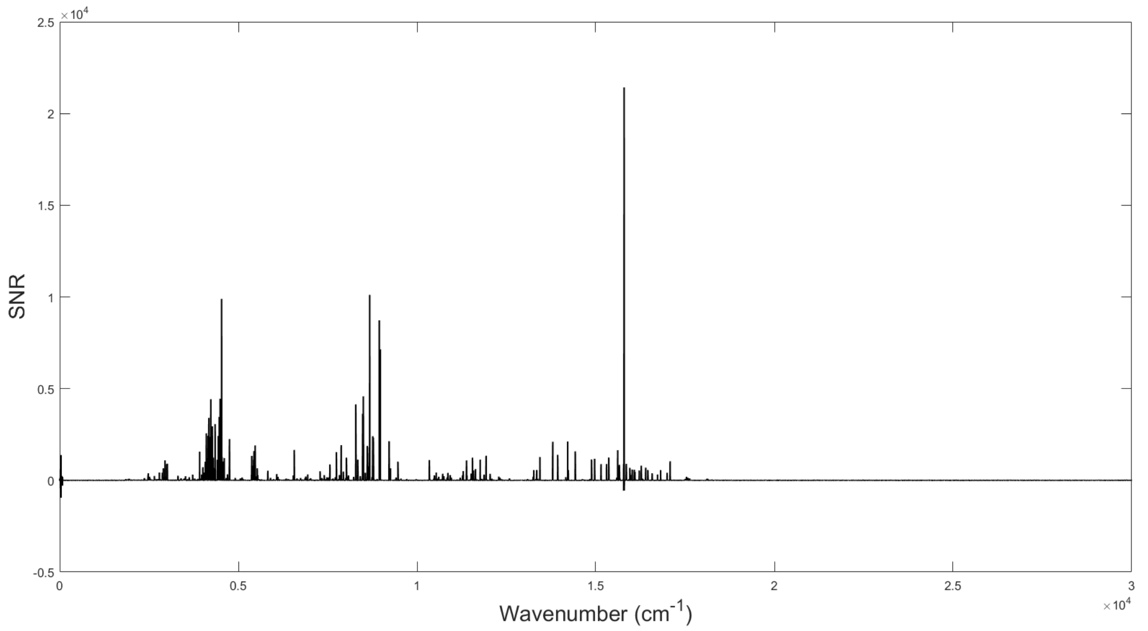

Figure 3.4: The observed spectrum as transformed from the interferogram in Fig. 3.3.

3.2 Model

In order to measure the hfs constants, a synthetic spectrum was fitted to the observed spectrum using the nonlinear least squares method. In this section, it will be discussed how the synthetic spectrum of a hfs multiplet can be modelled. Additionally, it is discussed how initial values were chosen.

3.2.1 Nonlinear least squares fit

In this section the principle of the nonlinear least squares method is explained in a summary of the theory given on the Matlab website (Mathworks). The observed spectrum is fitted by minimizing the summed square of the residuals, where the residual for the ith data point is defined as

$$r_i = y_i - \hat{y}_i \tag{3.6}$$

$\hat{y}_i$ is the modelled intensity at data point i. y_i is the observed intensity at the ith data point, which can be read directly from the FTS spectrum. In the FTS spectrum, the intensity and wavenumbers are given as arrays of length N. Since wavenumbers are given as an array, i can be related to the wavenumber. N is large, which makes the fitting procedure computationally heavy. For this reason, spectra of individual hfs multiplets are read in, and each multiplet is fitted separately. The summed square of residuals can be calculated as

$$S = \sum_{i=1}^{n} r_i^2 \tag{3.7}$$

where n is the number of data points within a hfs multiplet. In the method of least squares, intensities are calculated in the model $\hat{y}_i$ for various input parameters, starting with the given initial values for all parameters. For each set of parameters the summed squares of the residuals is calculated and the best fit is found when the summed square of the residuals is minimal. When a minimum is found, the program returns the set of parameters that fit the observed spectrum best.

To fit spectral lines, a *nonlinear* least squares method is generally used. A model is defined as nonlinear for a parameter when the model depends on a certain parameter after taking the partial derivative to this parameter. Mathematically, equation $f(x)$ is nonlinear in x when $\frac{\partial f(x)}{\partial x} = g(x)$. As will be shown in the next section, the model used in this project consists of a sum of several Gaussians, which are obviously nonlinear.

3.2.2 Synthetic spectra

To create a synthetic spectrum of a fine structure transition from E_{J_u} to E_{J_l}, one needs to determine what hfs transitions are allowed. The possible upper and lower hfs energy levels are calculated using $\boldsymbol{F} = \boldsymbol{J} + \boldsymbol{I}$. I is fixed for an isotope and J_u and J_l are known, as the fine structure transitions can be identified from the NIST database. The allowed hfs transitions can be found using the selection rule $\Delta F = 0, \pm 1$ *not* $F = 0 \rightarrow 0$. The wavenumbers for the allowed transitions are calculated using the hfs constants, as was shown in Eq. (2.29). The initial values of the hfs constants are given to the function as input parameters. It is assumed that spectral lines have a Gaussian profile, as explained in Sect. 2.2. For each allowed hfs transition, intensity values I_{mod} are computed following a Gaussian with the wavenumber of a hfs transition as mean and a standard deviation. This calculation is executed for all n wavenumbers using the built in Matlab function *normpdf*. Instead of the conventional symbol, *std* is used to refer to the standard deviation, as σ already refers to the wavenumber. *std* can be related to the temperature of the plasma as will be shown in Sect. 3.2.3.

The relative intensities can be calculated for given values of J_l, J_u, F_l and F_u, as was seen in Eq. (2.31). A separate function was written to execute this, called *sixjsymbol*. For each hfs component, I_{mod} is multiplied with the corresponding relative intensity. All Gaussians are summed into one array containing the total intensity I_{tot}. The intensity is normalized, so that the maximum intensity is equal to one. This intensity is multiplied by the maximum observed intensity, so that the observed and synthetic maximum intensity coincide.

The continuum of the synthetic spectrum can be lifted from zero using the input parameter *lift*. This parameter adds a constant intensity value to each element of the array I_{tot}. This additional parameter is necessary, since the HCL has a temperature of roughly 1000 K. Therefore it radiates as a black body, causing the continuum to have a small offset from zero.

In summary, J_u and J_l are given as input parameters. From these values the number of hfs transitions and the intensity of each component can be calculated. Furthermore, initial guesses for the hfs constants and σ_J are given as input parameters. From this the wavenumbers of each hfs component can be calculated. Assuming a Gaussian distribution for each component, a synthetic spectrum is produced. The hfs constants, σ_J, $lift$, std and the maximum synthetic intensity are fitted using the nonlinear least squares fitting method. An overview of the procedure for generating a synthetic spectrum of a hfs multiplet is given in a flow chart in Fig. 3.5.

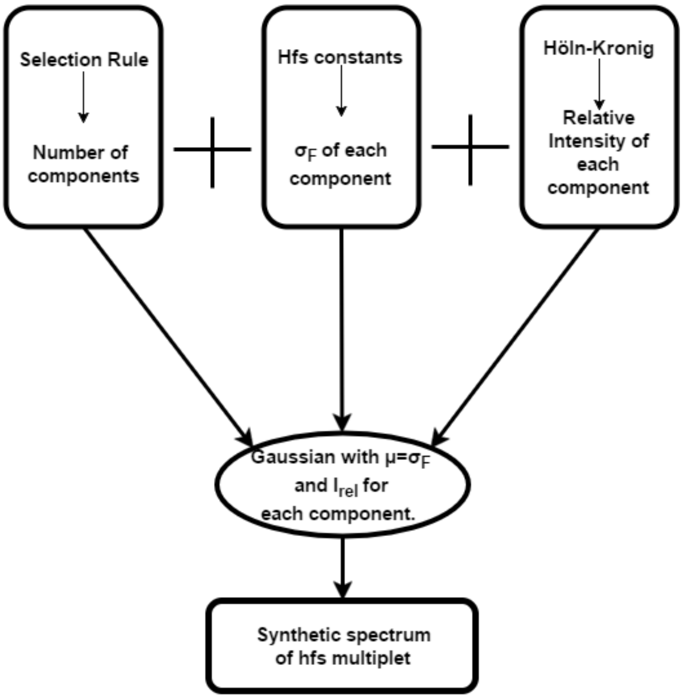

Figure 3.5: Procedure for generating the synthetic spectrum of a hfs multiplet. I_{rel} is the relative intensity of a hfs component.

3.2.3 Free parameters and initial values

There are 8 free parameters in the model, therefore the system is overdetermined and multiple best fit solutions will exist. There will exist local minima and it depends on the initial values which minimum will be found. In this section, constraints on the free parameters are discussed.

Hyperfine structure constants

Four hfs constants are involved in the calculation of the wavenumber of a hfs transition. One can use literature values as initial values. However, for many levels in scandium hfs data is unavailable. In this case initial values are determined manually, by plotting the synthetic versus the observed spectrum of the multiplet and searching for roughly similar profiles. For this purpose a GUI was developed. As a starting point one can set B to zero in most cases, as B is usually smaller than A. Also, as mentioned in Sect. 2.3.2, B is only non-zero when I and J both are greater or equal than one. Moreover, since hfs is caused by nuclear interactions, one might expect that when the valence electron is on a far out orbital, the nuclear interactions will be small and thus the hfs constants will be small.

Centre of gravity wavenumber

The centre of gravity wavenumbers for transitions in neutral scandium can be found in Kaufman and Sugar (1988) or in the NIST database (Kramida *et al.*, 2015). The centre of gravity wavenumber is usually accurately known. A shift in the wavenumber can easily be detected by comparing the initial synthetic spectrum with the observed spectrum. In this case, the wavenumber is shifted until the observed wavenumber is matched.

Line width

Each hfs component is modelled as a Gaussian with a mean and standard deviation. The standard deviation is set as a free parameter and an initial value can be calculated from the temperature of the emitting plasma. From Eq. (2.10) one can see that the Doppler width is related to the temperature of the emitting plasma. The Doppler width is the same as the Full Width Half Max (FWHM) of a line. According to Weisstein the FWHM can be related to the standard deviation of a Gaussian by $std = \text{FWHM}2\sqrt{2\ln 2}$. Combining this with the equation for the Doppler width, one can relate the standard deviation to the wavenumber of a transition and the temperature of the emitting plasma

$$std = \frac{7.16 \cdot 10^{-7}}{2\sqrt{2ln(2)}}\sigma\sqrt{\frac{T}{M}} \approx 3.04 \cdot 10^{-7}\sigma\sqrt{\frac{T}{45}} \tag{3.8}$$

A plasma temperature of $500K$ was assumed. This temperature probably underestimates the actual temperature, resulting in slightly too narrow initial widths.

Lift

The initial value for the parameter that lifts the entire spectrum is set to 0. The black body radiation causes the continuum to have a small slope, so an initial value of 0 should suffice.

Maximum intensity

In the fitting procedure, the relative intensities are kept constant while the maximum intensity of the synthetic spectrum is fitted. An initial value for the maximum intensity can be found by determining the maximum observed intensity within the hfs multiplet. It is important to note that an incorrect initial maximum intensity is found when there is a line close by with a stronger intensity. In this case, the initial maximum intensity is entered manually.

3.2.4 Locking parameters

It is useful to be able to lock certain parameters in the fitting routine. Consider for instance the case where the fitting routine finds a best fit solution for extremely large B values. It is known that usually $A > B$, so one might expect the solution that was found is incorrect. By locking parameters B_u and B_l, the fitting routine will search for a solution by varying the remaining free parameters, but keeping the B values constant. In the program this is achieved by setting upper and lower boundaries for the locked parameter equal to the initial value. Another case where it is useful to lock free parameters is when one of the levels has accurately known hfs constants. If a line is unresolved or too weak, a local minimum can be found in the fitting routine. By locking the upper or lower hfs constants, the degrees of freedom are limited and more accurate hfs constants for the opposite level could be found.

3.3 Analysis

3.3.1 Transition selection

As mentioned in the previous section, it is possible that the fitting routine ends in a local minimum, which would return incorrect hfs constants. For this reason, it is important to compare the best fit hfs constants for a certain level with other transitions involving the same level. The hfs constants for a level as found from various transitions should be the same. When the hfs constants are not the same, this indicates a local minimum might have been found. In this case, either some parameters are locked or the initial values are adjusted, until a consistent set of hfs constants is found. If for a certain level only one transition was observed, it is not clear whether the right minimum was found. For this reason, the hfs constant found in this work will be presented along with the number of transitions that returned consistent hfs constants. If a transition is too weak or unresolved, it might return wrong hfs constants. Some lines are therefore excluded from the set of consistent hfs constants.

For levels that are involved in multiple observed transitions, the “best” transition was selected and the hfs constants are presented as they were found from this transition. The selection of a transition is based on the signal to noise ratio (SNR), whether the line is resolved and the consistency and value of the opposite hfs constants. The fitting routine returns a parameter Υ to indicate if the line is resolved. Υ is defined as the width of the hfs multiplet divided by the number of hfs transitions (n_{hfs}) times the Doppler width

$$\Upsilon = \frac{max(\sigma_F) - min(\sigma_F) + \Delta\sigma_D}{\Delta\sigma_D \cdot n_{hfs}} \tag{3.9}$$

Whether all hfs components are resolved, also depends on what pattern is formed, which is determined by the hfs constants. In general, individual hfs components are resolved if $\Upsilon > 2$.

3.3.2 Wavenumber calibration

By imperfect alignment between the light beam from the HCL and the laser, a linear shift in the wavenumber is introduced. The hfs constants are not affected by this. Nonetheless, centre of gravity wavenumbers of a hfs multiplet will be affected and therefore the wavenumbers must be calibrated. This can be done by comparing literature wavenumbers (σ_{true}) of several well-known neon lines with the wavenumbers as observed in the spectrum (σ_{obs}). A correction factor k will be determined using the following relation

$$\sigma_{true} = \sigma_{obs}(1 + k) \tag{3.10}$$

The centre of gravity wavenumbers of the observed neon lines were determined using the program *Gfit* (Engström, 1998). Literature values for neon transitions have been taken from Sansonetti *et al.* (2004); Humphreys *et al.* (1961); Burns *et al.* (1950) and Meggers and Humphreys (1934). The correction factor was calculated using 42 lines, which is shown in Table 3.1. A mean correction factor of $7.66E - 07$ was found, which was used to correct all observed wavenumbers following Eq. (3.10). It can be seen from Table 3.1 that the correction factors are the same order of magnitude for different lines, but there does seem to be a trend between k and the wavenumber. For this reason it was investigated how k behaves with wavenumber, which is shown in Fig. 3.6. k has been calculated for three wavenumber regions, i.e. wavenumbers near 3000 cm^{-1}, 5500 cm^{-1} and 11000 cm^{-1}. From Fig. 3.6 it can be seen that k does have different value depending on the wavenumber region, but there is no obvious relation between the two. The observed trend could be explained by considering that there exist multiple stable neon isotopes. Isotopes differ in nuclear mass and volume, which gives rise to differential energy levels shifts between isotopes (Thorne *et al.*, 1999). If a spectral line is affected by *isotope shift*, the line profile will not be completely Gaussian and the centre of gravity wavelength will shift. Since isotope shift is a nuclear effect, it will influence electrons that are close to the nucleus the strongest. One can expect electrons in the s orbital to be affected the most, as these electrons penetrate the nucleus. The region around 3000 cm^{-1} has mainly transitions from $2s^22p^5(^2P_{1/2,3/2})5s$ to $2s^22p^5(^2P_{1/2,3/2})4p$. As the upper level has an electron in the $5s$ orbital, these transitions could be affected strongly by isotope shift. The region around 5500 cm^{-1} has transitions from $2s^22p^5(^2P_{1/2,3/2})4f$ to $2s^22p^5(^2P_{1/2,3/2})3d$. The region around 11000 cm^{-1} has transitions from $2s^22p^5(^2P_{1/2,3/2})3d$ to $2s^22p^5(^2P_{1/2,3/2})3p$. The wavenumbers of the transitions in the latter two regions are likely less affected by isotope shift, as the electrons are further away from the nucleus. One could therefore argue that the spread in the value of k is caused by a difference in how strong the centre of gravity wavenumber was affected by isotope shift.

If one would use the correction factor as obtained from the 3000 cm^{-1} region instead of the mean correction factor, one would find slightly different results for the centre of gravity wavenumbers compared to the wavenumbers presented in the results section. The change in wavenumber ($\Delta\sigma$) ranges from $\Delta\sigma = 0.001$ cm^{-1} for lines at 3000 cm^{-1} to $\Delta\sigma = 0.004$ cm^{-1} for lines at 12000 cm^{-1}. To avoid this, it might be better to use argon as a carrier gas, which is less affected by isotope shift and for which the wavenumbers of transitions are known more accurately.

Table 3.1: The correction factor as determined for several neon lines. The first column shows the wavenumber as observed in the uncorrected spectrum (σ_{obs}). The second column gives the reference value (σ_{ref}), with the reference in the last column. In the third column, the corresponding calculated correction factors k are shown. References 1-4 are respectively Sansonetti *et al.* (2004); Humphreys *et al.* (1961); Burns *et al.* (1950) and Meggers and Humphreys (1934).

σ_{obs} cm^{-1}	σ_{ref} cm^{-1}	k	Ref
2511.4774	2511.9867	1.23E-06	1
2874.4286	2874.4317	1.08E-06	1
2900.1584	2900.1617	1.10E-06	1
2929.0565	2929.0598	1.13E-06	1
2948.7826	2948.7858	1.09E-06	1
2949.0617	2949.0649	1.09E-06	1
2997.4568	2997.4691	1.10E-06	1
2999.2358	2999.2391	1.10E-06	1
3013.6622	3013.6695	1.10E-06	1
3310.2974	3310.3011	1.12E-06	1
5411.0047	5411.0081	6.28E-07	1
5426.6891	5426.6921	5.53E-07	1
5432.4588	5432.4618	5.71E-07	1
5436.2689	5436.2722	6.07E-07	1
5436.4964	5436.4996	5.89E-07	1
5437.7802	5437.7835	6.07E-07	1
5438.0285	5438.0319	6.25E-07	1
5445.4011	5445.4048	6.79E-07	1
5468.1810	5468.1842	5.85E-07	1
5469.9678	5469.9711	6.03E-07	1
5484.8608	5484.8639	5.65E-07	1
5486.6454	5486.6486	5.83E-07	1
5543.0076	5543.0107	5.59E-07	1
10343.3180	10343.3251	6.86E-07	2
10485.7129	10485.7203	7.06E-07	1
10538.1947	10538.2018	6.74E-07	1
10606.7353	10606.7422	6.51E-07	1
10719.1789	10719.1864	7.09E-07	1
10748.7455	10748.7524	6.51E-07	1
11276.2505	11276.2575	6.21E-07	3
11276.8227	11276.8305	7.01E-07	3
11291.3916	11291.3996	7.17E-07	3
11381.5205	11381.5286	7.29E-07	3
11385.5802	11385.5878	6.76E-07	3
11515.0178	11515.0247	5.99E-07	3
11518.2383	11518.2459	6.60E-07	1
11551.6583	11551.6661	6.84E-07	1
11578.0607	11578.0688	7.00E-07	3
11636.5338	11636.5419	7.05E-07	3
11767.8909	11767.8995	7.39E-07	3
11875.4325	11875.4411	7.33E-07	3
11933.2960	11933.3034	6.28E-07	4

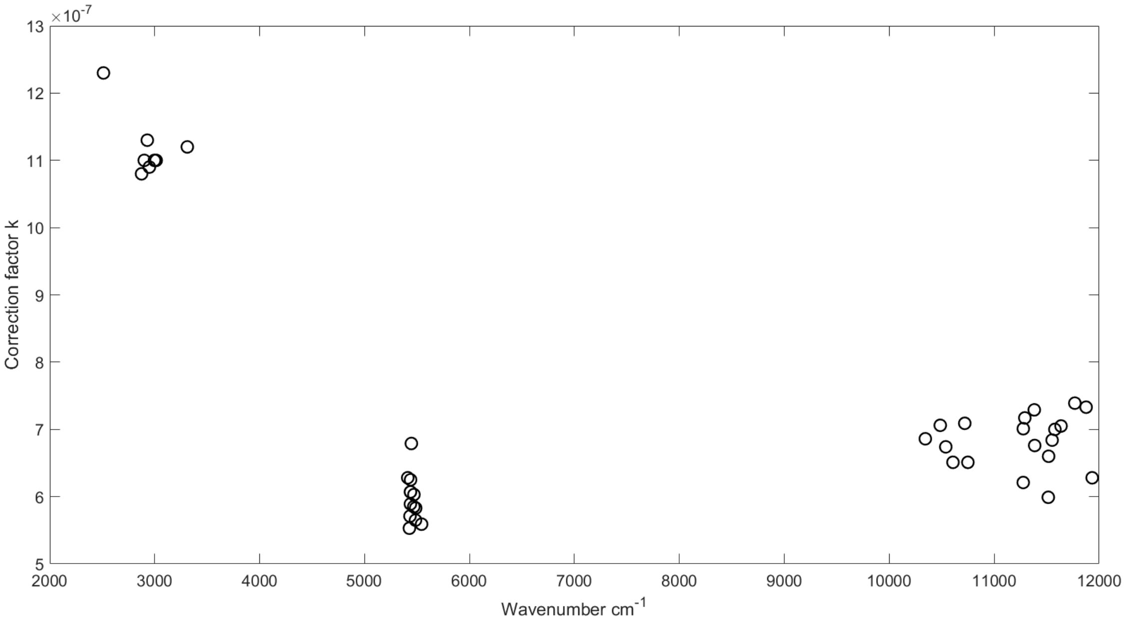

Figure 3.6: Correction factor k as calculated from various lines in the observed spectrum. k seems to depend on the wavenumber.

3.3.3 Oscillator strengths

A code was written to derive the oscillator strengths of hfs components for a given fine structure oscillator strength. One can derive this quantity using Eq. (2.31), which returns the relative intensity of a hfs transition within a hfs multiplet given the F upper and lower quantum numbers of the transition. The F values can be calculated from Eq. (2.22). One adds all relative intensities together and normalizes this, so that the total intensity of all hfs components is 1. Fine structure transition $\log gf$ values have been measured accurately by Pehlivan *et al.* (2015). The fine structure gf value is multiplied with the normalized relative intensity and a hfs oscillator strength f_{hfs} value is obtained. Mathematically this can be written as

$$gf_{hfs} = gf \frac{(2F_u+1)(2F_l+1)\begin{Bmatrix} J_l & I & F_l \\ F_u & 1 & J_u \end{Bmatrix}}{I_{tot}} \tag{3.11}$$

where I_{tot} is defined as

$$I_{tot} = \sum_i \sum_j (2F_{ui}+1)(2F_{lj}+1)\begin{Bmatrix} J_{lj} & I & F_{jl} \\ F_{ui} & 1 & J_{ui} \end{Bmatrix} \tag{3.12}$$

3.4 Uncertainties in the hfs constants

A function was written in Matlab to determine the uncertainties in the hfs constants. This function takes the best fit solution for the hfs constants and centre of gravity wavenumber. These parameters are treated as if they were the “true” values. A synthetic spectrum of the hfs multiplet is created using the “true” parameters and is normalized so that the maximum intensity is equal to the maximum intensity that was observed within the hfs multiplet. The synthetic spectrum is an array of intensity values. Random noise is added to each element of this array. The noise is generated using the built in Matlab function *randn*, so that the noise has a normal distribution with $\mu = 0$ and a standard deviation equal to that of the noise in the observed spectrum. How the noise level in the observed spectrum was determined, is described at the end of this section. The "pure+noise" spectrum is fitted using the same routine as described in Sect. 3.2.2. Here, initial values for hfs constants have a ten percent offset from the real value. The fitting routine is repeated 500 times, each time for new random noise and each time returning best fit parameters. Since the true hfs constant (A_{true}) is known in this case, the difference between the true and fitted constants can be calculated as $A_{true} - A_{fit}$. Moreover, the sample standard deviations in the hfs constants are calculated, which is equal to the uncertainty in the hfs constants. The method to derive uncertainties in the hfs constants is summarized in a flow chart in Fig. 3.7.

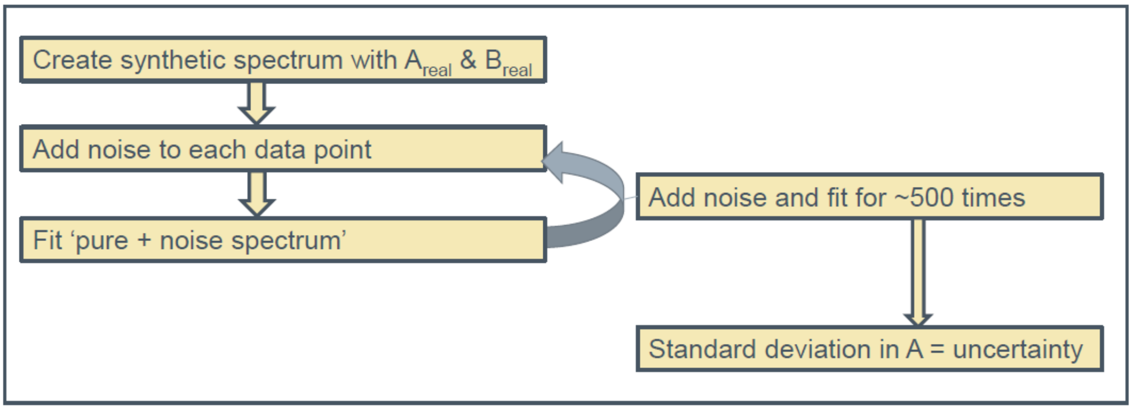

Figure 3.7: Flow chart describing how the uncertainties in the hfs constants were derived.

Noise in the observed spectrum

A property of a spectrum recorded by the FTS is that the uncertainty in the measured intensity is equal at all wavenumbers. The standard deviation of the noise can therefore be determined by calculating the sample standard deviation (s) in the intensity signal for various parts of the spectrum where there are no spectral lines. s is defined as

$$s = \sqrt{\frac{1}{N-1}\sum_{i=1}^{N}|I_i - \hat{I}|^2} \tag{3.13}$$

where N is the number of data points, I_i is the ith element of the intensity array and $\hat{I}$ is the mean intensity. After calculating s for various wavenumber regions, a weighed mean can be taken.

3.5 Sensitivity of the model

A code was written in Matlab to test how the best fit hfs constants behave with certain input parameters such as SNR, values of the hfs constants and an offset in initial values. The method to test the sensitivity to a certain parameter, for instance SNR, is as follows. Start by defining SNR as an array containing all the values one wants to test. SNR ranging from 0.1 to $7.5 \cdot 10^3$ were tested, as $7.5 \cdot 10^3$ is the intensity of the strongest line that was fitted. For each value of the SNR array a similar procedure as in Sect. 3.4 is carried out 200 times, which determines the uncertainty in the hfs constants given a SNR. The method described to probe the sensitivity to the SNR is summarized a flow chart in Fig. 3.8. It should be noted that this method is very time consuming. If for instance 50 different SNR values are tested, and each element of the SNR array is fitted 200 times, the program will execute $200 * 50 = 10000$ least squares fits, which takes approximately 10 hours.

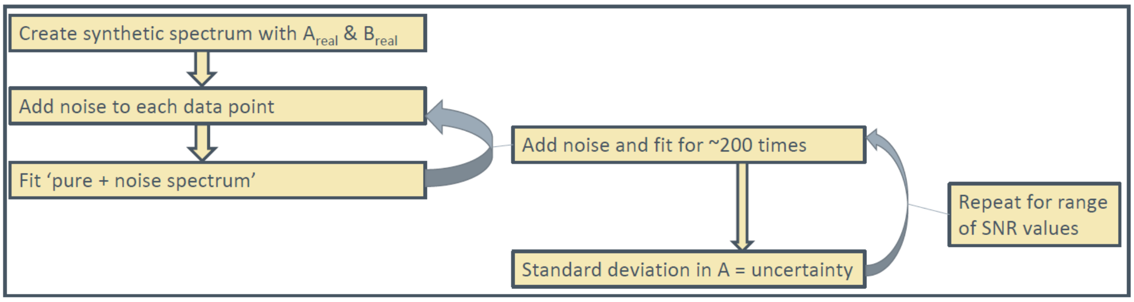

Figure 3.8: Flow chart describing how the models sensitivity to SNR was probed. It is essentially the same chart as shown in Fig. 3.7, but now repeated for a range of SNR values.

Chapter 4

Results

4.1 Hyperfine structure constants

In this project hfs constants have been determined for 95 levels of scandium. For 52 levels, the hfs constants have been determined for the first time. The hfs constants and their uncertainties are shown in Table 4.1 at the end of this section. For some levels the B values were locked to 0 cm^{-1} in the fitting procedure. In this case $B(thiswork)$ is left empty in column 5. The five columns on the right contain information on additional transitions involving the same level. n_{fit} indicates how many transitions involving this level have been fitted. $n_{checkfit}$ shows how many transitions have been fitted, while locking the hfs constants of the opposite level. The absolute deviation on A ($|dev.A|$) and B ($|dev.B|$) are also given, which is defined as the difference between the maximum and minimum hfs constant of the fitted/checkfitted transitions. Some transitions were too weak or unresolved to be fitted. However, by comparing the observed spectrum of such a transition with a synthetic spectrum generated using hfs constants from other transitions, one can check whether the least squares fitting routine has found the right minimum. Column 14 shows how many transitions were used to check on the hfs constants. In Fig. 4.1 a comparison between the hfs constant A as determined in this work and from literature values is shown for several levels. The y-axis shows the value of hfs constant A in cm^{-1}, while the x-axis separates the levels. It can be seen that for most levels the A values from this work have similar values compared to the literature values. Additionally, in this figure the uncertainty for each hfs constant is compared with uncertainty found by other studies. It can be seen that the uncertainty in A is of the same order for most levels. There are 5 levels for which the A value is remarkably different than the literature values. These levels are discussed in more detail in the discussion.

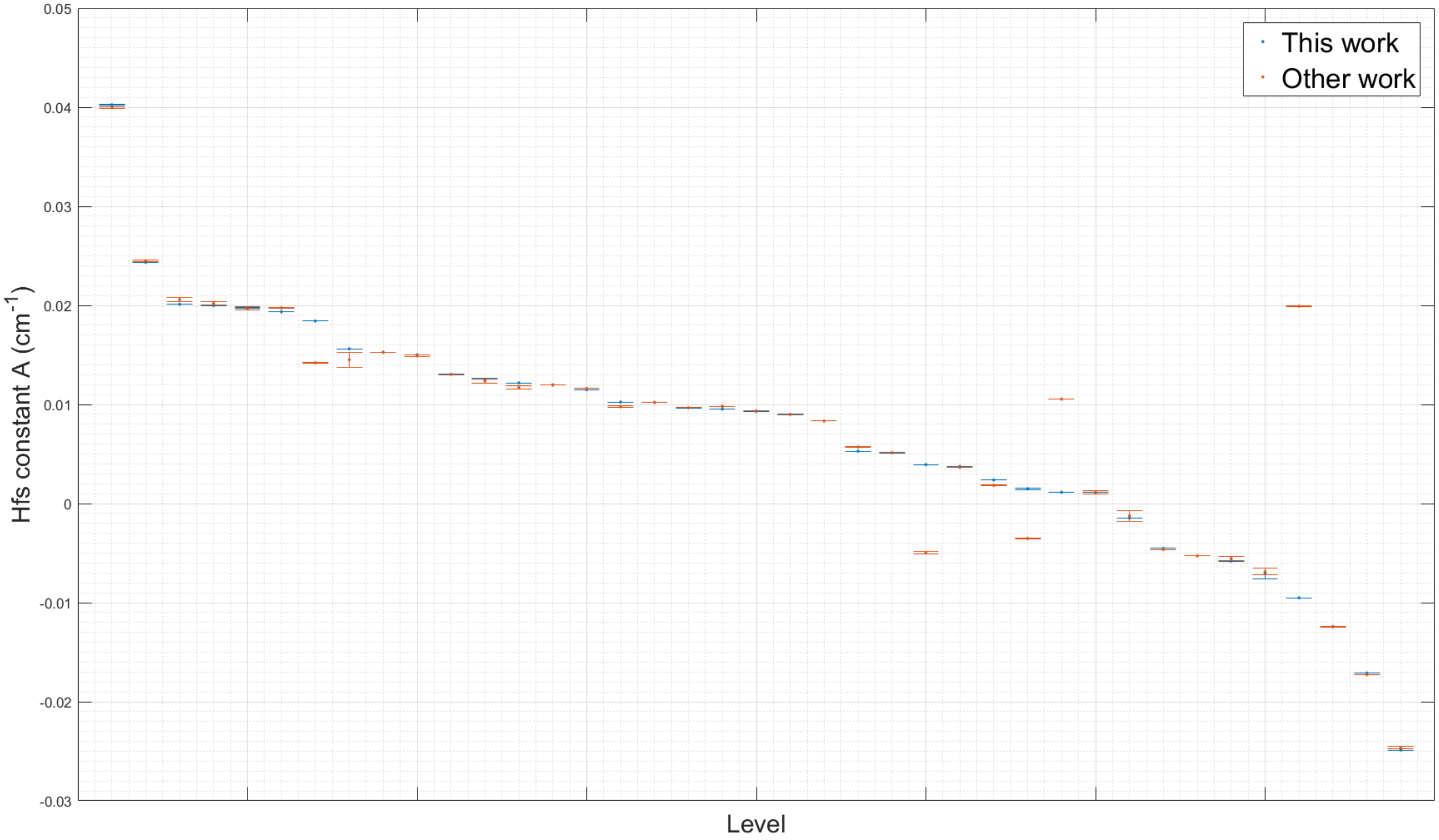

Figure 4.1: The hfs constants and their uncertainties compared with literature values. Blue dots represent hfs constants as determined in this work, while red dots represent those determined in other studies. See Table 4.1 for references. The hfs constants for levels for which no literature values exist are not shown in this plot.

In Fig. 4.2, 4.3 and 4.4 examples are shown of the synthetic spectrum after executing the fitting routine. In all three figures the black dots represent the observed spectrum and the red line represents the synthetic spectrum as found with the nonlinear least squares fit. The blue bars are used to indicate the wavenumbers of single hfs transitions. In all three figures a residual plot was added below the spectrum. Fig. 4.2 shows the transition from $3d4s(^1D)4p\ ^2D_{3/2}$ to $3d^2(^3F)4s\ ^4F_{5/2}$. As can be seen the fit is excellent and the residuals are small compared to the SNR. Most hfs components are resolved. Fig. 4.3 shows the transition from $3d4s(^3D)4p\ ^4F_{9/2}$ to $3d^2(^3F)4s\ ^4F_{7/2}$. Due to the large J values, this transition consists out of many components. Not all components are resolved. Again the fit is excellent and the residuals are small compared to the SNR. Fig. 4.4 shows the transition from $3d^2(^1S)4s\ ^2S_{1/2}$ to $3d4s(^3D)4p\ ^4P_{3/2}$. It can be seen the SNR is low for this line. Due to the small J values this transition consists out of few hfs components. Moreover, hfs constant A for the upper level is large and all hfs components are resolved. The observed wavenumbers of hfs components seem to be reproduced, however, the observed relative intensities are not reproduced.

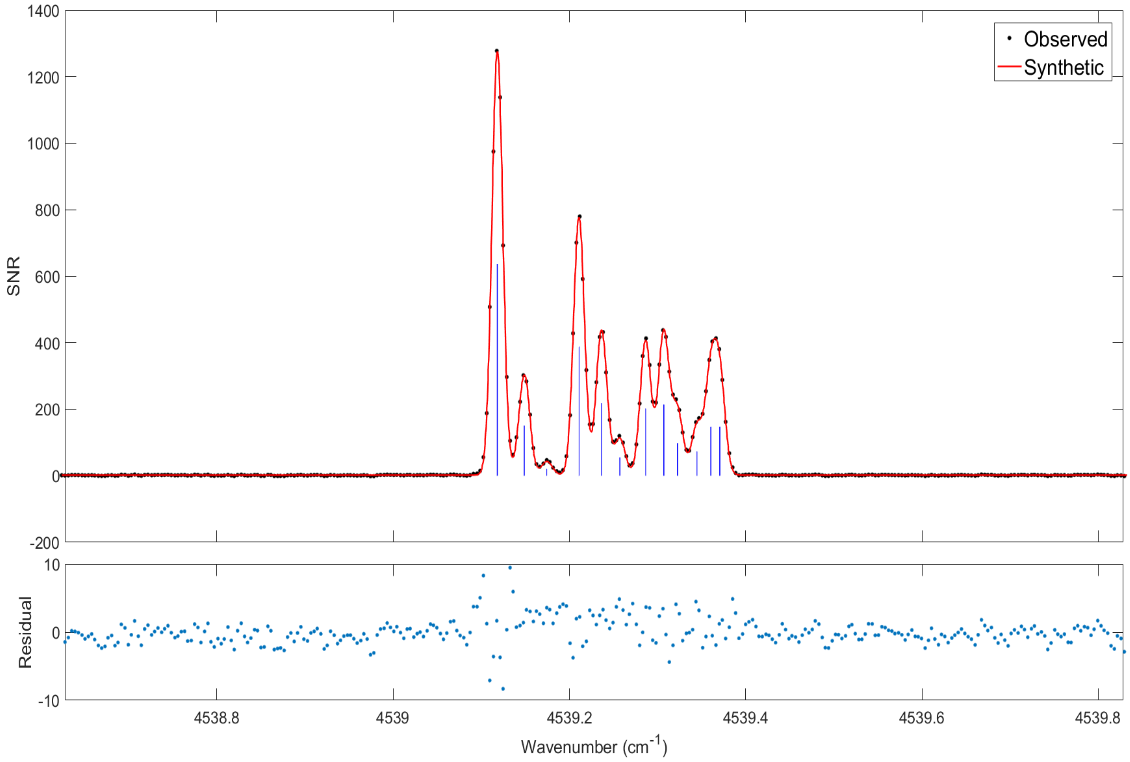

Figure 4.2: Synthetic and observed spectrum for a transition from $3d4s(^1D)4p\ ^2D_{3/2}$ to $3d^2(^3F)4s\ ^4F_{5/2}$. The black dots represent the observed spectrum and the red line is the synthetic spectrum as produced from the nonlinear least squares fit. The blue bars are used to indicate the wavenumber of single hfs transitions. Below the spectrum a residual plot is shown.

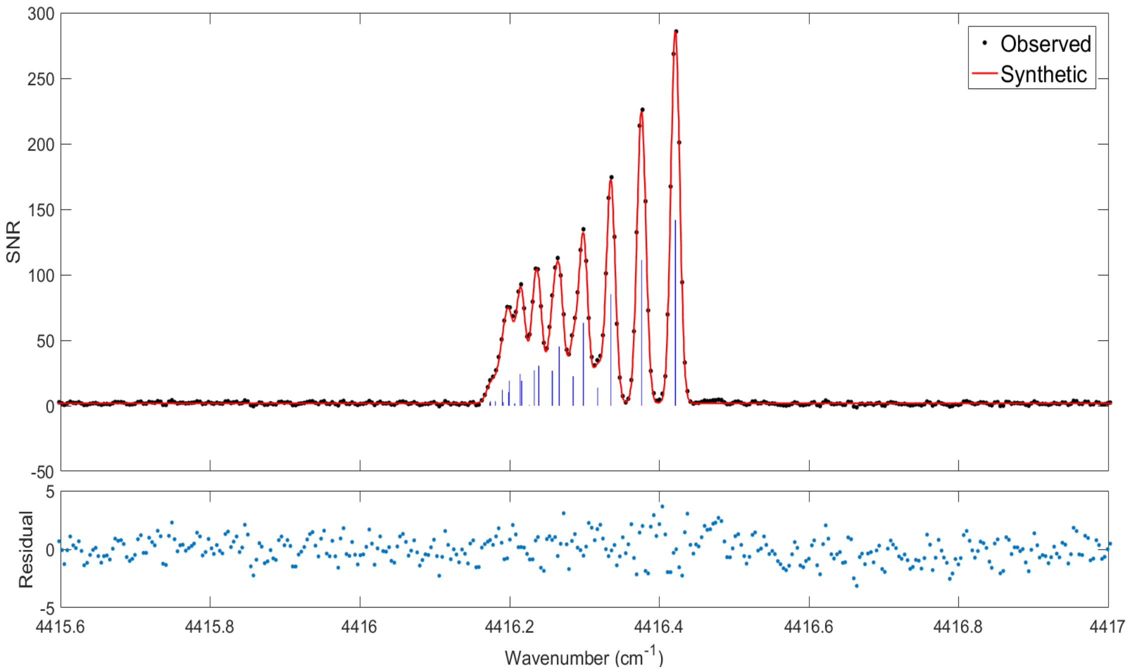

Figure 4.3: Synthetic and observed spectrum for a transition from $3d4s(^3D)4p\ ^4F_{9/2}$ to $3d^2(^3F)4s\ ^4F_{7/2}$. The black dots represent the observed spectrum and the red line is the synthetic spectrum as produced from the nonlinear least squares fit. The blue bars are used to indicate the wavenumber of single hfs transitions. Below the spectrum a residual plot is shown.

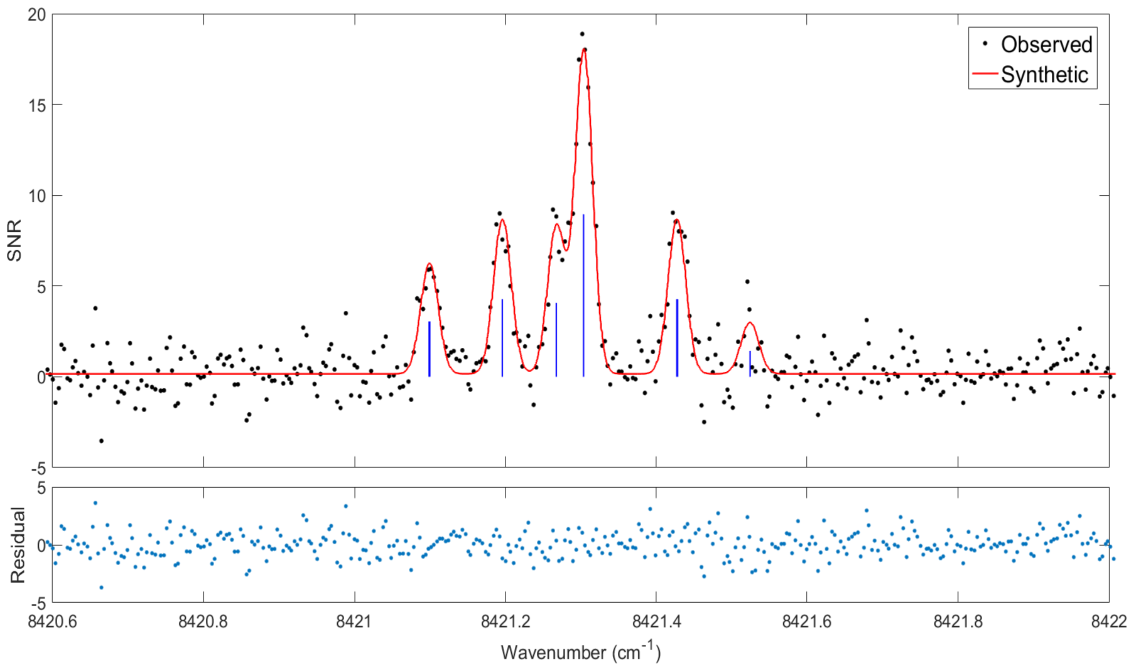

Figure 4.4: Synthetic and observed spectrum for a transition from $3d^2(^1S)4s\ ^2S_{1/2}$ to $3d4s(^3D)4p\ ^4P_{3/2}$. The black dots represent the observed spectrum and the red line is the synthetic spectrum as produced from the nonlinear least squares fit. The blue bars are used to indicate the wavenumber of single hfs transitions. Below the spectrum a residual plot is shown.

4.2 Recorded lines

230 electric dipole transitions in neutral scandium have been analysed, which is shown in Table 4.2 at the end of this section. Line properties as SNR and Υ are also given. Additionally, one can find the hfs constants for the upper and lower level, either determined in this work or from the literature. In the last column one can see what a transition was used for. A line can be used to *fit* or *check* or it can be excluded from the analysis because of *mixing* or if the line is unresolved or too weak. In total 118 lines have been fitted, which returned a consistent set of A values. Moreover, the hfs constants found from the fitted transitions, could reproduce the spectra of 44 lines that were too weak or unresolved to be fitted. Two transitions did not fit with the hfs constants as presented in Table 4.1. These two transitions are discussed in more detail in the discussion.

4.3 Oscillator strengths

Oscillator strengths were derived for 590 hfs transitions. In Table 4.3 oscillator strengths for all hfs transitions belonging to the fine structure transition from $3d4s(^3D)4p\ ^3D_{7/2}$ to $3d^2(^3F)4s\ ^4F_{7/2}$ are shown. Table B.1 shows $\log gf$ values of hfs transitions belonging to 44 additional fine structure transitions.

Table 4.1: The measured hfs constants for 95 levels in neutral scandium. Columns 3 to 6 show the hfs constants and their uncertainties as determined in this work. The next three columns give literature hfs constant A if available. Column n_{fit} shows how many transitions were fitted for this level. Column $n_{checkfit}$ gives how many lines were fitted while locking the hfs constants of the opposite level. The next two columns show the absolute deviation in A and B within the transitions that were fitted/checkfitted. The last column gives the number of lines for which the hfs constants could reproduce the observed spectrum.

Configuration	Term	A(this work) cm^{-1}	ΔA cm^{-1}	B(this work) cm^{-1}	ΔB cm^{-1}	A(Ref.) cm^{-1}	ΔA cm^{-1}	Ref.	n_{fit}	$n_{checkfit}$	$\|dev.A\|$ cm^{-1}	$\|dev.B\|$ cm^{-1}	n_{check}
$4s^2(^1S)4p$	$^2P_{1/2}$	0.00294	5.4E-06						1				1
$4s^2(^1S)4p$	$^2P_{3/2}$	0.02036	3.3E-07	-0.00098	3.1E-06				2		1.5E-03	2.5E-03	
$3d4s(^1D)4d$	$^2F_{7/2}$	0.00114	1.8E-06			0.01054	3.3E-05	[7]	1				1
$3d4s(^1D)4p$	$^2D_{3/2}$	-0.01245	3.4E-07	0.00030	2.3E-06	-0.01241	4.7E-05	[6]	5		3.6E-05	3.7E-04	
$3d4s(^1D)4p$	$^2D_{5/2}$	0.02202	1.1E-06	-0.01639	6.0E-06	-0.00687	3.3E-04	[8]	4		9.5E-05	7.6E-04	
$3d4s(^1D)4p$	$^2F_{5/2}$	-0.00146	1.6E-06			-0.00123	5.3E-04	[6]	3		3.7E-04		3
$3d4s(^1D)4p$	$^2F_{7/2}$	0.01254	2.6E-07	-0.00261	2.8E-06	0.01238	2.7E-04	[6]	3		1.7E-04	1.0E-04	1
$3d4s(^1D)4p$	$^2P_{1/2}$	0.01432	8.2E-06						1				1
$3d4s(^1D)4p$	$^2P_{3/2}$	-0.00094	1.5E-05						1				2
$3d4s(^1D)5p$	$^2D_{3/2}$	0.01108	1.4E-05	-0.00122	1.5E-04				1				
$3d4s(^1D)5p$	$^2F_{7/2}$	0.00224	9.0E-07						1				1
$3d4s(^1D)5p$	$^2P_{3/2}$	0.02593	2.8E-05	-0.00779	2.2E-04				1				
$3d4s(^1D)5s$	$^2D_{3/2}$	0.01023	1.1E-05	0.00225	1.3E-04	0.00977	1.0E-04	[7]	1				5
$3d4s(^1D)5s$	$^2D_{5/2}$	-0.00051	4.0E-06							4	1.0E-03		1
$3d4s(^3D)4d$	$^2F_{5/2}$	-0.00347	8.4E-06	0.00039						2	3.4E-04	3.9E-04	2
$3d4s(^3D)4d$	$^2F_{7/2}$	0.01089	1.0E-05						1				
$3d4s(^3D)4d$	$^2G_{7/2}$	0.00392	3.5E-06			-0.00497	1.3E-04	[7]		2	1.9E-04		1
$3d4s(^3D)4d$	$^2G_{9/2}$	0.00377	1.1E-05							1			1
$3d4s(^3D)4d$	$^2P_{1/2}$	-0.02455	4.9E-05						1				
$3d4s(^3D)4p$	$^2D_{3/2}$	0.00857	2.4E-05	-0.00057	2.3E-04	0.00920	0.0E+00	[4]	2		1.3E-03	5.8E-04	
$3d4s(^3D)4p$	$^2D_{5/2}$	0.00110	1.6E-06			0.00110	1.7E-04	[8]		2	2.7E-04		1
$3d4s(^3D)4p$	$^2F_{5/2}$	0.00588	1.0E-05			0.00570	0.0E+00	[4]	2		6.3E-04	1.8E-03	5

Table 4.1: Measured hfs constants for neutral scandium, continued.

Configuration	Term	A(this work) cm^{-1}	ΔA cm^{-1}	B(this work) cm^{-1}	ΔB cm^{-1}	A(Ref.) cm^{-1}	ΔA cm^{-1}	Ref.	n_{fit}	$n_{checkfit}$	$\|dev.A\|$ cm^{-1}	$\|dev.B\|$ cm^{-1}	n_{check}
$3d4s(^3D)4p$	$^2F_{7/2}$	0.00426	1.1E-05	0.00190	2.5E-04	0.00420	0.0E+00	[4]	3		5.2E-04	1.9E-03	2
$3d4s(^3D)4p$	$^2P_{1/2}$	0.00663	2.1E-05						2		7.1E-04		1
$3d4s(^3D)4p$	$^2P_{3/2}$	0.01026	1.0E-05	0.00058	1.1E-04				2		2.4E-03		
$3d4s(^3D)4p$	$^4D_{1/2}$	-0.01711	5.6E-08			-0.01727	4.7E-06	[6]	1				
$3d4s(^3D)4p$	$^4D_{3/2}$	0.01148	2.7E-07	0.00449	3.4E-06	0.01162	3.7E-06	[6]	4		6.2E-05	4.3E-03	
$3d4s(^3D)4p$	$^4D_{5/2}$	0.01019	2.9E-07	-0.00041	1.6E-06	0.01022	1.5E-07	[6]	3		2.9E-05	5.8E-04	3
$3d4s(^3D)4p$	$^4D_{7/2}$	0.01526	5.2E-08	0.00008	9.8E-07	0.01527	6.0E-08	[6]	3		1.1E-05	2.4E-04	1
$3d4s(^3D)4p$	$^4F_{3/2}$	-0.00453	1.5E-06	-0.00068	4.9E-06	-0.00463	2.3E-06	[6]	4		1.1E-04	2.8E-04	1
$3d4s(^3D)4p$	$^4F_{5/2}$	0.00965	2.1E-07	-0.00096	5.0E-06	0.00967	1.0E-06	[6]	4		9.2E-05	1.1E-03	2
$3d4s(^3D)4p$	$^4F_{7/2}$	0.01197	3.2E-07	-0.00164	6.9E-06	0.01198	6.7E-07	[6]	3		1.2E-04	7.1E-04	1
$3d4s(^3D)4p$	$^4F_{9/2}$	0.01305	4.1E-07	-0.00122	1.8E-05	0.01302	6.7E-07	[6]	2		4.1E-06	1.3E-03	1
$3d4s(^3D)4p$	$^4P_{1/2}$	0.04024	7.5E-05			0.03996	1.0E-04	[8]	1				
$3d4s(^3D)4p$	$^4P_{3/2}$	0.02433	7.9E-06	0.00226	1.0E-04	0.02448	1.0E-04	[8]	1	1	2.1E-03	6.3E-05	
$3d4s(^3D)4p$	$^4P_{5/2}$	0.01975	5.4E-05	-0.00001	8.5E-04	0.01968	1.7E-04	[8]	2		4.4E-05	1.8E-05	
$3d4s(^3D)5p$	$^2F_{5/2}$	0.00334	3.7E-06	-0.00113	4.4E-05				1				
$3d4s(^3D)5p$	$^2F_{7/2}$	0.01482	5.3E-06	-0.00335	1.5E-04				2		8.6E-04	-3.4E-03	1
$3d4s(^3D)5p$	$^4D_{1/2}$	-0.02452	1.1E-05						2		8.1E-05		
$3d4s(^3D)5p$	$^4D_{3/2}$	0.01170	1.1E-05	-0.00082	4.0E-05				3		8.5E-04	6.4E-03	
$3d4s(^3D)5p$	$^4D_{5/2}$	0.01395	1.1E-05						1				
$3d4s(^3D)5p$	$^4D_{7/2}$	0.01686	2.1E-06	0.00102	5.9E-05				1				1
$3d4s(^3D)5p$	$^4F_{3/2}$	-0.01103	1.1E-05	-0.00130					1				
$3d4s(^3D)5p$	$^4F_{5/2}$	0.00387	3.4E-06	-0.00017	4.5E-05				1				
$3d4s(^3D)5p$	$^4F_{7/2}$	0.01062	2.9E-06						1				
$3d4s(^3D)5p$	$^4F_{9/2}$	0.01439	3.4E-06	-0.00296	1.2E-04				1				
$3d4s(^3D)5p$	$^4P_{1/2}$	0.05694	3.2E-05						2		5.1E-04		
$3d4s(^3D)5p$	$^4P_{3/2}$	0.03090	1.6E-05	0.00056	1.4E-04				1				
$3d4s(^3D)5p$	$^4P_{5/2}$	0.02215	1.2E-05	-0.00152	1.7E-04				1				

Table 4.1: Measured hfs constants for neutral scandium, continued.

Configuration	Term	A(this work) cm^{-1}	ΔA cm^{-1}	B(this work) cm^{-1}	ΔB cm^{-1}	A(Ref.) cm^{-1}	ΔA cm^{-1}	Ref.	n_{fit}	$n_{checkfit}$	$\|dev.A\|$ cm^{-1}	$\|dev.B\|$ cm^{-1}	n_{check}
$3d4s(^3D)5s$	$^2D_{3/2}$	-0.00580	7.2E-06	-0.00069	2.5E-05	-0.00554	2.0E-04	[7]	4		4.0E-04	-4.5E-03	2
$3d4s(^3D)5s$	$^2D_{5/2}$	0.01998	1.2E-05	-0.00253	9.9E-05	0.02021	1.7E-04	[7]	7		1.3E-03	5.2E-03	1
$3d4s(^3D)5s$	$^4D_{1/2}$	-0.02489	1.1E-05			-0.02462	1.0E-04	[8]	4		2.0E-03		
$3d4s(^3D)5s$	$^4D_{3/2}$	0.01500	5.9E-06	-0.00049	6.1E-05	0.01491	1.0E-04	[8]	5		1.2E-03	2.4E-03	
$3d4s(^3D)5s$	$^4D_{5/2}$	0.01935	9.2E-06	-0.00102	1.7E-04	0.01975	6.7E-05	[7]	6		7.5E-04	4.0E-03	3
$3d4s(^3D)5s$	$^4D_{7/2}$	0.02012	2.1E-06	0.00016	4.8E-05	0.02058	2.0E-04	[7]	5		3.3E-05	8.3E-03	
$3d4s^2$	$^2D_{3/2}$	0.00901	5.1E-07	-0.00044	3.0E-06	0.00899	3.3E-08	[1]	5		7.2E-04	2.0E-03	
$3d4s^2$	$^2D_{5/2}$	0.00374	5.1E-07	0.00127	9.1E-06	0.00364	3.3E-08	[1]	1				3
$3d^2(^1D)4s$	$^2D_{3/2}$	-0.00952	4.2E-07	-0.00180		0.01991	2.3E-05	[5]	2		1.1E-04	2.1E-03	1
$3d^2(^1D)4s$	$^2D_{5/2}$	0.01842	1.5E-07	0.00227	1.9E-06	0.01419	1.3E-05	[5]	6		4.7E-04	-4.3E-03	
$3d^2(^1G)4p$	$^2F_{7/2}$	0.00777	3.9E-05						1				
$3d^2(^1G)4s$	$^2G_{7/2}$	-0.00383	7.7E-06						3		1.0E-04		
$3d^2(^1G)4s$	$^2G_{9/2}$	0.01170	3.6E-06						1				
$3d^2(1S)4s$	$^2S_{1/2}$	0.08208	8.9E-07						4		2.2E-04		
$3d^2(^3F)4d$	$^4D_{7/2}$	-0.00345	3.7E-05						1				
$3d^2(^3F)4d$	$^4H_{13/2}$	0.00105	1.7E-05						1				
$3d^2(^3F)4p$	$^2D_{5/2}$	0.00149	8.6E-05			-0.00352	1.7E-05	[5]	1				1
$3d^2(^3F)4p$	$^2F_{5/2}$	0.00764	5.9E-06							2	1.2E-05	1.1E-04	2
$3d^2(^3F)4p$	$^2G_{7/2}$	0.00562	9.8E-06						2		1.3E-04		2
$3d^2(^3F)4p$	$^2G_{9/2}$	0.00236	1.4E-05						1	2	7.6E-04		2
$3d^2(^3F)4p$	$^4D_{1/2}$	0.01686	2.0E-04						1				
$3d^2(^3F)4p$	$^4D_{7/2}$	-0.00266	1.9E-06						1				1
$3d^2(^3F)4p$	$^4G_{5/2}$	0.00930	9.2E-07	0.00102		0.00936	1.0E-05	[5]		2	4.0E-05	4.4E-03	
$3d^2(^3F)4p$	$^4G_{7/2}$	0.00503	1.9E-06			0.00494		[3]		1			1
$3d^2(^3F)4p$	$^4G_{11/2}$	0.00238	1.8E-05	0.00080		0.00183	3.3E-05	[5]	1				2
$3d^2(^3F)4s$	$^2F_{5/2}$	0.00919	1.1E-05	-0.00025	2.1E-04				1				2
$3d^2(^3F)4s$	$^2F_{7/2}$	-0.00054	1.8E-05						1				1

Table 4.1: Measured hfs constants for neutral scandium, continued.

Configuration	Term	A(this work) cm^{-1}	ΔA cm^{-1}	B(this work) cm^{-1}	ΔB cm^{-1}	A(Ref.) cm^{-1}	ΔA cm^{-1}	Ref.	n_{fit}	$n_{checkfit}$	$\|dev.A\|$ cm^{-1}	$\|dev.B\|$ cm^{-1}	n_{check}
$3d^2(^3F)4s$	$^4F_{3/2}$	-0.00529	4.2E-07	-0.00014	3.3E-06	-0.00529	1.0E-07	[3]	6		5.3E-05	1.7E-04	1
$3d^2(^3F)4s$	$^4F_{5/2}$	0.00512	2.4E-07	-0.00043	4.9E-06	0.00514	6.7E-08	[2]	7		2.9E-05	7.8E-04	2
$3d^2(^3F)4s$	$^4F_{7/2}$	0.00832	5.7E-08	-0.00055	1.2E-06	0.00834	6.7E-08	[2]	4		3.2E-05	9.9E-04	2
$3d^2(^3F)4s$	$^4F_{9/2}$	0.00953	5.3E-08	-0.00039	1.6E-06	0.00982	6.7E-06	[5]	4		1.4E-04	4.5E-04	
$3d^2(^3F)5s$	$^4F_{3/2}$	0.00166	1.3E-04						1				
$3d^2(^3F)5s$	$^4F_{9/2}$	0.00330	2.8E-05						1				
$3d^2(^3P)4p$	$^2D_{3/2}$	-0.00670	5.4E-06	0.00110	1.1E-04				1				
$3d^2(^3P)4p$	$^2D_{5/2}$	0.01567	4.3E-06	-0.00072	1.7E-04				1				
$3d^2(^3P)4p$	$^2S_{1/2}$	-0.01043	1.7E-05							1			1
$3d^2(^3P)4s$	$^2P_{1/2}$	0.01218	1.6E-06			0.01171	1.7E-04	[7]	3		8.0E-05		1
$3d^2(^3P)4s$	$^2P_{3/2}$	-0.00704	1.5E-06	0.00053	1.2E-05				4		1.4E-03	2.9E-03	3
$3d^2(^3P)4s$	$^4P_{5/2}$	0.01560	9.5E-06	-0.00039	5.4E-05	0.01451	7.3E-04	[7]		1			1
$3d^3$	$^2D_{5/2}$	0.00529	3.2E-06			0.00570	3.3E-05	[7]	1				
$3d^3$	$^2F_{7/2}$	0.00265	1.9E-05							1			
$3d^3$	$^2G_{7/2}$	0.00514	4.2E-06						1				1
$3d^3$	$^2G_{9/2}$	0.00175	3.2E-06						1				1
$3d^3$	$^2H_{11/2}$	0.00199	1.9E-06							1			
$3d^3$	$^4F_{7/2}$	0.00100	8.4E-06							2	1.7E-05		
$3d^3$	$^4F_{9/2}$	0.00144	2.3E-06						1				2

References 1-8 are respectively 1: Childs (1971), 2: Zeiske *et al.* (1976), 3: Ertmer and Hofer (1976), 4: Siefart (1977), 5: Singh *et al.* (1991), 6: Aboussaïd *et al.* (1996), 7: Krzykowski and Stefańska (2008), 8: Başar *et al.* (2004).

Table 4.2: Recorded scandium lines. SNR shows the maximum SNR within the hfs multiplet. Column Υ indicates whether hfs components were resolved. The next four columns show the hfs constants for the upper (A_u & B_u) and lower (A_l & B_l) level. The hfs constants are either from this work as shown in Table 4.1 or from literature values. The last column shows how the transition was used.

Nr	σ_J cm^{-1}	Upper Configuration	Term	Lower Configuration	Term	SNR	Υ	A_u cm^{-1}	B_u cm^{-1}	A_l cm^{-1}	B_l cm^{-1}	Upper Ref.	Lower Ref.	Comment
1	3778.7483	$3d4s(^1D)4p$	$^2F_{7/2}$	$3d^2(^3P)4s$	$^4P_{5/2}$	9.8E+01	3.7	0.01254	-0.00261	0.01560	-0.00039			fitted
2	3921.5174	$3d^3$	$^2G_{7/2}$	$3d^2(^3F)4p$	$^2G_{7/2}$	3.9E+01	1.4	0.00514		0.00562				fitted
3	4007.6079	$3d4s(^1D)4p$	$^2F_{5/2}$	$3d^2(^1D)4s$	$^2D_{3/2}$	7.1E+02	3.4	-0.00146		-0.00952	-0.00180			fitted
4	4019.9889	$3d4s(^1D)4p$	$^2F_{5/2}$	$3d^2(^1D)4s$	$^2D_{5/2}$	4.7E+01	9.0	-0.00146		0.01842	0.00227			fitted
5	4073.0782	$3d4s(^1D)4p$	$^2F_{7/2}$	$3d^2(^1D)4s$	$^2D_{5/2}$	1.0E+03	4.4	0.01254	-0.00261	0.01842	0.00227			fitted
6	4114.9033	$3d4s(^3D)4p$	$^4F_{3/2}$	$3d^2(^3F)4s$	$^4F_{5/2}$	2.0E+02	4.7	-0.00453	-0.00068	0.00512	-0.00043			fitted
7	4152.5987	$3d4s(^3D)4p$	$^4F_{3/2}$	$3d^2(^3F)4s$	$^4F_{3/2}$	2.4E+03	1.9	-0.00453	-0.00068	-0.00529	-0.00014			fitted
8	4198.8752	$3d4s(^3D)4p$	$^4F_{5/2}$	$3d^2(^3F)4s$	$^4F_{5/2}$	2.4E+03	2.9	0.00965	-0.00096	0.00512	-0.00043			fitted
9	4204.3971	$3d4s(^3D)4p$	$^4F_{7/2}$	$3d^2(^3F)4s$	$^4F_{9/2}$	2.2E+02	2.7	0.01197	-0.00164	0.00953	-0.00039			fitted
10	4236.5705	$3d4s(^3D)4p$	$^4F_{5/2}$	$3d^2(^3F)4s$	$^4F_{3/2}$	4.1E+02	7.4	0.00965	-0.00096	-0.00529	-0.00014			fitted
11	4271.4736	$3d4s(^3D)4p$	$^4F_{7/2}$	$3d^2(^3F)4s$	$^4F_{7/2}$	2.9E+03	2.9	0.01197	-0.00164	0.00832	-0.00055			fitted
12	4324.0539	$3d4s(^3D)4p$	$^4F_{7/2}$	$3d^2(^3F)4s$	$^4F_{5/2}$	4.7E+02	4.4	0.01197	-0.00164	0.00512	-0.00043			fitted
13	4349.2419	$3d4s(^3D)4p$	$^4F_{9/2}$	$3d^2(^3F)4s$	$^4F_{9/2}$	3.1E+03	3.4	0.01305	-0.00122	0.00953	-0.00039			fitted
14	4405.4678	$3d4s(^3D)5p$	$^2F_{7/2}$	$3d4s(^3D)5s$	$^2D_{5/2}$	4.1E+01	4.2	0.01482	-0.00335	0.01998	-0.00253			fitted
15	4412.4872	$3d4s(^1D)4p$	$^2D_{5/2}$	$3d^2(^3F)4s$	$^4F_{7/2}$	1.1E+03	6.3	-0.00704	0.00053	0.00832	-0.00055			fitted
16	4416.3183	$3d4s(^3D)4p$	$^4F_{9/2}$	$3d^2(^3F)4s$	$^4F_{7/2}$	2.9E+02	3.9	0.01305	-0.00122	0.00832	-0.00055			fitted
17	4433.1235	$3d4s(^3D)5p$	$^2F_{5/2}$	$3d4s(^3D)5s$	$^2D_{3/2}$	2.9E+01	3.8	0.00334	-0.00113	-0.00580	-0.00069			fitted
18	4464.0976	$3d4s(^3D)4p$	$^4D_{3/2}$	$3d^2(^3F)4s$	$^4F_{5/2}$	3.5E+03	3.3	0.01148	0.00449	0.00512	-0.00043			fitted
19	4489.7817	$3d4s(^3D)4p$	$^4D_{1/2}$	$3d^2(^3F)4s$	$^4F_{3/2}$	4.4E+03	5.1	-0.01711	0.00000	-0.00529	-0.00014			fitted
20	4501.8199	$3d4s(^3D)4p$	$^4D_{3/2}$	$3d^2(^3F)4s$	$^4F_{3/2}$	2.5E+02	6.6	0.01148	0.00449	-0.00529	-0.00014			fitted
21	4533.5030	$3d4s(^3D)4p$	$^4D_{7/2}$	$3d^2(^3F)4s$	$^4F_{9/2}$	7.6E+03	3.7	0.01526	0.00008	0.00953	-0.00039			fitted
22	4539.2283	$3d4s(^1D)4p$	$^2D_{3/2}$	$3d^2(^3F)4s$	$^4F_{5/2}$	1.3E+03	6.8	-0.01245	0.00030	0.00512	-0.00043			fitted
23	4576.9236	$3d4s(^1D)4p$	$^2D_{3/2}$	$3d^2(^3F)4s$	$^4F_{3/2}$	5.3E+02	4.2	-0.01245	0.00030	-0.00529	-0.00014			fitted

Table 4.2: Recorded scandium lines, continued.

Nr	σ_J cm^{-1}	Upper Configuration	Term	Lower Configuration	Term	SNR	Υ	A_u cm^{-1}	B_u cm^{-1}	A_l cm^{-1}	B_l cm^{-1}	Upper Ref.	Lower Ref.	Comment
24	4578.8232	$3d^2(^3P)4s$	$^2P_{3/2}$	$3d4s(^3D)4p$	$^4D_{5/2}$	7.3E+01	7.7	0.02202	-0.01639	0.01019	-0.00041			fitted
25	4583.3456	$3d4s(^3D)4p$	$^4D_{5/2}$	$3d^2(^3F)4s$	$^4F_{5/2}$	1.0E+03	2.9	0.01019	-0.00041	0.00512	-0.00043			fitted
26	4584.5289	$3d^2(^3P)4s$	$^2P_{1/2}$	$3d4s(^1D)4p$	$^2D_{3/2}$	1.7E+02	10.6	0.01218		-0.01245	0.00030			fitted
27	4600.5794	$3d4s(^3D)4p$	$^4D_{7/2}$	$3d^2(^3F)4s$	$^4F_{7/2}$	6.2E+02	4.0	0.01526	0.00008	0.00832	-0.00055			fitted
28	4621.0408	$3d4s(^3D)4p$	$^4D_{5/2}$	$3d^2(^3F)4s$	$^4F_{3/2}$	5.5E+01	7.1	0.01019	-0.00041	-0.00529	-0.00014			fitted
29	4622.9402	$3d^2(^3P)4s$	$^2P_{3/2}$	$3d4s(^1D)4p$	$^2D_{3/2}$	4.3E+01	3.9	0.02202	-0.01639	-0.01245	0.00030			fitted
30	4659.6327	$3d^2(^3P)4s$	$^2P_{1/2}$	$3d4s(^3D)4p$	$^4D_{3/2}$	1.2E+02	5.7	0.01218		0.01148	0.00449			fitted
31	4697.1012	$3d^2(^3P)4s$	$^2P_{3/2}$	$3d4s(^1D)4p$	$^2D_{5/2}$	3.3E+02	13.6	0.02202	-0.01639	-0.00704	0.00053			fitted
32	4963.2934	$3d^2(^3P)4s$	$^2P_{3/2}$	$3d4s(^3D)4p$	$^4F_{5/2}$	2.5E+01	6.8	0.02202	-0.01639	0.00965	-0.00096			fitted
33	5008.8545	$3d^2(^3P)4s$	$^2P_{1/2}$	$3d4s(^3D)4p$	$^4F_{3/2}$	2.2E+01	5.2	0.01218		-0.00453	-0.00068			fitted
34	5038.9463	$3d4s(^3D)5s$	$^2D_{5/2}$	$3d4s(^3D)4p$	$^2P_{3/2}$	1.4E+01	6.7	0.01998	-0.00253	0.01026	0.00058			fitted
35	5097.8937	$3d4s(^3D)5s$	$^2D_{3/2}$	$3d4s(^3D)4p$	$^2P_{1/2}$	1.1E+01	4.8	-0.00580	-0.00069	0.00663				fitted
36	5344.9699	$3d4s(^3D)4p$	$^2F_{5/2}$	$3d4s(^1G)4s$	$^2G_{7/2}$	1.4E+01	3.4	0.00588		-0.00383				fitted
37	5389.6079	$3d4s(^1D)5p$	$^2D_{3/2}$	$3d4s(^1D)5s$	$^2D_{3/2}$	1.2E+01	3.0	0.01108	-0.00122	0.01023	0.00225			fitted
38	5416.8848	$3d^2(^3P)4p$	$^2D_{5/2}$	$3d4s(^3D)5s$	$^2D_{5/2}$	1.9E+01	3.8	0.01567	-0.00072	0.01998	-0.00253			fitted
39	5482.3958	$3d^2(^3P)4p$	$^2D_{3/2}$	$3d4s(^3D)5s$	$^2D_{3/2}$	1.7E+01	1.8	-0.00670	0.00110	-0.00580	-0.00069			fitted
40	5487.8324	$3d4s(^3D)4p$	$^2F_{7/2}$	$3d4s(^1G)4s$	$^2G_{9/2}$	2.1E+01	3.9	0.00426	0.00190	0.01170				fitted
41	5559.4522	$3d4s(^3D)5p$	$^4F_{3/2}$	$3d4s(^3D)5s$	$^4D_{1/2}$	2.8E+01	6.8	-0.01302	-0.00130	-0.02489				fitted
42	5566.7279	$3d4s(^3D)5p$	$^4F_{5/2}$	$3d4s(^3D)5s$	$^4D_{3/2}$	3.5E+01	3.7	0.00387	-0.00017	0.01500	-0.00049			fitted
43	5568.6699	$3d4s(^3D)5p$	$^4F_{7/2}$	$3d4s(^3D)5s$	$^4D_{5/2}$	4.6E+01	3.8	0.01062	0.00000	0.01935	-0.00102			fitted
44	5578.6556	$3d4s(^3D)5p$	$^4F_{9/2}$	$3d4s(^3D)5s$	$^4D_{7/2}$	6.4E+01	3.6	0.01439	-0.00296	0.02012	0.00016			fitted
45	5583.9495	$3d4s(^3D)5p$	$^2F_{7/2}$	$3d4s(^3D)5s$	$^4D_{7/2}$	1.6E+01	3.5	0.01482	-0.00335	0.02012	0.00016			fitted
46	5593.5216	$3d4s(^3D)5p$	$^4D_{3/2}$	$3d4s(^3D)5s$	$^4D_{5/2}$	1.1E+01	5.4	0.01170	-0.00082	0.01935	-0.00102			fitted
47	5621.8290	$3d4s(^3D)5p$	$^4D_{1/2}$	$3d4s(^3D)5s$	$^4D_{3/2}$	1.0E+01	12.1	-0.02452		0.01500	-0.00049			fitted
48	5643.7513	$3d4s(^3D)5p$	$^4D_{7/2}$	$3d4s(^3D)5s$	$^4D_{7/2}$	5.3E+01	3.3	0.01686	0.00102	0.02012	0.00016			fitted
49	5650.6768	$3d4s(^3D)5p$	$^4D_{3/2}$	$3d4s(^3D)5s$	$^4D_{3/2}$	2.0E+01	3.6	0.01170	-0.00082	0.01500	-0.00049			fitted

Table 4.2: Recorded scandium lines, continued.

Nr	σ_J cm^{-1}	Upper Configuration	Term	Lower Configuration	Term	SNR	Υ	A_u cm^{-1}	B_u cm^{-1}	A_l cm^{-1}	B_l cm^{-1}	Upper Ref.	Lower Ref.	Comment
50	5654.4084	$3d4s(^3D)5p$	$^4D_{1/2}$	$3d4s(^3D)5s$	$^4D_{1/2}$	1.2E+01	13.0	-0.02452	0.00000	-0.02489				fitted
51	5683.2555	$3d4s(^3D)5p$	$^4D_{3/2}$	$3d4s(^3D)5s$	$^4D_{1/2}$	8.9E+00	10.4	0.01170	-0.00082	-0.02489				fitted
52	5807.9873	$3d4s(^3D)4d$	$^2F_{7/2}$	$3d^2(^3F)4p$	$^2G_{9/2}$	1.3E+01	3.1	0.01089		0.00236				fitted
53	5815.6981	$3d4s(^3D)4d$	$^2F_{5/2}$	$3d^2(^3F)4p$	$^2G_{7/2}$	1.3E+01	3.2	-0.00347	0.00039	0.00562				fitted
54	6043.9091	$3d4s(^1D)4p$	$^2F_{7/2}$	$3d^2(^3F)4s$	$^2F_{7/2}$	2.9E+01	4.2	0.01254	-0.00261	-0.01302	-0.00130			fitted
55	6148.2921	$3d4s(^3D)5p$	$^4P_{5/2}$	$3d4s(^3D)5s$	$^4D_{7/2}$	5.9E+01	3.5	0.02215	-0.00152	0.02012	0.00016			fitted
56	6164.6705	$3d4s(^3D)5p$	$^4P_{3/2}$	$3d4s(^3D)5s$	$^4D_{5/2}$	2.3E+01	5.8	0.03090	0.00056	0.01935	-0.00102			fitted
57	6172.4623	$3d4s(^3D)5p$	$^4P_{1/2}$	$3d4s(^3D)5s$	$^4D_{3/2}$	1.7E+01	11.5	0.05694		0.01500	-0.00049			fitted
58	6205.0420	$3d4s(^3D)5p$	$^4P_{1/2}$	$3d4s(^3D)5s$	$^4D_{1/2}$	9.2E+00	19.4	0.05694		-0.02489				fitted
59	7034.7833	$3d4s(^1D)5p$	$^2P_{3/2}$	$3d4s(^3D)5s$	$^2D_{5/2}$	1.5E+01	4.1	0.02593	-0.00779	0.01998	-0.00253			fitted
60	7148.9668	$3d4s(^1D)5s$	$^2D_{5/2}$	$3d4s(^3D)4p$	$^2P_{3/2}$	1.3E+01	2.4	-0.00051	0.00000	0.01026	0.00058			fitted
61	7631.5599	$3d4s(^1D)4p$	$^2P_{1/2}$	$3d^2(^1D)4s$	$^2D_{3/2}$	6.7E+01	5.7	0.01432		-0.00952	-0.00180			fitted
62	7644.1442	$3d4s(^1D)4p$	$^2P_{3/2}$	$3d^2(^1D)4s$	$^2D_{5/2}$	9.8E+01	6.1	-0.00094		0.01842	0.00227			fitted
63	8081.2385	$3d^2(^1S)4s$	$^2S_{1/2}$	$4s^2(^1S)4p$	$^2P_{3/2}$	2.7E+02	12.4	0.08208		0.02036	-0.00098			fitted
64	8114.5227	$3d^2(^1G)4p$	$^2F_{7/2}$	$3d4s(^3D)5s$	$^2D_{5/2}$	7.1E+00	3.1	0.00777		0.01998	-0.00253			fitted
65	8225.9703	$3d^2(^1S)4s$	$^2S_{1/2}$	$4s^2(^1S)4p$	$^2P_{1/2}$	1.9E+02	15.3	0.08208		0.00294				fitted
66	8421.2890	$3d^2(^1S)4s$	$^2S_{1/2}$	$3d4s(^3D)4p$	$^4P_{3/2}$	1.9E+01	12.4	0.08208		0.02433	0.00226			fitted
67	8432.9129	$3d^2(^1S)4s$	$^2S_{1/2}$	$3d4s(^3D)4p$	$^4P_{1/2}$	9.1E+00	21.2	0.08208		0.04024				fitted
68	8711.9370	$3d4s(^3D)4p$	$^2F_{7/2}$	$3d^2(^1D)4s$	$^2D_{5/2}$	1.2E+01	3.0	0.00426	0.00190	0.01842	0.00227			fitted
69	9284.5610	$3d^2(^3F)5s$	$^4F_{3/2}$	$3d^2(^3F)4p$	$^4D_{1/2}$	1.2E+01	2.2	0.00166		0.01686				fitted
70	9333.6800	$3d^2(^3F)5s$	$^4F_{9/2}$	$3d^2(^3F)4p$	$^4D_{7/2}$	1.6E+01	1.5	0.00330		-0.00266				fitted
71	9497.1568	$3d4s(^3D)4d$	$^2P_{1/2}$	$3d4s(^3D)4p$	$^2P_{1/2}$	8.0E+00	5.2	-0.02455		0.00663				fitted
72	9940.1325	$3d4s(^3D)4p$	$^2D_{3/2}$	$3d^2(^3F)4s$	$^2F_{5/2}$	2.8E+01	1.4	0.00857	-0.00057	0.00919	-0.00025			fitted
73	10020.9753	$3d4s(^3D)5s$	$^2D_{5/2}$	$3d4s(^3D)4p$	$^2F_{7/2}$	2.7E+01	2.9	0.01998	-0.00253	0.00426	0.00190			fitted
74	10086.4126	$3d4s(^3D)5s$	$^2D_{3/2}$	$3d4s(^3D)4p$	$^2F_{5/2}$	2.5E+01	2.4	-0.00580	-0.00069	0.00588				fitted
75	12816.3161	$3d^2(^3F)4p$	$^2G_{7/2}$	$3d4s(^1G)4s$	$^2G_{7/2}$	1.4E+01	1.5	0.00562		-0.00383				fitted

Table 4.2: Recorded scandium lines, continued.

Nr	σ_J cm^{-1}	Upper Configuration	Term	Lower Configuration	Term	SNR	Υ	A_u cm^{-1}	B_u cm^{-1}	A_l cm^{-1}	B_l cm^{-1}	Upper Ref.	Lower Ref.	Comment
76	14005.4864	$3d4s(^3D)4d$	$^2F_{5/2}$	$3d4s(^3D)4p$	$^2D_{3/2}$	7.6E+00	1.6	-0.00347	0.00039	0.00857	-0.00057			fitted
77	15672.5600	$3d4s(^3D)4p$	$^4F_{3/2}$	$3d4s^2(^1D)$	$^2D_{3/2}$	1.1E+02	1.7	-0.00453	-0.00068	0.00901	-0.00044			fitted
78	15854.3877	$3d4s(^1D)4p$	$^2D_{5/2}$	$3d4s^2(^1D)$	$^2D_{5/2}$	9.0E+02	2.4	-0.00704	0.00053	0.00374	0.00127			fitted
79	15908.6412	$3d4s(^3D)5s$	$^4D_{5/2}$	$3d4s(^3D)4p$	$^4P_{5/2}$	6.7E+00	1.4	0.01935	-0.00102	0.01975	-0.00001			fitted
80	15928.5437	$3d4s(^1D)4p$	$^2D_{3/2}$	$3d4s^2(^1D)$	$^2D_{5/2}$	5.5E+01	1.8	-0.01245	0.00030	0.00374	0.00127			fitted
81	15995.7870	$3d4s(^3D)5s$	$^4D_{7/2}$	$3d4s(^3D)4p$	$^4P_{5/2}$	1.7E+01	1.4	0.02012	0.00016	0.01975	-0.00001			fitted
82	16021.7788	$3d4s(^3D)4p$	$^4D_{3/2}$	$3d4s^2(^1D)$	$^2D_{3/2}$	5.9E+02	1.1	0.01148	0.00449	0.00901	-0.00044			fitted
83	16022.7364	$3d4s(^1D)4p$	$^2D_{5/2}$	$3d4s^2(^1D)$	$^2D_{3/2}$	1.3E+02	2.0	-0.00704	0.00053	0.00901	-0.00044			fitted
84	16096.8844	$3d4s(^1D)4p$	$^2D_{3/2}$	$3d4s^2(^1D)$	$^2D_{3/2}$	4.6E+02	2.5	-0.01245	0.00030	0.00901	-0.00044			fitted
85	16694.3166	$3d^2(^3F)4p$	$^2D_{5/2}$	$3d^2(^1D)4s$	$^2D_{5/2}$	7.0E+00	2.0	0.00149		0.01842	0.00227			fitted
86	16889.9195	$3d4s(^3D)5s$	$^2D_{5/2}$	$4s^2(^1S)4p$	$^2P_{3/2}$	1.2E+01	1.7	0.01998	-0.00253	0.02036	-0.00098			fitted
87	17626.1766	$3d^2(^3F)4p$	$^4G_{11/2}$	$3d^2(^3F)4s$	$^4F_{9/2}$	1.1E+02	1.2	0.00238	0.00080	0.00953	-0.00039			fitted
88	17964.8873	$3d^3$	$^4F_{7/2}$	$3d4s(^3D)4p$	$^4F_{7/2}$	8.5E+00	1.3	0.00100		0.01197	-0.00164			fitted
89	3823.6868	$3d^3$	$^2G_{7/2}$	$3d^2(^3F)4p$	$^2F_{5/2}$	2.3E+01	2.0	0.00514		-0.00266				checkfitted
90	3903.2857	$3d^3$	$^2G_{9/2}$	$3d^2(^3F)4p$	$^2G_{9/2}$	4.5E+01	0.7	0.00175		0.00236				checkfitted
91	4602.8869	$3d^3$	$^4F_{9/2}$	$3d^2(^3F)4p$	$^4G_{11/2}$	1.1E+01	0.9	0.00144		0.00238	0.00080			checkfitted
92	5123.1943	$3d4s(^1D)5p$	$^2F_{7/2}$	$3d4s(^1D)5s$	$^2D_{5/2}$	2.6E+01	1.2	0.00224	0.00000	-0.00051				checkfitted
93	6074.1428	$3d^3$	$^2H_{11/2}$	$3d^2(^3F)4p$	$^2G_{9/2}$	3.4E+02	0.5	0.00199		0.00236				checkfitted
94	6106.6855	$3d4s(^1D)4p$	$^2F_{5/2}$	$3d^2(^3F)4s$	$^2F_{5/2}$	1.2E+01	3.2	-0.00146		0.00919	-0.00025			checkfitted
95	6648.2693	$3d4s(^1D)5p$	$^2F_{7/2}$	$3d^3$	$^2D_{5/2}$	1.0E+01	1.1	0.00224		0.00529				checkfitted
96	7264.7610	$3d4s(^3D)4d$	$^2G_{7/2}$	$3d^2(^3F)4p$	$^2F_{5/2}$	1.6E+01	1.3	0.00392		-0.00266				checkfitted
97	7362.5950	$3d4s(^3D)4d$	$^2G_{7/2}$	$3d^2(^3F)4p$	$^2G_{7/2}$	1.1E+01	0.9	0.00392		0.00562				checkfitted
98	7410.8637	$3d4s(^3D)4d$	$^2G_{9/2}$	$3d^2(^3F)4p$	$^2G_{9/2}$	2.1E+01	0.7	0.00377		0.00236				checkfitted
99	7674.5720	$3d^3$	$^2F_{7/2}$	$3d^2(^3F)4p$	$^2G_{9/2}$	4.0E+01	0.4	0.00265		0.00236				checkfitted
100	8995.8902	$3d4s(^1D)4d$	$^2F_{5/2}$	$3d^2(^3F)4p$	$^2F_{5/2}$	1.5E+01	0.7			-0.00266				checkfitted
101	9047.6747	$3d4s(^1D)4d$	$^2F_{7/2}$	$3d^2(^3F)4p$	$^2G_{9/2}$	2.4E+01	0.5	0.00114		0.00236				checkfitted

Table 4.2: Recorded scandium lines, continued.

Nr	σ_J cm^{-1}	Upper Configuration	Term	Lower Configuration	Term	SNR	Υ	A_u cm^{-1}	B_u cm^{-1}	A_l cm^{-1}	B_l cm^{-1}	Upper Ref.	Lower Ref.	Comment
102	9093.7552	$3d4s(^1D)4d$	$^2F_{5/2}$	$3d^2(^3F)4p$	$^2G_{7/2}$	1.0E+01	1.5			0.00562				checkfitted
103	9972.2829	$3d4s(^3D)4p$	$^2D_{5/2}$	$3d^2(^3F)4s$	$^2F_{7/2}$	6.4E+01	0.4	0.00110		-0.01302	-0.00130			checkfitted
104	11316.3573	$3d^3$	$^2D_{5/2}$	$3d4s(^3D)4p$	$^2D_{5/2}$	1.1E+01	0.9	0.00529		0.00110	0.00000			checkfitted
105	11329.8001	$3d^3$	$^2G_{9/2}$	$3d4s(^3D)4p$	$^2F_{7/2}$	3.7E+01	0.6	0.00175		0.00426	0.00190			checkfitted
106	12130.9454	$3d4s(^1D)5s$	$^2D_{5/2}$	$3d4s(^3D)4p$	$^2F_{7/2}$	8.2E+00	1.0	-0.00051		0.00426	0.00190			checkfitted
107	13198.7343	$3d4s(^1D)5s$	$^2D_{5/2}$	$3d4s(^1D)4p$	$^2P_{3/2}$	2.5E+01	0.3	-0.00051		-0.00094				checkfitted
108	13291.1640	$3d^2(^3F)4d$	$^4D_{7/2}$	$3d^2(^3F)4p$	$^4D_{7/2}$	8.2E+00	0.3	-0.00345		-0.00266				checkfitted
109	14837.3795	$3d4s(^3D)4d$	$^2G_{9/2}$	$3d4s(^3D)4p$	$^2F_{7/2}$	7.6E+01	0.4	0.00377		0.00426	0.00190			checkfitted
110	15964.3454	$3d4s(^3D)5s$	$^4D_{5/2}$	$3d4s(^3D)4p$	$^4P_{3/2}$	1.4E+01	1.8	0.01935	-0.00102	0.02433	0.00226			checkfitted
111	16750.8530	$3d^2(^3F)4d$	$^4H_{13/2}$	$3d^2(^3F)4p$	$^4G_{11/2}$	1.2E+01	0.4	0.00105	0.00000	0.00238	0.00080			checkfitted
112	17465.2117	$3d^2(^3F)4p$	$^4G_{5/2}$	$3d^2(^3F)4s$	$^4F_{5/2}$	2.7E+01	0.8	0.00930	0.00102	0.00512	-0.00043			checkfitted
113	17485.9482	$3d^2(^3F)4p$	$^4G_{7/2}$	$3d^2(^3F)4s$	$^4F_{7/2}$	3.5E+01	0.6	0.00503		0.00832	-0.00055			checkfitted
114	17502.9086	$3d^2(^3F)4p$	$^4G_{5/2}$	$3d^2(^3F)4s$	$^4F_{3/2}$	7.7E+01	1.9	0.00930	0.00102	-0.00529	-0.00014			checkfitted
115	3821.2764	$3d^3$	$^4P_{5/2}$	$3d^2(^3F)4p$	$^4D_{7/2}$	7.6E+00	1.3	-0.00083		-0.00266		[2]		checked
116	4530.7653	$3d4s(^3D)4p$	$^4D_{5/2}$	$3d^2(^3F)4s$	$^4F_{7/2}$	9.9E+03	2.1	0.01019	-0.00041	0.00832	-0.00055			checked
117	4627.0751	$3d4s(^1D)5s$	$^2D_{3/2}$	$3d^2(^3F)4p$	$^2F_{5/2}$	1.3E+01	2.6	0.01023	0.00225	-0.00266				checked
118	4656.7514	$3d^3$	$^4F_{7/2}$	$3d^2(^3F)4p$	$^4G_{9/2}$	9.3E+00	1.2	0.00100		0.00287			[3]	checked
119	4831.9880	$3d^2(^3P)4p$	$^2D_{5/2}$	$3d^3$	$^2D_{5/2}$	7.6E+00	4.8	0.01567	-0.00072	0.00529				checked
120	4876.8170	$3d^2(^3P)4p$	$^2D_{3/2}$	$3d^3$	$^2D_{3/2}$	8.1E+00	3.1	-0.00670	0.00110	0.00143			[2]	checked
121	5047.2509	$3d^2(^3P)4s$	$^2P_{3/2}$	$3d4s(^3D)4p$	$^4F_{3/2}$	7.4E+00	9.4	0.02202	-0.01639	-0.00453	-0.00068			checked
122	5623.9842	$3d^3$	$^2D_{5/2}$	$3d4s(^3D)4p$	$^2P_{3/2}$	9.8E+00	2.3	0.00529		0.01026	0.00058			checked
123	5671.0898	$3d4s(^3D)5p$	$^2F_{7/2}$	$3d4s(^3D)5s$	$^4D_{5/2}$	6.8E+00	3.1	0.01482	-0.00335	0.01935	-0.00102			checked
124	5703.4693	$3d^3$	$^2D_{3/2}$	$3d4s(^3D)4p$	$^2P_{1/2}$	6.9E+00	1.7	0.00143		0.00663		[2]		checked
125	5705.3261	$3d4s(^3D)5p$	$^4D_{5/2}$	$3d4s(^3D)5s$	$^4D_{3/2}$	1.6E+01	3.4	0.01395		0.01500	-0.00049			checked
126	5730.8912	$3d4s(^3D)5p$	$^4D_{7/2}$	$3d4s(^3D)5s$	$^4D_{5/2}$	1.2E+01	3.2	0.01686	0.00102	0.01935	-0.00102			checked
127	7207.7266	$3d4s(^1D)5s$	$^2D_{3/2}$	$3d4s(^3D)4p$	$^2P_{1/2}$	7.7E+00	3.5	0.01023	0.00225	0.00663				checked

Table 4.2: Recorded scandium lines, continued.

Nr	σ_J cm^{-1}	Upper Configuration	Term	Lower Configuration	Term	SNR	Υ	A_u cm^{-1}	B_u cm^{-1}	A_l cm^{-1}	B_l cm^{-1}	Upper Ref.	Lower Ref.	Comment
128	7349.8149	$3d4s(^1D)4p$	$^2P_{3/2}$	$3d^2(^3P)4s$	$^4P_{5/2}$	7.5E+00	5.4	-0.00094		0.01560	-0.00039			checked
129	8559.5052	$3d4s(^3D)4p$	$^2F_{5/2}$	$3d^2(^1D)4s$	$^2D_{3/2}$	9.2E+00	3.4	0.00588		-0.00952	-0.00180			checked
130	10658.5838	$3d4s(^3D)4p$	$^2F_{5/2}$	$3d^2(^3F)4s$	$^2F_{5/2}$	5.5E+01	1.1	0.00588		0.00919	-0.00025			checked
131	12196.2409	$3d4s(^1D)5s$	$^2D_{3/2}$	$3d4s(^3D)4p$	$^2F_{5/2}$	8.6E+00	1.1	0.01023	0.00225	0.00588				checked
132	12841.4243	$3d4s(^1D)5s$	$^2D_{5/2}$	$3d4s(^3D)4p$	$^2D_{5/2}$	2.2E+01	0.3	-0.00051		0.00110				checked
133	12933.4835	$3d^2(^3F)4p$	$^2D_{3/2}$	$3d^2(^3P)4s$	$^2P_{1/2}$	9.1E+00	1.6	0.00498	0.00334	0.01218		[1]		checked
134	12987.2310	$3d^2(^3F)4p$	$^2D_{5/2}$	$3d^2(^3P)4s$	$^2P_{3/2}$	1.1E+01	1.2	0.00149		0.02202	-0.01639			checked
135	13124.1933	$3d4s(^1D)5s$	$^2D_{3/2}$	$3d4s(^1D)4p$	$^2P_{1/2}$	6.9E+00	2.1	0.01023	0.00225	0.01432				checked
136	13234.5030	$3d4s(^3D)4d$	$^2F_{7/2}$	$3d4s(^3D)4p$	$^2F_{7/2}$	6.5E+00	1.2	0.01089		0.00426	0.00190			checked
137	13287.0415	$3d4s(^3D)4d$	$^2F_{5/2}$	$3d4s(^3D)4p$	$^2F_{5/2}$	6.5E+00	1.4	-0.00347	0.00039	0.00588				checked
138	13944.9896	$3d4s(^3D)4d$	$^2F_{7/2}$	$3d4s(^3D)4p$	$^2D_{5/2}$	7.1E+00	1.7	0.01089		0.00110				checked
139	14626.5155	$3d^2(^3P)4p$	$^2S_{1/2}$	$3d^2(^3P)4s$	$^2P_{3/2}$	6.5E+01	1.4	-0.01000		0.02202	-0.01639			checked
140	14638.3104	$3d4s(^3D)5s$	$^2D_{3/2}$	$3d4s(^1D)4p$	$^2F_{5/2}$	4.4E+01	0.7	-0.00580	-0.00069	-0.00146				checked
141	14659.8330	$3d4s(^3D)5s$	$^2D_{5/2}$	$3d4s(^1D)4p$	$^2F_{7/2}$	4.1E+01	1.5	0.01998	-0.00253	0.01254	-0.00261			checked
142	14664.9270	$3d^2(^3P)4p$	$^2S_{1/2}$	$3d^2(^3P)4s$	$^2P_{1/2}$	3.6E+01	2.7	-0.01000		0.01218				checked
143	14833.9332	$3d4s(^3D)4d$	$^2G_{7/2}$	$3d4s(^3D)4p$	$^2F_{5/2}$	6.1E+01	0.5	0.00392		0.00588				checked
144	15320.1745	$3d4s(^3D)4d$	$^2D_{5/2}$	$3d4s(^3D)4p$	$^2D_{5/2}$	1.8E+01	1.0	0.00804		0.00110		[2]		checked
145	15504.2177	$3d4s(^3D)4p$	$^4F_{3/2}$	$3d4s^2(^1D)$	$^2D_{5/2}$	1.4E+01	1.2	-0.00453	-0.00068	0.00374	0.00127			checked
146	15588.1967	$3d4s(^3D)4p$	$^4F_{5/2}$	$3d4s^2(^1D)$	$^2D_{5/2}$	1.5E+02	1.0	0.00965	-0.00096	0.00374	0.00127			checked
147	15756.5297	$3d4s(^3D)4p$	$^4F_{5/2}$	$3d4s^2(^1D)$	$^2D_{3/2}$	2.9E+01	1.0	0.00965	-0.00096	0.00901	-0.00044			checked
148	15972.6659	$3d4s(^3D)4p$	$^4D_{5/2}$	$3d4s^2(^1D)$	$^2D_{5/2}$	3.0E+02	1.0	0.01019	-0.00041	0.00374	0.00127			checked
149	16748.1483	$3d4s(^1D)5s$	$^2D_{3/2}$	$3d4s(^1D)4p$	$^2F_{5/2}$	7.5E+00	1.2	0.01023	0.00225	-0.00146				checked
150	16769.7993	$3d4s(^1D)5s$	$^2D_{5/2}$	$3d4s(^1D)4p$	$^2F_{7/2}$	6.8E+00	1.8	-0.00051		0.01254	-0.00261			checked
151	16960.0433	$3d4s(^3D)5s$	$^2D_{3/2}$	$4s^2(^1S)4p$	$^2P_{1/2}$	7.7E+00	1.5	-0.00580	-0.00069	0.00294				checked
152	17512.5333	$3d^2(^3F)4p$	$^4G_{9/2}$	$3d^2(^3F)4s$	$^4F_{9/2}$	1.4E+01	1.1	0.00287		0.00953	-0.00039	[3]		checked
153	17538.5318	$3d^2(^3F)4p$	$^4G_{7/2}$	$3d^2(^3F)4s$	$^4F_{5/2}$	1.9E+02	0.4	0.00503		0.00512	-0.00043			checked

Table 4.2: Recorded scandium lines, continued.

Nr	σ_J cm^{-1}	Upper Configuration	Term	Lower Configuration	Term	SNR	Υ	A_u cm^{-1}	B_u cm^{-1}	A_l cm^{-1}	B_l cm^{-1}	Upper Ref.	Lower Ref.	Comment
154	17695.5565	$3d^3$	$^4F_{9/2}$	$3d4s(^3D)4p$	$^4D_{7/2}$	7.0E+00	1.6	0.00144		0.01526	0.00008			checked
155	17705.5942	$3d^3$	$^4F_{7/2}$	$3d4s(^3D)4p$	$^4D_{5/2}$	6.6E+00	1.0	0.00100		0.01019	-0.00041			checked
156	17838.9494	$3d4s(^3D)4d$	$^2F_{5/2}$	$3d4s(^1D)4p$	$^2F_{5/2}$	6.2E+00	0.4	-0.00347	0.00039	-0.00146				checked
157	17873.3593	$3d4s(^3D)4d$	$^2F_{7/2}$	$3d4s(^1D)4p$	$^2F_{7/2}$	6.7E+00	0.7	0.01089		0.01254	-0.00261			checked
158	17879.8161	$3d^3$	$^4F_{9/2}$	$3d4s(^3D)4p$	$^4F_{9/2}$	1.1E+01	1.6	0.00144		0.01305	-0.00122			checked
159	3013.6688	$3d^2(^3P)4p$	$^4D_{5/2}$	$3d^3$	$^4F_{7/2}$	9.1E+02	0.9			0.00100				not used
160	3776.1	$3d^3$	$^2G_{9/2}$	$3d^2(^3F)4p$	$^2F_{7/2}$	2.8E+01	2.6	0.00175					[1]	not used
161	4676.2860	$3d4s(^3D)5p$	$^2D_{3/2}$	$3d4s(^3D)5s$	$^2D_{3/2}$	1.4E+01	2.3			-0.00580	-0.00069			not used
162	4702.5128	$3d^3$	$^4F_{5/2}$	$3d^2(^3F)4p$	$^4G_{7/2}$	7.3E+00	2.5			0.00503				not used
163	4740.7082	$3d^3$	$^4F_{3/2}$	$3d^2(^3F)4p$	$^4G_{5/2}$	8.4E+00	4.8			0.00930	0.00102			not used
164	4828.6858	$3d4s(^3D)5p$	$^2P_{1/2}$	$3d4s(^3D)5s$	$^2D_{3/2}$	7.7E+00	3.8			-0.00580	-0.00069			not used
165	5396.9964	$3d4s(^1D)5p$	$^2D_{5/2}$	$3d4s(^1D)5s$	$^2D_{5/2}$	2.7E+01	0.3			-0.00051				not used
166	5977.9948	$3d^2(^3F)4d$	$^4D_{1/2}$	$3d4s(^3D)5p$	$^4F_{3/2}$	1.7E+01	6.5			-0.01302	-0.00130			not used
167	5983.9199	$3d^3$	$^2D_{5/2}$	$3d^2(^1D)4p$	$^2D_{3/2}$	6.6E+01	2.3	0.00529						not used
168	6108.1010	$3d^3$	$^2H_{9/2}$	$3d^2(^3F)4p$	$^2G_{7/2}$	1.9E+02	1.9			0.00562				not used
169	6333.7312	$3d^2(^3P)4p$	$^2P_{3/2}$	$3d4s(^1D)5s$	$^2D_{5/2}$	1.5E+01	0.4			-0.00051				not used
170	6921.9794	$3d4s(^1D)5p$	$^2D_{5/2}$	$3d^3$	$^2D_{5/2}$	5.0E+01	1.5			0.00529				not used
171	7148.3280	$3d4s(^1D)5p$	$^2P_{1/2}$	$3d4s(^3D)5s$	$^2D_{3/2}$	1.3E+01	2.6			-0.00580	-0.00069			not used
172	7746.8062	$3d^3$	$^2F_{5/2}$	$3d^2(^3F)4p$	$^2G_{7/2}$	9.5E+00	1.7			0.00562				not used
173	8159.1516	$3d^2(^1G)4p$	$^2F_{5/2}$	$3d4s(^3D)5s$	$^2D_{3/2}$	6.2E+00	1.2			-0.00580	-0.00069			not used
174	8920.4674	$3d4s(^1D)4d$	$^2F_{7/2}$	$3d^2(^3F)4p$	$^2F_{7/2}$	1.8E+01	0.9	0.00114					[1]	not used
175	9301.6906	$3d^2(^3F)5s$	$^4F_{5/2}$	$3d^2(^3F)4p$	$^4D_{3/2}$	1.7E+01	0.2							not used
176	9318.7695	$3d^2(^3F)5s$	$^4F_{7/2}$	$3d^2(^3F)4p$	$^4D_{5/2}$	1.3E+01	0.1							not used
177	9328.5016	$3d4s(^3D)4d$	$^4F_{7/2}$	$3d^2(^3F)4p$	$^4F_{7/2}$	4.0E+00	0.1							not used
178	9339.1801	$3d4s(^3D)4d$	$^4F_{5/2}$	$3d^2(^3F)4p$	$^4F_{5/2}$	6.9E+00	0.1							not used
179	9357.1592	$3d4s(^3D)4d$	$^2P_{3/2}$	$3d4s(^3D)4p$	$^2P_{3/2}$	1.2E+01	2.1			0.01026	0.00058			not used

Table 4.2: Recorded scandium lines, continued.

Nr	σ_J cm^{-1}	Upper Configuration	Term	Lower Configuration	Term	SNR	Υ	A_u cm^{-1}	B_u cm^{-1}	A_l cm^{-1}	B_l cm^{-1}	Upper Ref.	Lower Ref.	Comment
180	11458.7695	$3d4s(^3D)4d$	$^4F_{5/2}$	$3d^2(^3F)4p$	$^4G_{7/2}$	6.6E+00	1.1			0.00503				not used
181	12825.7628	$3d^2(^3F)5s$	$^4F_{7/2}$	$3d^2(^3F)4p$	$^4G_{9/2}$	7.3E+00	0.6			0.00287			[3]	not used
182	12864.8053	$3d^2(^3F)5s$	$^4F_{5/2}$	$3d^2(^3F)4p$	$^4G_{7/2}$	7.6E+00	1.0			0.00503				not used
183	13310.0759	$3d^2(^3F)4d$	$^4D_{3/2}$	$3d^2(^3F)4p$	$^4D_{1/2}$	2.2E+01	1.5			0.01686				not used
184	13322.7720		$^2F_{5/2}$	$3d^2(^3F)4p$	$^2G_{7/2}$	6.4E+01	1.1			0.00562				not used
185	13774.9241	$3d(^2D)4p^2(^3P)$	$^4F_{9/2}$	$3d^2(^3F)4p$	$^4F_{9/2}$	6.6E+00	0.1							not used
186	14528.7601	$3d^2(^3F)4d$	$^4G_{9/2}$	$3d^2(^3F)4p$	$^4F_{7/2}$	6.5E+00	0.1							not used
187	14888.8077	$3d4s(^3D)4d$	$^4D_{5/2}$	$3d4s(^3D)4p$	$^2D_{3/2}$	8.8E+00	1.0			0.00857	-0.00057			not used
188	16796.0652	$3d^2(^3F)4d$	$^4H_{11/2}$	$3d^2(^3F)4p$	$^4G_{9/2}$	1.0E+01	0.5			0.00287	0.00000		[3]	not used
189	16828.9930	$3d^2(^3F)4d$	$^4H_{9/2}$	$3d^2(^3F)4p$	$^4G_{7/2}$	7.3E+00	0.7			0.00503				not used
190	3975.4	$3d4s(^1D)4p$	$^2P_{1/2}$	$3d^2(^3P)4s$	$^2P_{1/2}$	1.2E+01	10.0	0.01432		0.01218				mixing
191	3975.4	$3d4s(^1D)4p$	$^2P_{3/2}$	$3d^2(^3P)4s$	$^2P_{1/2}$	1.2E+01	3.9	-0.00094		0.01218				mixing
192	4146.3	$3d4s(^3D)4p$	$^2D_{3/2}$	$3d^2(^3P)4s$	$^2P_{3/2}$	3.5E+02	8.3	0.00857	-0.00057	0.02202	-0.01639			mixing
193	4146.3	$3d4s(^3D)4p$	$^4F_{5/2}$	$3d^2(^3F)4s$	$^4F_{7/2}$	3.5E+02	2.2	0.00965	-0.00096	0.00832	-0.00055			mixing
194	4184.8	$3d4s(^3D)4p$	$^2D_{3/2}$	$3d^2(^3P)4s$	$^2P_{1/2}$	1.2E+01	5.1	0.00857	-0.00057	0.01218				mixing
195	4184.8	$3d4s(^1D)4d$	$^2F_{5/2}$	$3d^2(^3P)4p$	$^4P_{5/2}$	1.2E+01	0.1							mixing
196	4294.4	$3d4s(^3D)4p$	$^2D_{5/2}$	$3d^2(^3P)4s$	$^2P_{3/2}$	1.9E+01	7.5	0.00110		0.02202	-0.01639			mixing
197	4294.4	$3d^2(^3F)5p$	$^4F_{5/2}$	$3d^2(^3F)5s$	$^4F_{5/2}$	1.9E+01	0.1							mixing
198	4653.2	$3d4s(^3D)4p$	$^4D_{7/2}$	$3d^2(^3F)4s$	$^4F_{5/2}$	2.2E+01	5.7	0.01526	0.00008	0.00512	-0.00043			mixing
199	4653.2	$3d4s(^3D)4d$	$^4P_{1/2}$	$3d^2(^3P)4p$	$^4D_{3/2}$	2.2E+01	0.3	0.00000		0.00000				mixing
200	5157.91	$3d4s(^1D)5p$	$^2F_{5/2}$	$3d4s(^1D)5s$	$^2D_{3/2}$	3.0E+01	3.0			0.01023	0.00225			mixing
201	5157.91	$3d^3$	$^2D_{5/2}$	$3d^2(^3F)4p$	$^4F_{3/2}$	3.0E+01	2.6	0.00529						mixing
202	5526.94	$3d4s(^3D)5p$	$^4F_{3/2}$	$3d4s(^3D)5s$	$^4D_{3/2}$	8.0E+00	8.9	-0.01302	-0.00130	0.01500	-0.00049			mixing
203	5526.94	$3d4s(^1D)4d$	$^2P_{3/2}$	$3d^2(^3P)4p$	$^4P_{3/2}$	8.0E+00	0.2							mixing
204	5648.1	$3d4s(^3D)5p$	$^4D_{5/2}$	$3d4s(^3D)5s$	$^4D_{5/2}$	2.7E+01	3.6	0.01395		0.01935	-0.00102			mixing
205	5648.1	$3d^2(^3F)4d$	$^4G_{7/2}$	$3d4s(^3D)5p$	$^2F_{5/2}$	2.7E+01	1.1			0.00334	-0.00113			mixing

Table 4.2: Recorded scandium lines, continued.

Nr	σ_J cm^{-1}	Upper Configuration	Term	Lower Configuration	Term	SNR	Υ	A_u cm^{-1}	B_u cm^{-1}	A_l cm^{-1}	B_l cm^{-1}	Upper Ref.	Lower Ref.	Comment
206	6235.4	$3d4s(^3D)5p$	$^4P_{5/2}$	$3d4s(^3D)5s$	$^4D_{5/2}$	8.3E+00	3.7	0.02215	-0.00152	0.01935	-0.00102			mixing
207	6235.4	$3d^2(^3F)5p$	$^4D_{3/2}$	$3d4s(^3D)4d$	$^4S_{3/2}$	8.3E+00	0.2							mixing
208	9264.1	$3d^2(^3F)5s$	$^4F_{7/2}$	$3d^2(^3F)4p$	$^4D_{7/2}$	8.7E+00	0.6			-0.00266				mixing
209	9264.1	$3d^2(^3F)5s$	$^4F_{5/2}$	$3d^2(^3F)4p$	$^4D_{5/2}$	8.7E+00	0.1							mixing
210	11392.86	$3d^3$	$^2G_{7/2}$	$3d4s(^3D)4p$	$^2F_{5/2}$	2.1E+01	0.6	0.00514		0.00588				mixing
211	11392.86	$3d(^2D)4p^2(^3P)$	$^4P_{1/2}$	$3d^2(^3F)4p$	$^4D_{1/2}$	2.1E+01	2.6			0.01686				mixing
212	11410.42	$3d(^2D)4p^2(^3P)$	$^4P_{3/2}$	$3d^2(^3F)4p$	$^4D_{5/2}$	8.5E+00	0.2							mixing
213	11410.42	$3d^3$	$^2D_{3/2}$	$3d4s(^3D)4p$	$^2D_{3/2}$	8.5E+00	1.4	0.00143		0.00857	-0.00057	[2]		mixing
214	12914.21	$3d^2(^3F)4p$	$^2F_{5/2}$	$3d4s(^1G)4s$	$^2G_{7/2}$	1.6E+01	0.5	-0.00266		-0.00383				mixing
215	12914.41	$3d^2(^3F)4p$	$^2G_{9/2}$	$3d4s(^1G)4s$	$^2G_{9/2}$	1.6E+01	1.9	0.00236		0.01170				mixing
216	15243.88		$^2F_{7/2}$	$3d^2(^3F)4p$	$^4F_{5/2}$	6.5E+00	0.1	0.00000		0.00000				mixing
217	15243.88	$3d^3$	$^2D_{3/2}$	$3d4s(^1D)4p$	$^2F_{5/2}$	6.5E+00	0.5	0.00143		-0.00146		[2]		mixing
218	15918.83	$3d(^2D)4p^2(^3P)$	$^2F_{7/2}$	$3d^2(^3F)4p$	$^4G_{5/2}$	6.5E+00	1.0			0.00930	0.00102			mixing
219	15918.83	$3d4s(^3D)5s$	$^4D_{3/2}$	$3d4s(^3D)4p$	$^4P_{1/2}$	6.5E+00	3.6	0.01500	-0.00049	0.04024				mixing
220	16140.97	$3d4s(^3D)4p$	$^4D_{5/2}$	$3d4s^2(^1D)$	$^2D_{3/2}$	3.5E+01	1.0	0.01019	-0.00041	0.00901	-0.00044			mixing
221	16140.97	$3d^2(^3F)4p$	$^2F_{5/2}$	$3d^2(^1D)4s$	$^2D_{5/2}$	3.5E+01	2.5	-0.00266		0.01842	0.00227			mixing
222	17579.531	$3d4s(^1D)4d$	$^2D_{5/2}$	$3d4s(^3D)4p$	$^2D_{3/2}$	1.4E+02	0.9			0.00857	-0.00057			mixing
223	17579.531	$3d^2(^3F)4p$	$^4G_{9/2}$	$3d^2(^3F)4s$	$^4F_{7/2}$	1.4E+02	0.8	0.00287		0.00832	-0.00055	[3]		mixing
224	3937.0083	$3d4s(^1D)4p$	$^2P_{3/2}$	$3d^2(^3P)4s$	$^2P_{3/2}$	8.5E+01	3.1	-0.00094		0.02202	-0.01639			mixing Ne I
225	5537.06	$3d4s(^3D)5p$	$^2F_{5/2}$	$3d4s(^3D)5s$	$^4D_{7/2}$	2.4E+01	7.2	0.00334	-0.00113	0.02012	0.00016			mixing Fe I
226	7283.7038	$3d4s(^3D)4d$	$^2G_{9/2}$	$3d^2(^3F)4p$	$^2F_{7/2}$	1.6E+01	2.0	0.00377					[1]	mixing Fe I
227	4465.0	$3d4s(^1D)4p$	$^2D_{5/2}$	$3d^2(^3F)4s$	$^4F_{5/2}$	7.2E+01	5.0	0.00512	-0.00043	0.02202	-0.01639			no fit
228	5990.8017	$3d4s(^1D)4p$	$^2F_{5/2}$	$3d^2(^3F)4s$	$^2F_{7/2}$	6.8E+00	4.6	-0.00146		-0.01302	-0.00130			no fit

---

References: 1: Singh *et al.* (1991), 2: Krzykowski and Stefańska (2008), 3: Ertmer and Hofer (1976). Empty reference for hfs constants from this work.

Table 4.3: $\log gf$ values for hfs components belonging to the transition from $3d4s(^3D)4p\ ^3D_{7/2}$ to $3d^2(^3F)4s\ ^4F_{7/2}$. The oscillator strength for the fine structure transition is shown in column $\log gf$. In the next 2 columns the quantum numbers F for the hfs levels are given. Column σ_F gives the wavenumbers of hfs transitions. The next column shows the relative intensity of each hfs component in percentages. The last column gives the oscillator strength for the hfs components.

Upper Configuration	Term	Lower Configuration	Term	σ_J cm^-1	$log(gf)$	Uncertainty %	F_u	F_l	σ_F cm^-1	Percentage %	Hfs $log(gf)$
3d4s(^{3}D)4p	$^4D_{7/2}$	3d^2(^{3}F)4s	$^4F_{7/2}$	4600.5820	-1.766	23	0	1	4600.4648	1.6	-3.572
							1	0	4600.4884	1.6	-3.572
							1	1	4600.4801	0.1	-4.593
							1	2	4600.4634	3.0	-3.292
							2	1	4600.5106	3.0	-3.292
							2	2	4600.4939	0.7	-3.894
							2	3	4600.4690	4.1	-3.154
							3	2	4600.5397	4.1	-3.154
							3	3	4600.5147	2.1	-3.447
							3	4	4600.4814	4.8	-3.088
							4	3	4600.5757	4.8	-3.088
							4	4	4600.5424	4.5	-3.116
							4	5	4600.5007	4.8	-3.081
							5	4	4600.6187	4.8	-3.081
							5	5	4600.5769	8.2	-2.853
							5	6	4600.5267	4.2	-3.146
							6	5	4600.6685	4.2	-3.146
							6	6	4600.6183	13.5	-2.634
							6	7	4600.5596	2.6	-3.350
							7	6	4600.7251	2.6	-3.350
							7	7	4600.6664	20.8	-2.447

Chapter 5

Discussion

5.1 Hyperfine structure constants

The hfs constant A has been determined for 95 levels. The A values as found from transitions involving the same level were consistent. Moreover, the A values are in agreement with literature values, as was shown in Fig. 4.1. In this figure it can be seen that for 38 levels, the hfs constants deviate no more than 0.001 cm^{-1} from the literature values. For 5 levels a larger deviation was found, which are discussed in the next section. It was not possible to derive the hfs constant B for all 95 levels. For some transitions it was necessary to lock B to zero, to prevent finding a local minimum. Furthermore, the B values as found for various transitions involving the same level were not always consistent. This can be seen for each level separately from the absolute deviation in B as shown in Table 4.1.

5.1.1 Levels in disagreement with literature

For the level $\boldsymbol{3d^2(^1D)4s\ ^2D_{3/2}}$ a hfs constant A of -0.00951 cm^{-1} was found, while the Singh *et al.* (1991) report a value of 0.01991 cm^{-1}. This is an extremely large difference and the patterns produced for transitions involving this level will look completely different depending on which hfs constant is used. The best fit hfs constant A for various lines involving this level are shown in Table 5.1. In this table, one can see that for 2 lines consistent hfs constants were found and for 1 other line it was possible to reproduce the observed pattern with this hfs constant. Moreover, for the transition at 4007.6079 cm^{-1}, the opposite hfs constant is known accurately from other transitions. The line patterns could not be reproduced using the value found in Singh *et al.* (1991), therefore it is likely that the hfs constant found is this work is the correct.

Table 5.1: The hfs constants as determined from various lines involving the level $3d^2(^1D)4s\ ^2D_{3/2}$. The first two lines were fitted and the third lines was used to check the hfs constants found from the other lines.

σ_J (cm^{-1})	A (cm^{-1})	use
4007.6079	-0.00952	fitted
7631.5599	-0.00963	fitted
8559.5052	*-0.00952*	*checked*

For the level **$3d^2(^1D)4s\ ^2D_{5/2}$** a hfs constant A of 0.01842 cm^{-1} was found, while Singh *et al.* (1991) report a value of 0.01419 cm^{-1}. In Singh *et al.* (1991), two resolved lines were used. One of these transitions involved the level discussed above, for which Singh *et al.* (1991) found a doubtful value. In this work, four resolved lines were used to determine hfs constants for this level. The resulting best fit hfs constants A for these lines are shown in Table 5.2.

Table 5.2: The hfs constants as determined from various lines involving the level $3d^2(^1D)4s\ ^2D_{5/2}$. The top 4 lines were resolved, the last line was unresolved. All lines were fitted.

σ_J (cm^{-1})	A (cm^{-1})	use
4019.9889	0.01830	fitted
8711.9370	0.01842	fitted
7644.1442	0.01802	fitted
4073.0782	0.01842	fitted
16694.3166	0.01848	fitted

For the level **$3d^2(^3F)4p\ ^2D_{5/2}$** a hfs constant A of 0.00149 cm^{-1} was found, while the in Singh *et al.* (1991) report a value of -0.00352 cm^{-1}. For this level, the hfs constant found in this work is uncertain. There was only 1 transition available to fit, which has a SNR of 7. The hfs constant of the opposite level is consistent with the values from other transitions. However, it is likely that the low SNR of this line causes the best fit hfs constant to deviate from the value reported in Singh *et al.* (1991).

For the level **$3d4s(^1D)4d\ ^2F_{7/2}$** it is more difficult to draw a conclusion. A hfs constant A of 0.00114 cm^{-1} was found in this work, while the in Başar *et al.* (2004) report a value of 0.01054 cm^{-1}. There is one line available to fit for this level, which lies close to a neon line. It is possible that part of the intensity of these lines is shared, influencing the best fit parameters. However, the pattern produced using the value from Başar *et al.* (2004) does not reproduce the observed pattern at all. To determine what the correct hfs constant is, one should record a spectrum of a wavelength region where multiple lines involving this level can be observed.

For the level **$3d4s(^3D)4d\ ^2G_{7/2}$** a hfs constant A of 0.003923 cm^{-1} was found in this work, while the in Başar *et al.* (2004) report a value of -0.00497 cm^{-1}. In this work, the lines used to determine hfs constants for this level were all unresolved. Therefore, the hfs constants for this level as determined in this work is uncertain. Transitions involving this level have not been used to determine hfs constants for the opposite level, to prevent the potentially wrong hfs constant to contaminate the values of the opposite hfs constants.

It would be useful to record a spectrum in the visible region, so that the contradicting hfs constants could be determined from the same transitions as used by Başar *et al.* (2004) and Singh *et al.* (1991) used.

5.1.2 Uncertainties in the hfs constants

The uncertainties in the hfs constants as shown in Table 4.1 might underestimate the actual uncertainties. One can compare the uncertainties with the deviation of the hfs constants within a set of transitions involving the same level. In Table 5.3 one can for instance see several best fit hfs constants A and B for the level $3d4s(^1D)4p$ $^2D_{3/2}$. The uncertainties in A and B found using the method described in Sect. 3.4 are ΔA =3.4E-07 cm^{-1} and ΔB =2.4E-06 cm^{-1}. The deviation in A between the transitions shown in Table 5.3 is two orders of magnitude larger, and for B the deviation is 3 orders of magnitude larger. The uncertainties that were derived in this work can be used as relative uncertainties, to compare two lines that were analysed within this work. When comparing the hfs constants and their uncertainties with literature values, one should be aware that the uncertainties as shown in Table 4.1 could be underestimated.

The reason this method might underestimate the actual uncertainty could be because the noise level is underestimated. A better method to determine the uncertainties might be to record multiple spectra, and fit the same line several times for different spectra. The standard deviation in the best fit hfs constant would than represent the uncertainty.

Table 5.3: The hfs constants for the level $3d4s(^1D)4p$ $^2D_{3/2}$ as determined from various transitions involving this level. The deviation between the values for A and B is larger than the uncertainties ΔA =3.4E-07 cm^{-1} and ΔB =2.4E-06 cm^{-1}.

σ_J (cm^{-1})	A (cm^{-1})	B (cm^{-1})
4622.9402	-0.01245	0.00043
4584.5289	-0.01242	0.00036
4576.9236	-0.01244	0.00023
4539.2283	-0.01245	0.00030
16096.8844	-0.01243	0.00060

5.1.3 Transition selection

A consistent set of hfs constants was produced from the lines that were analysed. It should be noted however that some lines have been excluded from this set. Lines were excluded when the SNR was too low or when hfs components were unresolved. For transitions with a low SNR, the best fit solution will depend on the noise. For unresolved patterns, multiple best fit solutions exist, and there is a probability the fitting routine finds a local minimum. This effect can be illustrated by looking at the scandium line at 4530.7653 cm^{-1}, shown in Fig. 5.1. This line is the strongest observed scandium line (SNR $\approx 10^4$), however the hfs components are unresolved. Two peaks can were observed, while the lines consist of 18 hfs components. Even though this line has a large SNR, one can expect that this line might give incorrect best fit hfs constants. One can see the best fit hfs constants for several transitions involving the same upper and lower level as the 4530.7653 cm^{-1} line in Table 5.4 a and b respectively. The hfs constant A from the unresolved level returns a best fit value which deviates 10^{-4} cm^{-1} compared to the resolved lines. One can therefore conclude that this line should not be selected to represent the hfs constants of this level. In general one can conclude that SNR is not the only important parameter when selecting lines to represent the hfs constants.

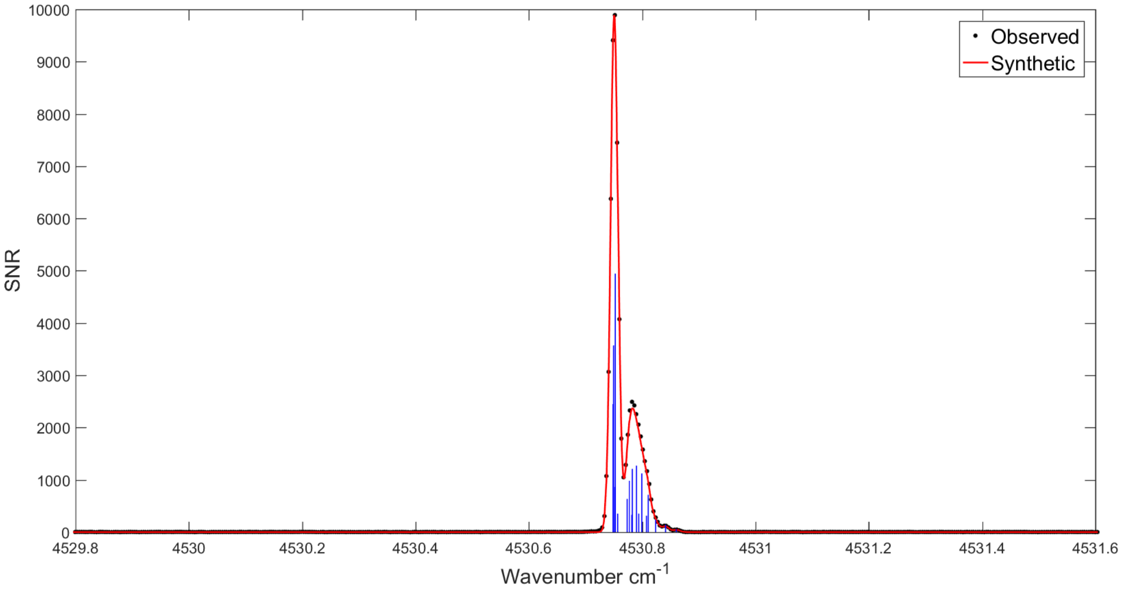

Figure 5.1: Observed and synthetic spectrum of the strongest scandium line. The hfs components are unresolved and many best fit solutions exist for this line.

Table 5.4: The hfs constants for the levels involved in the transition from at 4530.7653 cm^{-1}, as determined for lines involving one of these levels. (a) Best fit hfs constants for the level $3d^2(^3F)4s\ ^4F_{7/2}$ as determined from various lines. (b) Best fit hfs constants for the level $3d4s(^3D)4p\ ^4D_{5/2}$ as determined from various lines.

(a)

σ_J (cm^{-1})	A (cm^{-1})
4416.3183	0.00836
4600.5794	0.00834
4412.4872	0.00834
4271.4763	0.008323
4530.7653	0.00825

(b)

σ_J (cm^{-1})	A (cm^{-1})
4578.8232	0.01022
4621.0408	0.01020
4583.3456	0.01019
4530.7653	0.01006

Some levels were involved in few observed transitions, which complicates determining whether the fitting routine returned a local minimum. It would be useful to record spectra of wavelength regions containing more transitions involving these levels. Moreover, the unresolved lines could be investigated in more detail by reducing the Doppler width. The Doppler width could for instance be reduced by cooling the HCL with liquid nitrogen instead of water, as the Doppler width depends on the temperature of the emitting plasma.

5.1.4 Misidentified lines

For two of the recorded lines it was not possible to reproduce the observed spectrum of the hfs multiplet using the hfs constants that were found. This could indicate that the hfs constants for this level found from other transitions are not correct, but this could also be caused by misidentification of a line. If a line is misidentified, the profile will be fitted with the hfs constants from the wrong level. The transition from $3d4s(^1D)4p\ ^2D_{5/2}$ to $3d^2(^3F)4s\ ^4F_{5/2}$ at 4465.0 cm^{-1} might be misidentified. The hfs constants have been determined for five transitions, as shown in Table 5.5a. The hfs constants of the upper level has been determined for three transitions, as shown in Table 5.5b. It can be seen that the hfs constants are consistent for both the upper and lower level. However, the observed spectrum of this hfs multiplet is not reproduced using these hfs constants, as is shown in Fig. 5.2. This indicates that the line might be misidentified. Neither was the pattern at 5990.802 cm^{-1} reproduced by the hfs constants found from other transitions. It is less clear whether this line is misidentified, as this line is weak (SNR $\approx$ 7). Moreover, the hfs constants for the levels involved in this transition, as determined from other lines showed less consistent results.

Table 5.5: The hfs constants for the levels involved in the transition from at 4465.0 cm^{-1}, as determined for lines involving one of these levels. (a) Best fit hfs constants for the level $3d^2(^3F)4s\ ^4F_{5/2}$ as determined from various lines. (b) Best fit hfs constants for the level $3d4s(^1D)4p\ ^2D_{5/2}$ as determined from various lines.

(a)

σ_J (cm^{-1})	A (cm^{-1})	B (cm^{-1})
4114.9033	0.00514	0.00029
4324.0539	0.00511	-0.00043
4539.2283	0.00513	-0.00044
4583.3456	0.00511	-0.00049
4198.8752	0.00511	-0.00036

(b)

σ_J (cm^{-1})	A (cm^{-1})	B (cm^{-1})
4697.1012	0.02202	-0.01639
4412.4872	0.02203	-0.01589
16022.7364	0.02078	-0.01640

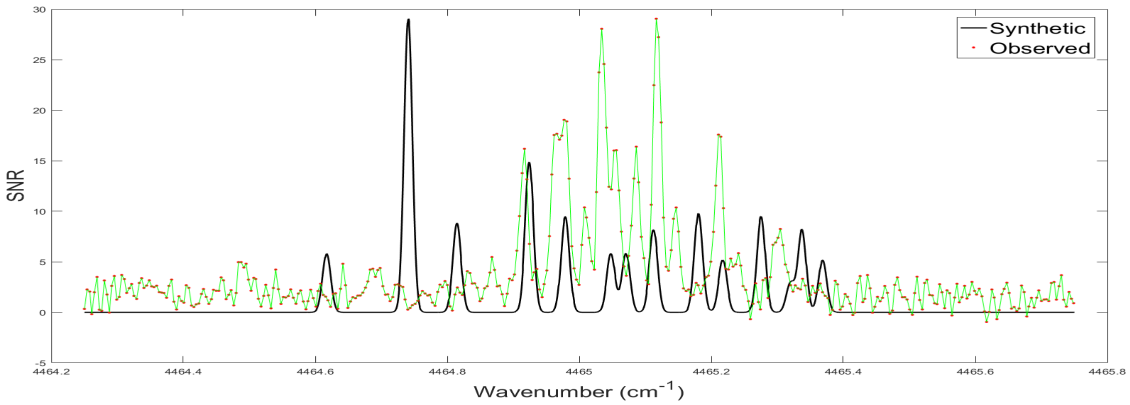

Figure 5.2: The spectrum of a possibly misidentified line at 4465 cm^{-1}. The synthetic spectrum is shown asa black line, the observed spectrum is shown as red dots and the green line. The green line is used to guide the eye. The synthetic spectrum was created using the best fit hfs constants as found from other transitions. The observed spectrum is not reproduced at all.

5.2 hfs in the spectrum of a star

A scandium line in the spectrum of the star Alpha Boo was reproduced using the hfs constants that were found in this work. Fig. 5.3 shows a part of the observed spectrum were a scandium transition from $3d^2(^3F)4s\ ^4F_{7/2}$ to $3d4s(^3D)4p\ ^4D_{7/2}$ was observed. In this figure, two synthetic spectra are shown as well, which were produced using atlas scandium abundance values for Alpha Boo. The fine structure spectrum (green) was produced ignoring hfs, while the hfs spectrum (red) used the hfs constants as found in this work. The synthetic and observed spectra were provided by Ryde (private communication). It can be seen that the hfs spectrum reproduces the width and depth of the observed line better compared to the fine structure spectrum.

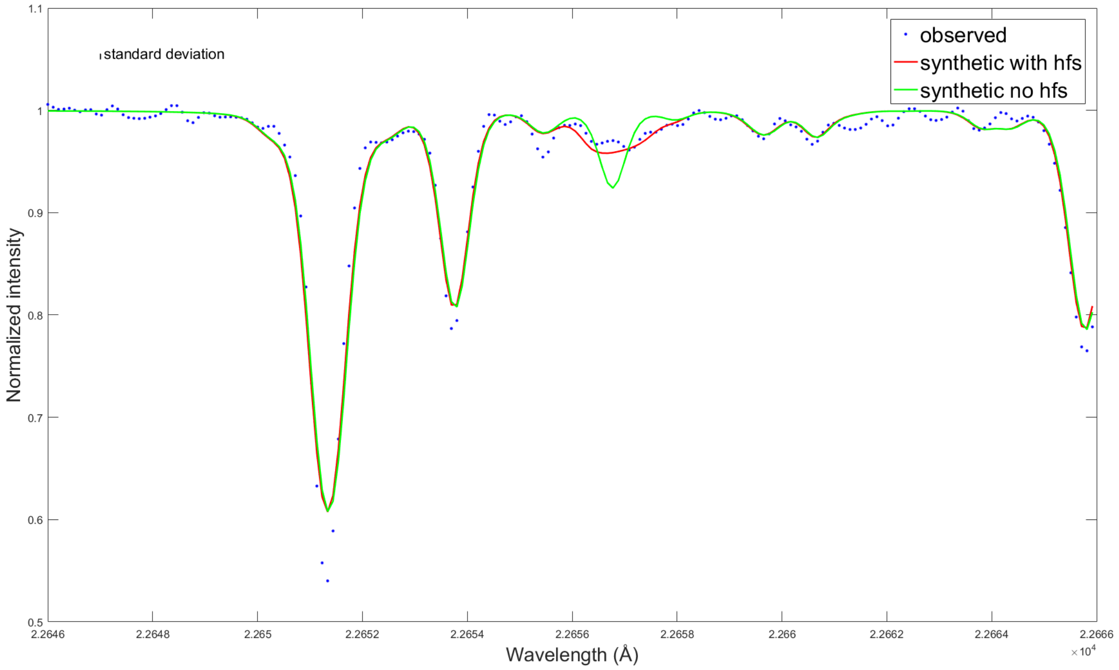

Figure 5.3: The transition from $3d^2(^3F)4s\ ^4F_{7/2}$ to $3d4s(^3D)4p\ ^4D_{7/2}$ observed in the spectrum of Alpha Boo. Blue dots represent measured intensities. The red and green line represent synthetic spectra produced using an atlas scandium abundance value for Alpha Boo. The red line is a spectrum produced using the hfs constants found in this work. The green line represents a spectrum were hfs is ignored. The standard deviation is indicated in the top left of the figure. The observed and synthetic spectrum were provided by Ryde (private communication).

5.3 Sensitivity of the model

The behaviour of the program that was developed to perform a nonlinear least squares fit was extensively tested given various sets of input parameters. The outcome of these tests is discussed in this section.

The most obvious parameter to test is the SNR. One can expect that if the SNR is low, the noise will be fitted instead of the signal and wrong hfs constants could be returned. In Fig. 5.4 the uncertainty on A_u is shown for a range of SNR in a log-log scale plot. One can see that the uncertainty in A_u decreases as the SNR increases. The same trend was observed for A_l. It can be seen that for SNR smaller than 40, the uncertainties are of the order of 10^{-2} cm^{-1}. For larger SNR the uncertainty decreases rapidly. At SNR larger than 400, the uncertainty seems to flatten out.

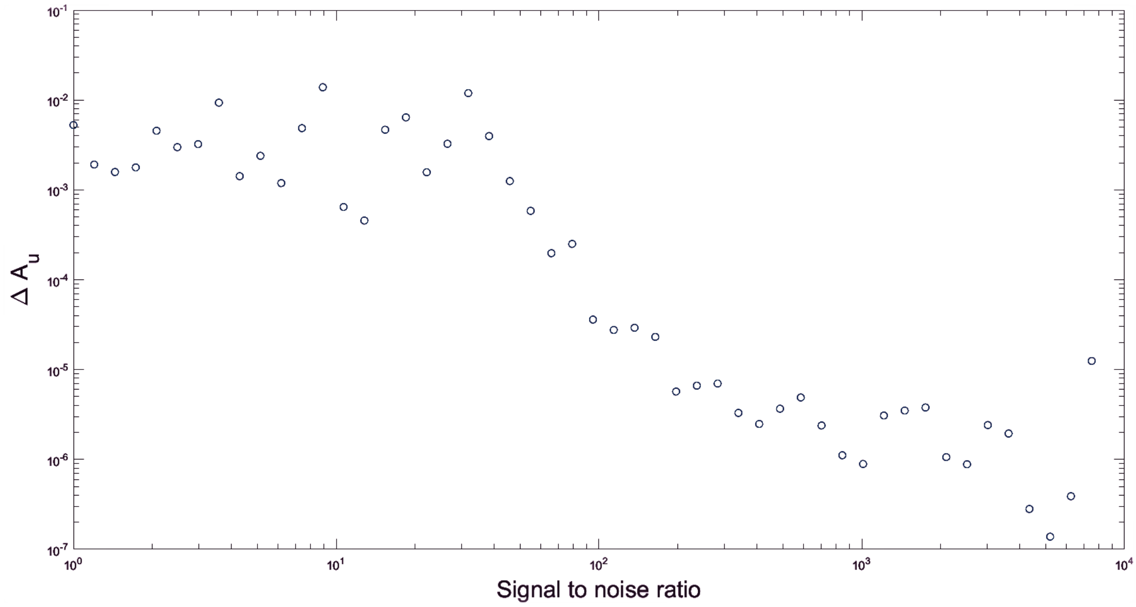

Figure 5.4: A log-log scale plot of the uncertainty on A_u as a function of the SNR. The uncertainty drops at SNR of 40.

Apart from SNR, the uncertainties on the hfs constants also depend on the width of the hfs multiplet. Broad patterns contain more data points and individual hfs components are resolved. The width of a hfs multiplet depends on the values of the hfs constants. If A of both levels is small, the splitting will be small as well and the line could become unresolved. Moreover, depending on the quantum number J of the upper and lower level, some combinations of hfs constants can cancel out the energy splitting of both levels, producing a narrow line. In Fig. 5.5 the uncertainty for all four hfs constants are shown for a given combination of values for A_u and A_l. It can be seen that the uncertainty is largest for A values near zero. From the top right plot, one can also see a slightly higher uncertainty around regions were $A_u = A_l$. Along this line, the energy splitting is cancelled given these J values.

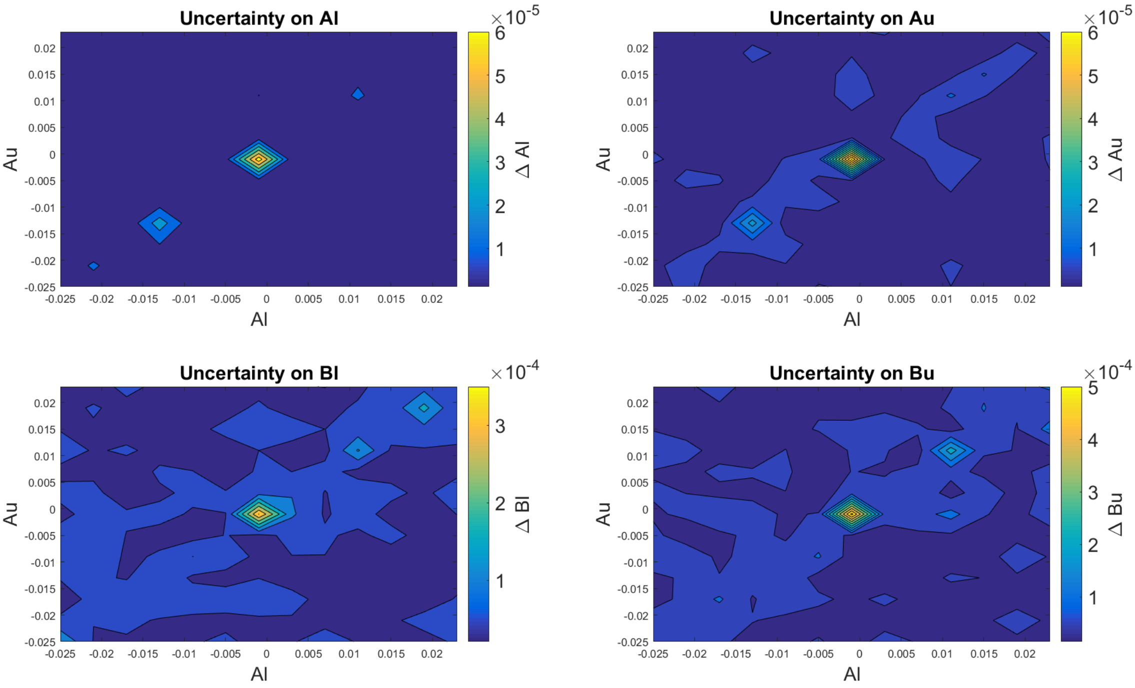

Figure 5.5: The uncertainty on the hfs constants for the upper and lower level (ΔA_l, ΔA_u, ΔB_l, ΔB_u respectively), given a combination of A_u and A_l. SNR was set to $2 \cdot 10^3$. The uncertainties are largest when both A values are near zero.

The best fit parameters are sensitive to the initial values of all free parameters. If the initial values are wrong, the fitting routine could end up in a local minimum, returning incorrect hfs constants. The sensitivity to the initial value for A_l was tested and the results are shown in Fig. 5.6. A spectrum generated was with A^{true} and B^{true} and random noise. This spectrum was fitted, but each time with new random noise. The initial value A_u^{IV} was varied as a fraction of A_u^{true}, which is shown on the x-axis. The true hfs constants are known, and the difference between the true and fitted parameter can be calculated as $A^{true} - A^{fit}$ which is shown on the y-axis. The behaviour for both A_u and A_l are shown. It can be seen that for fractions between 0.9 and 1.1 hfs constants close to the true values were returned. For fractions smaller than 0.9, too small hfs constants are returned. If the fraction is larger than 1.1, A_u is overestimated while A_l is underestimated. If A_u is overestimated, A_l can compensate so that the width of a hfs multiplet is reproduced. It should be noted that for this test, only A_l had an offset in its initial value, while the other hfs constants were set to the true values. In reality the true values are not known, and whether the model finds the right minimum depends on the offset in initial value for all hfs constants.

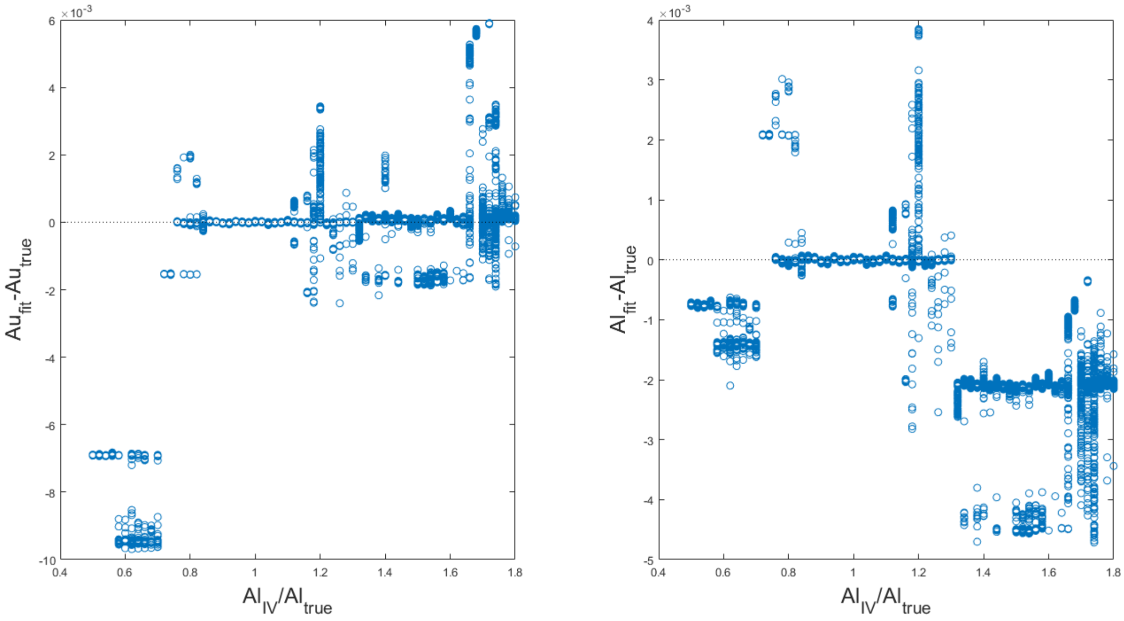

Figure 5.6: The initial value as a fraction of A^{true} is shown on x-axis. The y-axis shows the difference between the true A value and the A value as returned from the fit. For fractions between 0.9 and 1.1 hfs constants were returned which were close to the true values.

5.4 Noise in the recorded spectrum: an unexpected trend

For a spectrum recorded by the FTS, the noise level is expected to be equal throughout the whole spectrum. In Fig. 5.7 the sample standard deviation is shown as determined for various wavenumber regions of the spectrum. There seems to exist a trend between the wavenumber and the noise level, which is unexpected. The sample standard deviation has been determined for 2 spectra and the same trend was observed. It might be possible that this trend is caused by ringing. Narrow, unresolved lines can show a *sinc* function, which is caused by having finite integration limits in Eq. (3.5). In the wings this unresolved line, the *sinc* function produces an intensity value that is oscillating with a small amplitude. This might have been observed as noise in the spectrum. At a wavenumber around 0 cm^{-1} an intensity peak was recorded, as can be seen in Fig. 5.8. Ringing of this peak might have caused to sample standard deviation to be higher at low wavenumbers.

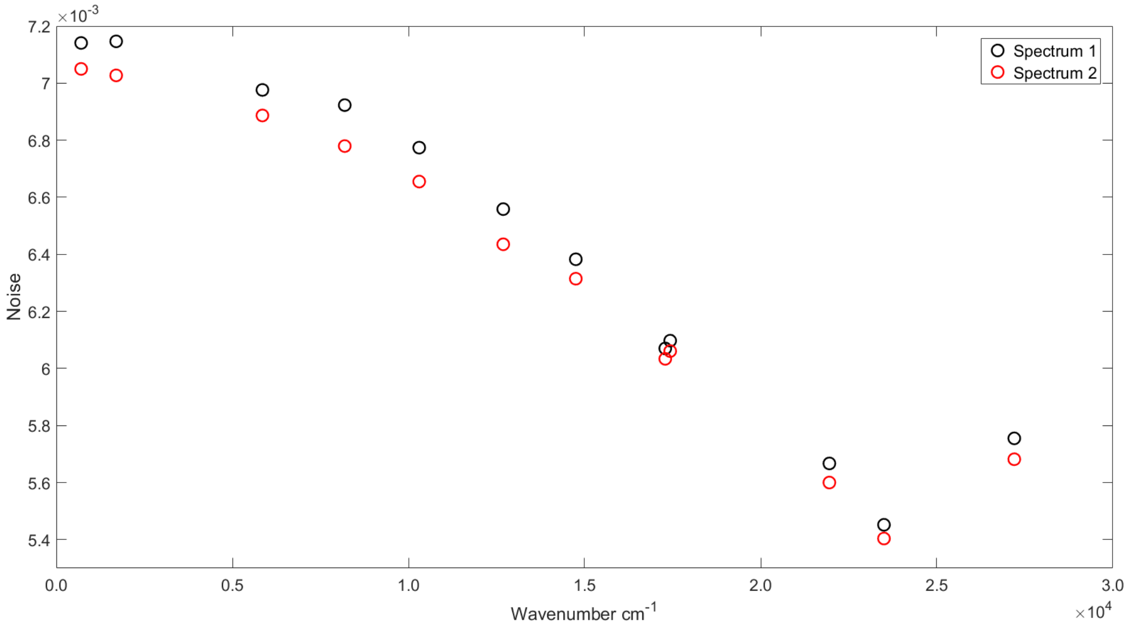

Figure 5.7: The sample standard deviation as determined for various spectral regions for two recorded two spectra. For a spectrum recorded with the FTS, it is expected that the noise level does not depend on the wavenumber region. In contrast, this plot suggests the noise level is higher for low wavenumbers.

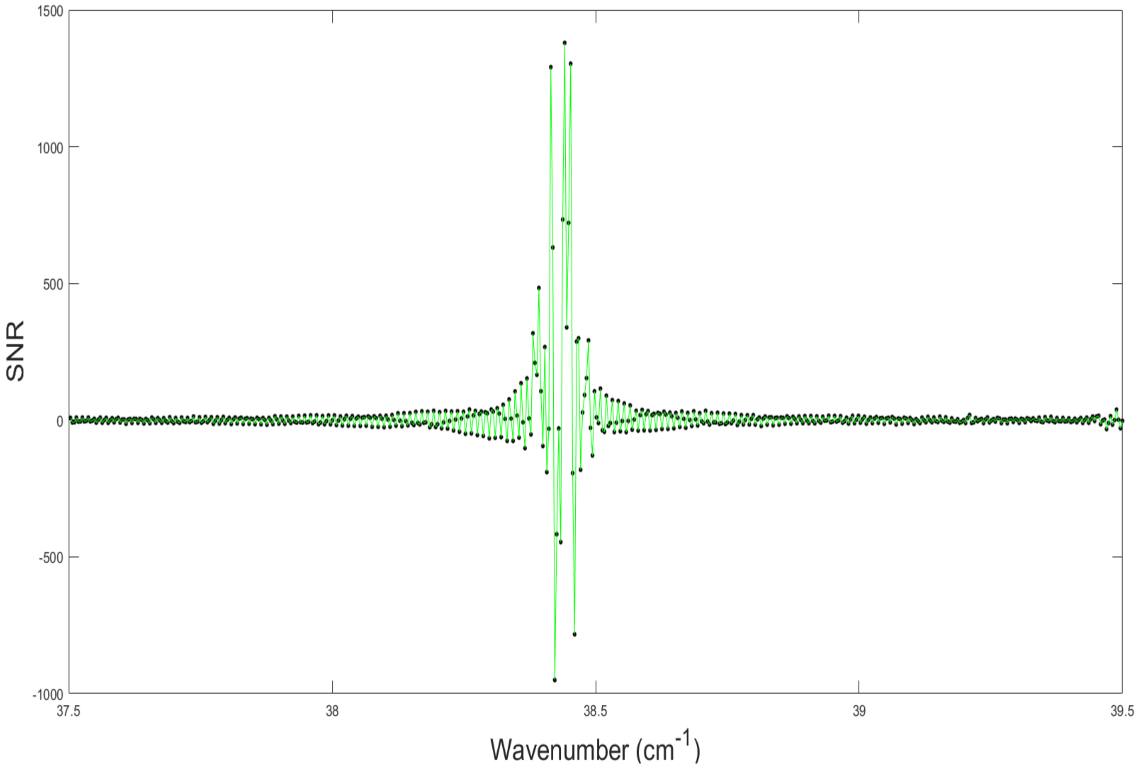

Figure 5.8: An intensity pattern observed at an extremely low wavenumber. The black dots represent the observed spectrum, while the green line guides the eye. The line is too narrow to be resolved and a *sinc* is measured. The wings of this *sinc* function might add to the noise level at low wavenumbers.

Chapter 6

Conclusion

In this project, hfs constants have been determined for 95 levels in neutral scandium. For 52 of these levels the hfs constants have been determined for the first time. The recorded transitions returned a consistent set of best fit hfs constants. For determining the hfs constants from a laboratory spectrum, a program was developed to model synthetic spectra of hfs multiplets and fit these using the nonlinear least squares method. For the levels for which hfs data already existed, the program returned hfs constants that were in agreement with literature values. The sensitivity of the program to input parameters SNR, width of the structure and an offset in initial values was probed. Additionally, a program was developed to derive the oscillator strengths of hfs components, given the oscillator strength of the fine structure transition. Oscillator strengths have been derived for 590 hfs transitions.

The program that determines hfs constants from an observed spectrum is attached in Appendix A. This program is of general nature and could also be used to measure hfs constants for other elements. The program that derives $\log gf$ values for hfs transitions is attached to appendix B. One can use this program to derive the $\log gf$ values of hfs components for any transition given the oscillator strength of the fine structure transition.

With known hfs constants and oscillator strengths, one can generate the synthetic spectrum of a hfs multiplet. For instance, using the new hfs data it was possible to reproduce the profile of the scandium transition from $3d^2(^3F)4s\ ^4F_{7/2}$ to$3d4s(^3D)4p$ $^4D_{7/2}$ in the observed spectrum of the star Alpha Boo. The new hfs data will allow for more accurate analysis of scandium lines in stellar spectra. Next to this, the new hfs data can be of use when analysing laboratory spectra. For lines that have shared intensities, the relative intensities are unknown. If the hfs constants are available, one could generate a synthetic spectrum of both lines. By adding these spectra together and fitting this to the observed spectrum the relative intensities could be obtained.

Bibliography

A. Aboussaïd, M. Carleer, D. Hurtmans, E. Biémontb, and M. R. Godefroid. Hyperfine Structure of Sc I by Infrared Fourier Transform Spectroscopy. *Phys. Scr.*, 53:28–32, 1996.

W. D. Arnett. On the bulk yields of nucleosynthesis from massive stars. *Astrophysical Journal*, 219:1008–1016, February 1978.

G. Başar, G. Başar, F. G. Acar, I. K. Öztürk, and S. Kröger. Experimental Investigation of the Hyperfine Structure and Theoretical Studies of the Even Configurations of Sc I. *Phys. Scr.*, 69(3):189–195, 2004.

C. Battistini and T. Bensby. The origin and evolution of the odd-Z iron-peak elements Sc, V, Mn, and Co in the Milky Way stellar disk. *Astronomy and Astrophysics*, 577:A9, May 2015.

J. Bieron, C. Froese-Fischer, and Godefroid. M. Hyperfine-structure calculations of excited levels in neutral scandium. *Journal of Physics B: Atomic, Molecular and Optical Physics*, 35(15):3337, 2002.

K. Burns, K. B. Adams, and J. Longwell. Interference measurements in the spectra of neon and natural mercury. *J. Opt. Soc. Am.*, 40(6):339–344, Jun 1950.

J. Cernicharo, A. M. Heras, A. G. G. M. Tielens, J. R. Pardo, F. Herpin, M. Gulin, and L. B. F. M. Waters. Infrared space observatory's discovery of c4h2, c6h2, and benzene in crl 618. *The Astrophysical Journal Letters*, 546(2):L123, 2001.

W. J. Childs. *Phys. Rev. A*, 4, 1971.

R. D. Cowan. *The Theory Of Atomic Structure And Spectra.* January 1981.

L. Engström. *GFit, A Computer Program to Determine Peak Positions and Intensities in Experimental Spectra.*, volume LRAP-232 of *Lund Reports in Atomic Physics.* Atomic Physics, Department of Physics, Lund University, 1998.

W. Ertmer and B. Hofer. Zero-field hyperfine structure measurements of the metastable states 3d2 4s4f3/2, 9/2 of45sc using laser-fluorescence atomic-beam-magnetic-resonance technique. *Zeitschrift für Physik A Atoms and Nuclei*, 276(1):9–14, 1976.

R. B. Firestone, C. M. Baglin, and S. Y. Frank Chu. *Table of Isotopes.* October 1999.

G. Fricke, H. Kopfermann, S. Penselin, and K. Schlüpmann. Bestimmung der hyperfeinstrukturaufspaltungen der scandium-grundzustände2d3/2 und2d5/2 und des quadrupolmomentes des sc45-kernes. *Zeitschrift für Physik*, 156(3):416–424, 1959.

R. G. Gratton and C. Sneden. Abundances of elements of the Fe-group in metal-poor stars. *Astronomy & Astrophysics*, 241:501–525, 1991.

U. Heiter, K. Lind, M. Asplund, P. S. Barklem, M. Bergemann, L. Magrini, T. Masseron, Š. Mikolaitis, J. C. Pickering, and M. P. Ruffoni. Atomic and molecular data for optical stellar spectroscopy. *Phys Scr*, 90(5):054010, May 2015.

C. J. Humphreys, E. Paul, and K. B. Adams. Infrared atomic spectra. *J Res Natl Inst Stand Technol.*, 109(3):371–389, 1961.

P. Jofré, U. Heiter, C. Soubiran, S. Blanco-Cuaresma, T. Masseron, T. Nordlander, L. Chemin, C. C. Worley, S. Van Eck, A. Hourihane, G. Gilmore, V. Adibekyan, M. Bergemann, T. Cantat-Gaudin, E. Delgado-Mena, J. I. González Hernández, G. Guiglion, C. Lardo, P. de Laverny, K. Lind, L. Magrini, S. Mikolaitis, D. Montes, E. Pancino, A. Recio-Blanco, R. Sordo, S. Sousa, H. M. Tabernero, and A. Vallenari. Gaia FGK benchmark stars: abundances of α and iron-peak elements. *Astronomy and Astrophysics*, 582:A81, October 2015.

V. Kaufman and J. Sugar. Wavelengths and energy level classifications of scandium spectra for all stages of ionization. *Journal of Physical and Chemical Reference Data*, 17:1679–1789, October 1988.

H. Kopfermann and E. Rasmussen. *Z. Phys.*, 92:82, 1934.

A. Kramida, Yu. Ralchenko, J. Reader, and and NIST ASD Team. NIST Atomic Spectra Database (ver. 5.3), [Online]. Available: `http://physics.nist.gov/asd` [2017, April 24]. National Institute of Standards and Technology, Gaithersburg, MD., 2015.

A. Krzykowski and D. Stefańska. Hyperfine structure measurements of the even electron levels in scandium atom. *Journal of Physics B: Atomic, Molecular and Optical Physics*, 41(5):055001, 2008.

H. G. Kuhn. *Atomic Spectra.* October 1969.

G. Ledrew. The Real Starry Sky. *Journal of the Royal Astronomical Society of Canada*, 95:32, 2001.

R. B. Leighton and W. H. Furry. Principles of Modern Physics. *American Journal of Physics*, 28:510–511, May 1960.

Mathworks least-squares (model fitting) algorithms. `https://se.mathworks.com/help/optim/ug/least-squares-model-fitting-algorithms.html`.

F. Matteucci, editor. *The chemical evolution of the Galaxy*, volume 253 of *Astrophysics and Space Science Library*, 2001.

W. F. Meggers and C. J. Humphreys. Interference measurements in the spectra of noble gases. *J. Res. Natl. Bur. Stand. (U.S.)*, 13:293–309, 1934.

I. Mills, T. Cvitas, K. Homann, N. Kallay, and K. Kuchitsu. *Quantities, Units and Symbols in Physical Chemistry.* January 1988.

F. Molster and C. Kemper. *Crystalline Silicates*, pages 3–28. Springer Netherlands, Dordrecht, 2005.

C. P. Nicholls, Lebzelter, T., Smette, A., Wolff, B., Hartman, H., Kufl, H.-U., Przybilla, N., Ramsay, S., Uttenthaler, S., Wahlgren, G. M., Bagnulo, S., Hussain, G. A. J., Nieva, M.-F., Seemann, U., and Seifahrt, A. Crires-pop: a library of high resolution spectra in the near-infrared - ii. data reduction and the spectrum of the k giant 10 leonis. *A&A*, 598:A79, 2017.

P. E. Nissen, Y. Q. Chen, W. J. Schuster, and G Zhao. Sc and Mn abundances in disk and metal-rich halo stars. *Astronomy and Astrophysics*, 353:722, 2000.

K. Nomoto, F.K. Thielemann, and K. Yokoi. Accreting white dwarf models of Type I supernovae. III - Carbon deflagration supernovae. *The Astrophysical Journal*, 286:644, 1984.

K. Nomoto, C. Kobayashi, and N. Tominaga. Nucleosynthesis in Stars and the Chemical Enrichment of Galaxies. *Annual Review of Astron and Astrophys*, 51:457–509, August 2013.

A. Pehlivan, H. Nilsson, and H. Hartman. Laboratory oscillator strengths of Sc i in the near-infrared region for astrophysical applications. *The Astrophysical Journal*, 582:A98, October 2015.

D. Prialnik. *An Introduction to the Theory of Stellar Structure and Evolution.* October 2009.

J.X. Prochaska, S.O. Naumov, B.W. Carney, A McWilliam, and A.M. Wolfe. The Galactic Thick Disk Stellar Abundances. *Apj*, 120:2513–2549, 2000.

N. Ramsey. The Nuclear Magnetic Moment of Scandium45. *Physical Review*, 79(6):1010–1010, 1950.

R. J. Rutten. *Radiative Transfer in Stellar Atmospheres.* May 2003.

C. J. Sansonetti, M. M. Blackwell, and E. B. Saloman. High-resolution observations of the infrared spectrum of neutral neon. *J. Phys. Chem. Ref. Data*, 33:11131158, 2004.

P. Schneider. *Extragalactic Astronomy and Cosmology: An Introduction.* 2015.

Pat Scott, Asplund, Martin, Grevesse, Nicolas, Bergemann, Maria, and Jacques Sauval, A. The elemental composition of the sun - ii. the iron group elements sc to ni. *A&A*, 573:A26, 2015.

E. Siefart. Calculation of the hyperfinestructure and gj-values of the 3d 4s 4p-configuration of scandium. *Annalen der Physik*, 489(4):286–294, 1977.

R. Singh, G. N. Rao, and R. K. Thareja. Laser optogalvanic spectroscopy of sci: hyperfine-structure studies. *Journal of the Optical Society of America, Part B: Optical Physics; (USA)*, 8:1, Jan 1991.

J. Sugar and C. Corliss. *Atomic energy levels of the iron-period elements : potassium through nickel.* New York : published by the American Chemical Society and the American Institute of Physics for the National Bureau of Standards, 1985. Includes bibliography.

A. Thorne, U. Litzén, and S. Johansson. *Spectrophysics*. February 1999.

F. X. Timmes, S. E. Woosley, and T. A. Weaver. Galactic chemical evolution: Hydrogen through zinc. *Astrophysical Journal, Supplement*, 98:617–658, June 1995.

B. M. Tinsley. Stellar lifetimes and abundance ratios in chemical evolution. *The Astrophysical Journal*, 229:1046, 1979.

J. A. Valenti and N. Piskunov. Spectroscopy made easy: A new tool for fitting observations with synthetic spectra. *Astronomy and Astrophysics Supplement Series*, 118(3):595–603, 1996.

G. M. Wahlgren. Inputting hyperfine structure into synthetic spectrum codes. *Mem. S.A. It.*, 8:108–113, 2005.

E. W. Weisstein. Gaussian function. From MathWorld—A Wolfram Web Resource. Last updated on 21/04/2017.

W. H. Wollaston. A Method of Examining Refractive and Dispersive Powers, by Prismatic Reflection. *Phil. Trans. R. Soc. Lond*, 92:365–380, January 1802.

W. Zeiske, G. Meisel, H. Gebauer, B. Hofer, and W. Ertmer. Hyperfine structure of cw dye laser populated high lying levels of 45sc by atomic-beam magnetic-resonance. *Physics Letters A*, 55(7):405 – 406, 1976.

H. W. Zhang, T. Gehren, and G. Zhao. A non-local thermodynamic equilibrum study of scandium in the Sun. *Astronomy and Astrophysics*, 481:489–497, April 2008.

G. Zhao and P. Magain. The chemical composition of the extreme halo stars. II - Green spectra of 20 dwarfs. *Astronomy and Astrophysics*, 238:242–248, November 1990.

Appendix A

The hfs constants

The program that was developed to determine hfs constants from an observed spectrum of a hfs multiplet is attached in this section. Additionally, an example of how to use the code is given.

A.1 Code

The program can be divided into three parts. The main program is called *LSQcurvefit*, which executes the nonlinear least squares fit. A synthetic spectrum of the hfs multiplet is generated using the function *Icreator*. The uncertainties in the hfs constants are derived by the function *determine_delta*. The code below only works for a single hfs multiplet, so that one can easily see how to use program. When analysing multiple fine structure transitions, one should read the data file just once, since this is very time consuming. A program to analyse multiple fine structure transitions can be found at `https://drive.google.com/drive/folders/0B_Rc6gvqtyT6ajFqaVdxbjB5N0U?usp=sharing`. Here, one can also find a GUI that was developed in this project, which can be used to find initial values for the hfs constants.

A.1.1 Nonlinear least squares

```
function [HF_constants,HF_uncert,lineprop, x, warnings]=
   LSQcurvefit_read(Ju,Jl,wavenrJ,Au,Bu,Al,Bl, lock,
   uncert,letplot)
%This function fits the spectrum of hfs multiplet and
   returns the best fit
% (...)
%for plots set letplot=1. For uncertainties set uncert=1.

%% Read data: Observed spectrum:
data = dlmread('Scdata18_cal_SNR.txt', ','); %Reads
   entire file
wavenrOBS=data(:,1); %observed wavenumbers
IOBS=data(:,2); %observed intensities

%% Select data: Extract hfs multiplet from observed
   spectrum.
```

```
mask = (wavenrOBS >= (wavenrJ-0.8)) & (wavenrOBS<=(
   wavenrJ+0.8)); %select only the transition
wavenrOBS=wavenrOBS(mask);
IOBS=IOBS(mask);

%% Model: Generating a synthetic spectrum of the hfs
   multiplet.
fun=@(x,wavenrOBS) IcreatorB_lift_fixI(Ju, Jl, x(1), x(2)
   , x(3), x(4), x(5), wavenrOBS, x(6), x(7),x(8));
%anonymous function for the syntethic spectrum.

%% Initial values
%line width guess
T=500; % Temperature in K
FWHM=7.16*10^-7*wavenrJ*sqrt(T/45)*1.38; %calculates FWHM
    from Doppler width
stdev=FWHM/2.3548; %std FWHM relation, see Wolfram Alpha

liftguess=0;
MaxIOBS=max(IOBS);
x0=[wavenrJ, Au, Bu, Al, Bl, stdev, liftguess, MaxIOBS];
   %initial guesses

%% locking parameters
%standard boundaries for free parameters
lb=[-Inf,-0.2,-0.03,-0.2,-0.03,stdev*0.5,-Inf,-Inf];
ub=[+Inf,+0.2,+0.03,+0.2,+0.03,stdev*1.5,+Inf,+Inf];

if nargin == 10
    lock2=find(lock); %input parameter 'lock' is an array
        of zeros and 1s. 1 means locking this parameter
    lb(lock2)=x0(lock2);
    ub(lock2)=x0(lock2);
end

%% Least Squares minimization
[x, ~]=lsqcurvefit(fun,x0,wavenrOBS',IOBS',lb,ub); % this
    executes the fit.

% Generate synthetic spectrum with the found best fit
   parameters.
Imodres=fun(x,wavenrOBS);

%% Compare synthetic and observed spectra with new hfs
   constants
if letplot==1
    width = 3;     % Width in inches
    height = 3;    % Height in inches
    alw = 0.75;    % AxesLineWidth
```

```
fsz = 11;       % Fontsize
lw = 1.5;       % LineWidth
msz = 8;        % MarkerSize

figureindex=1;
figure(figureindex)
pos = get(gcf, 'Position');
set(gcf, 'Position', [pos(1) pos(2) width*100, height
   *100]); %<- Set size
set(gca, 'FontSize', fsz, 'LineWidth', alw); %<- Set
   properties

figure(figureindex) %plot observed spectrum
plot(wavenrOBS, IOBS, '.r' ,'LineWidth',lw,'
   MarkerSize',msz*1.2)
hold on

minwav=min(wavenrOBS);
maxwav=max(wavenrOBS);
wavenrstotest=minwav:0.0038/10:maxwav;%get a higher
   resolution on calculated values

[Imod,xbar,ybar]=fun(x,wavenrstotest);
plot(wavenrstotest, Imod, 'k', 'LineWidth',lw*0.9,'
   MarkerSize',msz*1.2) % plot synthetic spectrum

xlabel('Wavenumber (cm^-^1)', 'FontSize',16)
ylabel('SNR', 'FontSize',16)
h_legend=legend('Observed','Synthetic');
set(gca,'fontsize',14)
set(h_legend,'FontSize',18);

%add bars at line centres
for i=1:size(xbar,1)
    hold on
    plot(xbar(i,:), ybar(i,:), 'b', 'LineWidth',lw
       *0.6,'MarkerSize',msz)
    hold on
end

hold off

figure(figureindex+1) % residual plot
pos = get(gcf, 'Position');
set(gcf, 'Position', [pos(1) pos(2) width*100, height
   *100]); %<- Set size
set(gca, 'FontSize', fsz, 'LineWidth', alw); %<- Set
   properties
```

```
    Res=IOBS-Imodres';
    plot(wavenrOBS, Res, '.', 'MarkerSize',msz*1.2)

    xlabel('Wavenumber (cm^-^1)', 'FontSize',16)
    ylabel('Residual', 'FontSize',16)
    set(gca,'fontsize',14)


end



%% Uncertainties on the hfs constants
%if not asked for uncertainty, set to NaN
delAu=NaN; %uncertainty on Au
delBu=NaN;
delAl=NaN;
delBl=NaN;

if uncert==1
    rms2=0.006628; % noise level was determined from
       observed spectrum

    [delAu,delBu,delAl,delBl]=determine_delta(rms2,
       MaxIOBS,Ju,Jl,x(1),x(2),x(3),x(4),x(5), lock); %
       returns uncertainty on hfs constants

end

%return hfs constants and uncertainties
HF_constants=[x(2), x(3), x(4), x(5)];
HF_uncert=[delAu, delBu,delAl,delBl];

%% check if large changes
changes=x-x0;
warnings=1+find(abs(changes(2:6)>0.003));
warnings(length(warnings)+1:7)=NaN;

%% line properties
[~,xbar,~]=fun(x,wavenrOBS);
hfwidth=max(xbar(:,1))-min(xbar(:,1))+x(6);
resolved=hfwidth./(x(6)*length(xbar(:,1))*0.5);
lineprop=[MaxIOBS, resolved];
```

A.1.2 Synthetic spectra

```
function [Itot, xbar, ybar]=IcreatorB(Ju, Jl, wavenrJ, Au
   , Bu, Al, Bl, wavenrs, stdev,lift, MaxIOBS)
%this function creates a model of the intensity for some
   range of wavenumbers.


Iqnr=7/2; %nuclear spin quantum nr. 7/2 for Scandium %9/2
    for Nb!


%% Possible F values
Fu=abs(Iqnr-Ju):Iqnr+Ju; %possible values for upper F
Fl=abs(Iqnr-Jl):Iqnr+Jl; %possible values for lower F

%% Allowed transitions.
transition_index=0;%use as index, but also to see total
   nr of possible transitions.
transitions=[];%store allowed transitions in this matrix
wavenr=[];%store wavenrs of transitions in here
for i=1:length(Fu)
    for j=1:length(Fl)
        dF=Fu(i)-Fl(j);
        if dF==0 && Fu(i)+Fl(j)~=0 || abs(dF)==1 && Fu(i)
           +Fl(j)~=0;%selection rules
        transition_index=transition_index+1;
        transitions(1,transition_index)=Fu(i);
        transitions(2,transition_index)=Fl(j);

        %% Find wavenr for each transition
        wavenr(transition_index)=wavenrJ+(0.5*Au*Ccalc(Fu
           (i),Ju))-(0.5*Al*Ccalc(Fl(j),Jl))+(Bu*
           function_calc(Fu(i),Ju))-(Bl*function_calc(Fl(
           j),Jl)); %contains wavenr of each transition

        %% Relative Intensities
        sixj=sixjsymbol(Jl, Fl(j), Fu(i), Ju);
        I(transition_index)=(2*Fu(i)+1)*(2*Fl(j)+1)*sixj
           ^2;%contains relative intensities for each
           transition
        end
    end
end

%% Gaussian for each hfs transition
yvalues=[];
for k=1:transition_index; % for each transition create a
   Gaussian profile.
```

```
    Iuse=normpdf(wavenrs, wavenr(k), stdev);
    yvalues(k,:)=Iuse*I(k); % in the end contains
       intensity values for each hfs lines on seperate
       row
end
Itot=sum(yvalues); %lines are not in seperate rows
   anymore, only total intensity

% normalize intensity
Itot=Itot.*MaxIOBS/max(Itot);
%Lift continuum (caused by blackbody radiation)
Itot=Itot+lift;


%return line centres for plots
xbar=[];
ybar=[];

for k=1:transition_index;
    xbar(k,:)=[wavenr(k),wavenr(k)];
    ybar(k,:)=[0, I(k)*MaxIOBS/(2*max(I))]; %not actual
       intensities, just scaling
end
```

Ccalc

```
function C=Ccalc(F,J)
I=7/2; %for Sc
C=F*(F+1)-J*(J+1)-I*(I+1);
end
```

Dcalc

```
function D=Dcalc(F,J)
I=7/2; %for Sc

C=F*(F+1)-J*(J+1)-I*(I+1);
upper=(3*C*(C+1)-4*I*J*(I+1)*(J+1));
lower=(8*I*J*(2*I-1)*(2*J-1));


if upper==0
    D=0;
elseif lower==0
    D=0;
else
    D=upper/lower;
end


end
```

sixjsymbol

```
function I=sixjsymbol(j1, j3, l1, l3)
%Calculate sixjsymbol with j2=7/2 and l2=1.


j2=7/2;
l2=1;
A=delta6j(j1,j2,j3)*delta6j(j1,l2,l3)*delta6j(l1,j2,l3)*
   delta6j(l1,l2,j3);

lowerk=max(max(j1+j2+j3, j1+l2+l3), max(l1+j2+l3, l1+l2+
   j3));
upperk=min(min(j1+j2+l1+l2, j2+j3+l2+l3), j3+j1+l3+l1);



B=0;
for k=lowerk:upperk; %steps of 1

    C=(((-1)^k)*factorial(k+1))/(factorial(k-j1-j2-j3)*
       factorial(k-j1-l2-l3)*factorial(k-l1-j2-l3)*
       factorial(k-l1-l2-j3));

    D=1/(factorial(j1+j2+l1+l2-k)*factorial(j2+j3+l2+l3-k
       )*factorial(j3+j1+l3+l1-k));
    E=C*D;
    B=B+E;
end
I=A*B;
```

delta6j

```
function [y]=delta6j(a,b,c)
%this function calculates delta(abc) for the 6j wigner
   symbol

%use gamma function instead of factorial in case of half
   integers
A=gamma(a+b-c+1);
B=gamma(a-b+c+1);
C=gamma(b+c-a+1);
D=gamma(a+b+c+1+1);

y=sqrt(A*B*C/D);
end
```

A.1.3 Uncertainties

determine_delta

```
function [delAus,delBus,delAls,delBls]=determine_delta(
   rms,MaxIOBS,Ju,Jl,wavenrJ, Au, Bu, Al, Bl,lock)
%This function returns the uncertainty on the hfs
   constants by generating
%spectra with artificial noise and calculating the sample
    standard
%deviation in the best fit hfs constants. rms is the
   sample standard
%deviation as determined from the observed spectrum.


%% Create pure hfs pattern
[wavenumbers, intensity]=create_hfpat(wavenrJ, Ju, Jl, Au
   , Bu, Al, Bl); %creates 'pure' hfs pattern
intensity=(MaxIOBS.*intensity)./(max(intensity));

%% Add noise to pure pattern
n=500; %add random error for n times
for i=1:n


%error is gaussian with rms as standard deviation.
    for j=1:length(intensity) % add an error in intensity
        at each point.
        intensity(j)=intensity(j)+(randn*rms); %add noise
            to intensity
    end



    [ABfit,~]=fitpure_del_fixI(wavenumbers,intensity,Ju,
       Jl,wavenrJ,Au*1.1,Bu*1.1,Al*1.1,Bl*1.1, lock); %
       small ofset in initial values
    saveAB(:,i)=ABfit;






end

delAus=std(saveAB(1,:)); %sample standard deviation
delBus=std(saveAB(2,:));
delAls=std(saveAB(3,:));
delBls=std(saveAB(4,:));
```

create_hfpat

```
function [wavenumbers, intensity, resolved]=create_hfpat(
   wavenrJ, Ju, Jl, Au, Bu, Al, Bl)
%this function generates the spectrum of a hfs multiplet
   given the hfs
%constants, centre of gravity wavenumber and J quantum
   numbers.

I=7/2; %nuclear spin quantum nr. 7/2 for Scandium


%% Possible F values
Fu=abs(I-Ju):I+Ju; %possible values for upper F
Fl=abs(I-Jl):I+Jl; %possible values for lower F


%% Allowed transitions.
transition_index=0;%use as index, and total nr of allowed
    transitions.
transitions=[];%store allowed transitions
wavenr=[];%store wavenrs of hfs transitions
for i=1:length(Fu)
    for j=1:length(Fl)
        dF=Fu(i)-Fl(j);
        if dF==0 && Fu(i)+Fl(j)~=0 || abs(dF)==1 && Fu(i)
           +Fl(j)~=0;%selection rules
        transition_index=transition_index+1;
        transitions(1,transition_index)=Fu(i);
        transitions(2,transition_index)=Fl(j);

        %% Find wavenr for ech transition
        wavenr(transition_index)=wavenrJ+(0.5*Au*Ccalc(Fu
           (i),Ju))-(0.5*Al*Ccalc(Fl(j),Jl))+(Bu*
           function_calc(Fu(i),Ju))-(Bl*function_calc(Fl(
           j),Jl)); %contains wavenr of each transition

        %% Intensities
        sixj=sixjsymbol(Jl, Fl(j), Fu(i), Ju);
%         sixj;
        I(transition_index)=(2*Fu(i)+1)*(2*Fl(j)+1)*sixj
           ^2;%contains relative intensities for each
           transition
        end
    end
end

%range of wavenumbers to test
wavenumbers=(min(wavenr)-1):0.0038:(max(wavenr)+1);
```

```
%% Line width
T=500; % put in temperature in K
FWHM=7.16*10^-7*wavenrJ*sqrt(T/45)*1.38; %calculates FWHM
    or Doppler width
width=FWHM/2.3548; %std dev. found 2,4548 on wolfram


yvalues=[]; %this will be the intensity values for a
   single hfs lines
for k=1:transition_index; % for each transition create a
   Gaussian profile.
    Iuse=normpdf(wavenumbers, wavenr(k), width);
    yvalues(k,:)=Iuse*I(k); % in the end contains
       intensity values for each hfs lines on seperate
       row. multiplied by their relative intensity
end

intensity=sum(yvalues); %lines are not in seperate rows
   anymore, only total intensity.



hfwidth=max(wavenr)-min(wavenr)+width;
resolved=hfwidth./(width*length(wavenr));
```

fitpure_del

```
function [ABfit,Imod]=fitpure(wavenrOBS, IOBS, Ju,Jl,
   wavenrJ,Au,Bu,Al,Bl, lock)

% max intensity for normalization
MaxIOBS=max(IOBS);

%% Model
fun=@(x,wavenrOBS) IcreatorB_lift_fixI(Ju, Jl, x(1), x(2)
   , x(3), x(4), x(5), wavenrOBS, x(6), x(7),x(8));


%% Initial guesses
%line width
T=500; %Temperature in K
FWHM=7.16*10^-7*wavenrJ*sqrt(T/45)*1.38; %calculates FWHM
    from Doppler width
stdev=FWHM/2.3548;


x0=[wavenrJ, Au, Bu, Al, Bl, stdev, 0, MaxIOBS]; %initial
```

```
   guesses
lb=[-Inf,-0.2,-0.03,-0.2,-0.03,stdev*0.5,-Inf,-Inf]; %if
   lock is not given, no boundaries
ub=[+Inf,+0.2,+0.03,+0.2,+0.03,stdev*1.5,+Inf,+Inf];

%% lock parameters
if nargin == 10


    lock2=find(lock); %input parameter 'lock' is an array
        of zeros and 1s. 1 means locking this parameter
    lb(lock2)=x0(lock2);
    ub(lock2)=x0(lock2);
end

%% Least Squares minimization
[x, ~]=lsqcurvefit(fun,x0,wavenrOBS,IOBS,lb,ub);
ABfit=x(2:5);

Imod=fun(x,wavenrOBS);
```

A.2 Using the program

A.2.1 Fitting a hfs multiplet

In this section it will be shown how to use the program by investigating the transition at 4539.2283 cm^{-1}. The input parameters for this line can be found in Table 4.1. So we have $Ju = 3/2$, $Jl = 5/2$, $wavenrJ = 4539.2283$, $Au = -0.01245$, $Bu = 0.00030$, $Al = 0.00512$ and $Bl = -0.00043$. We want the program to look for the right values, so we can for instance change A_u to -0.01 and $wavenrJ$ to 4539.21. In this example, the B values will be locked, so input parameter *lock* is given as the following array [0 0 1 0 1 0 0 0]. In general a parameter is locked if its element in the array *lock* is set to 1, where the order is as follows: [$wavenrJ$, A_u, B_u, A_l, B_l, *std*, $lift$, *maxIOBS*]. Additionally, one can set *uncert* and *letplot* to 1 or 0 to specify whether uncertainties in the hfs constants should be derived and if the resulting synthetic spectrum should be plotted respectively. In this example, we are not interested in the uncertainties but we do want to see the resulting fit, so one can use *uncert* = 0 and *letplot* = 1. The function should now return a plot of the resulting fitted spectrum and the residuals, as is shown in Fig. A.1. From this plot it can be seen whether a local minimum is found. The best fit hfs constants are returned in matrix $HF\_constants$, and it can be seen A_u changed back to the same value as in Table 4.1. Additional best fit parameters are given in x.

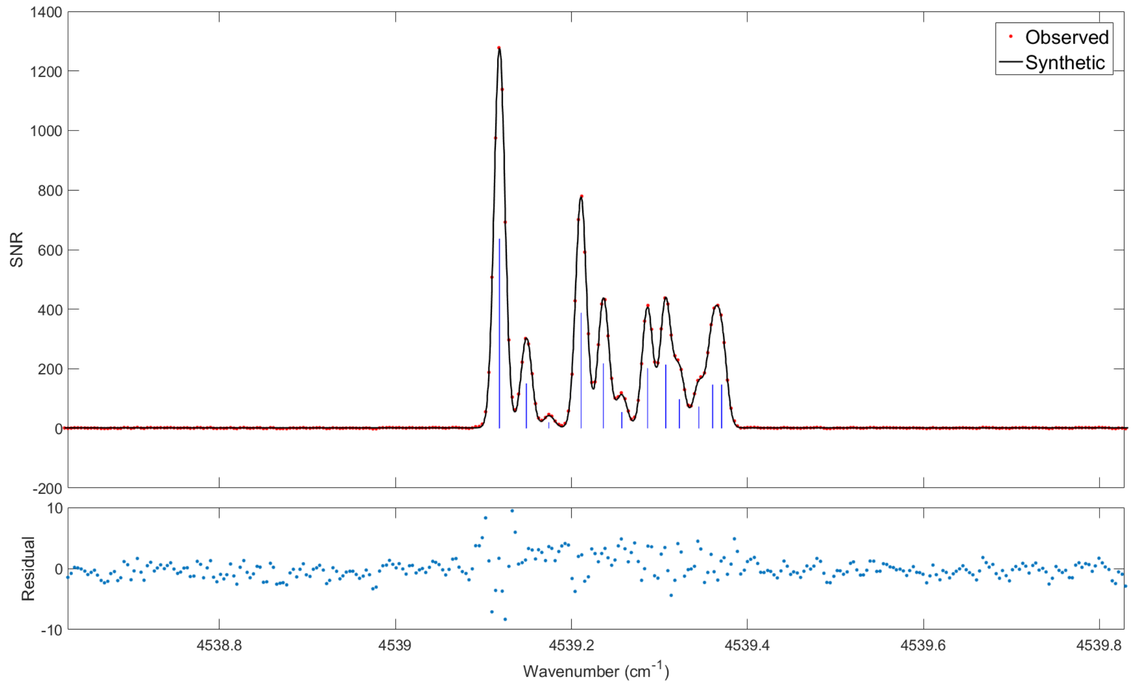

Figure A.1: The plot that is returned after running *LSQcurvefit*. The fitted synthetic spectrum is shown as a black line, and the observed spectrum is shown as red dots. The blue lines indicate the wavenumbers of individual hfs components.

A.2.2 Finding initial values

A GUI was developed for choosing initial values. In this section it will be shown how to use this GUI. First, the spectrum needs to be read in, which can be done by clicking *Read data*. One should then see a plot of the full spectrum, as is shown in Fig. A.2. Using $wavenrJ = 4539.1$ and the same input values as in the example above and pressing *Update observed* should produce a synthetic spectrum as shown in Fig. A.3. The patterns look similar, but it is clear that the wavenumber should be shifted. Changing the wavenumber to 4539.22 returns a better match. If the patterns are similar and the centre of gravity wavenumbers coincide, one can press *Autofit*. The program will then search for the combination of parameters that fits the observed spectrum best. The best fit hfs constants are returned under *results*. The resulting fitted spectrum is plotted, as is shown in Fig. A.4. Additionally, parameters can be locked during the fit under *Fit settings*.

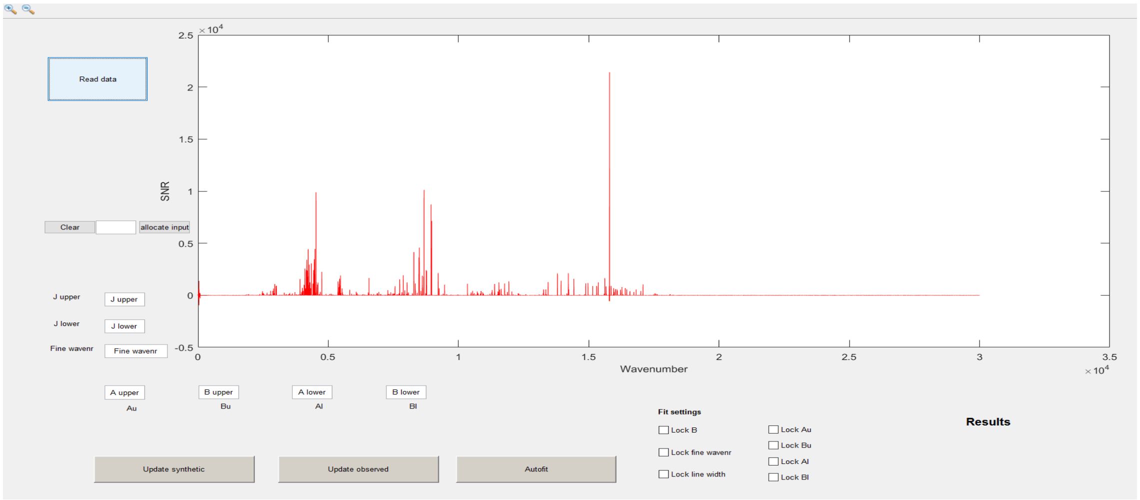

Fit settings
☐ Lock B
☐ Lock fine wavenr
☐ Lock line width
☐ Lock Au
☐ Lock Bu
☐ Lock Al
☐ Lock Bl

Figure A.2: A screen shot of the GUI after reading in the data.

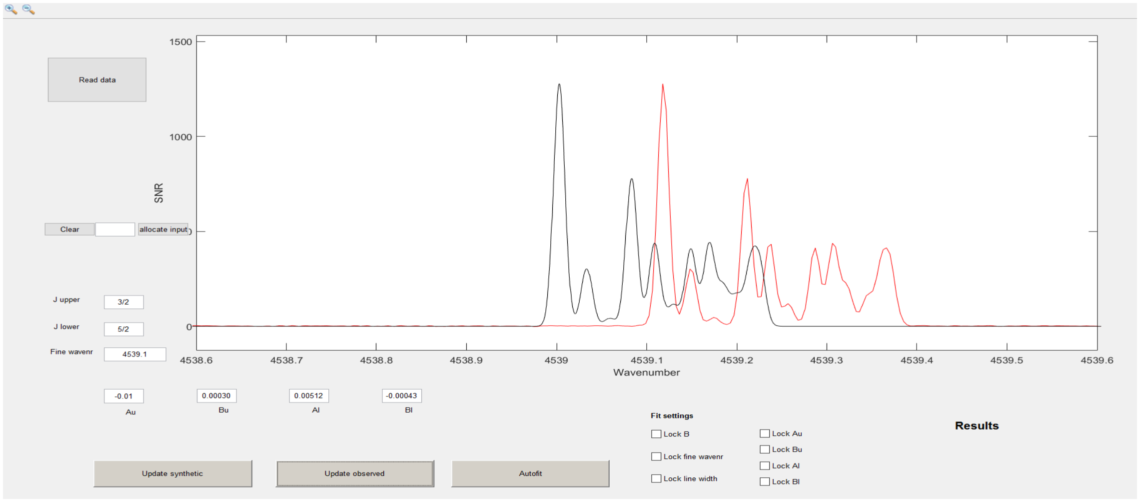

J upper 3/2
J lower 5/2
Fine wavenr 4539.1
Au -0.01
Bu 0.00030
Al 0.00512
Bl -0.00043

Fit settings
☐ Lock B
☐ Lock fine wavenr
☐ Lock line width
☐ Lock Au
☐ Lock Bu
☐ Lock Al
☐ Lock Bl

Figure A.3: Pressing *Update observed* zooms in on a wavenumber region of 1 cm^{-1}. A synthetic spectrum is also plotted using the input values.

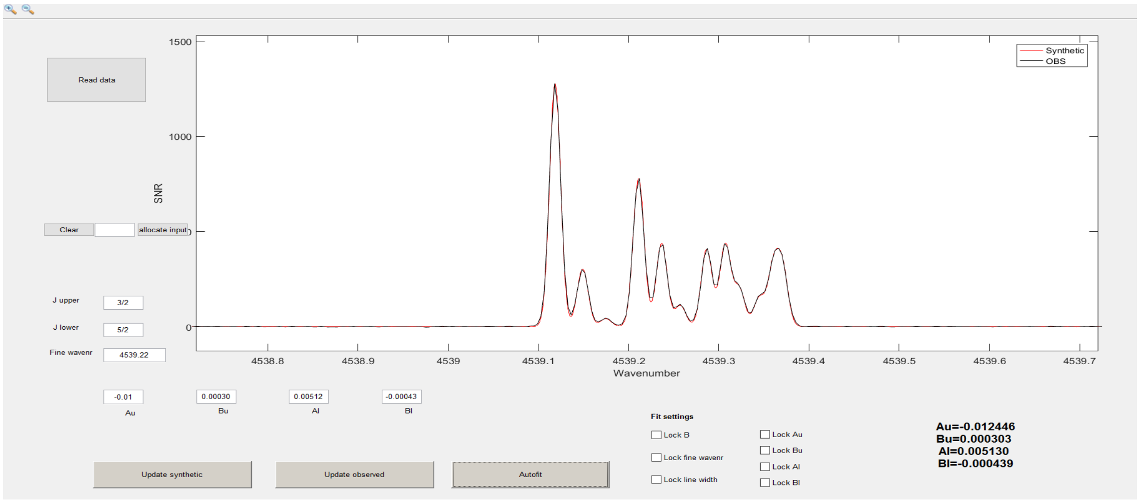

J upper 3/2
J lower 5/2
Fine wavenr 4539.22
Au -0.01
Bu 0.00030
Al 0.00512
Bl -0.00043

Fit settings
☐ Lock B
☐ Lock fine wavenr
☐ Lock line width
☐ Lock Au
☐ Lock Bu
☐ Lock Al
☐ Lock Bl

Au=-0.012446
Bu=0.000303
Al=0.005130
Bl=-0.000439

Figure A.4: Pressing *Autofit* fits the synthetic spectrum and returns the best fit hfs constants.

Appendix B

Oscillator strengths

B.1 Code

log gf values for hfs transitions can be derived using the program *hfgf_calc*, which is added in this section. The program also returns the wavenumber of each hfs component.

hfgf_calc

```
function output=hfgf_calc(Jl,Ju,wavenrJ,Au, Bu, Al, Bl,
   loggf)
clear I3 transitions wavenr

%% Constants
Iqnr=7/2; %nuclear spin quantum nr. 7/2 for Scandium

%% start calculations

%possible transitions
Fu=abs(Iqnr-Ju):Iqnr+Ju; %possible values for upper F
Fl=abs(Iqnr-Jl):Iqnr+Jl; %possible values for lower F
transition_index=0;%use as index, but also to see total
   nr of possible transitions.
transitions=[];%store allowed transitions in this matrix
wavenr=[];%store wavenrs of transitions in here

I3=[];

for i=1:length(Fu)
    for j=1:length(Fl)
        dF=Fu(i)-Fl(j);
        if dF==0 && (Fu(i)+Fl(j))~=0 || abs(dF)==1 && Fu(
           i)+Fl(j)~=0;%selection rules
        transition_index=transition_index+1;
        transitions(1,transition_index)=Fu(i);
        transitions(2,transition_index)=Fl(j);
```

```
        %% Find wavenr for ech transition
        wavenr(transition_index)=wavenrJ+(0.5*Au*Ccalc(Fu
           (i),Ju))-(0.5*Al*Ccalc(Fl(j),Jl))+(Bu*
           function_calc(Fu(i),Ju))-(Bl*function_calc(Fl(
           j),Jl)); %contains wavenr of each transition

        %% Intensities
        sixj=sixjsymbol(Jl, Fl(j), Fu(i), Ju);
        I3(transition_index)=(2*Fu(i)+1)*(2*Fl(j)+1)*sixj
           ^2;

        end
    end
    perlineresult=[transitions(1,:);transitions(2,:);
       wavenr; I3];


end

%% convert
totalI3=sum(I3);
fract=I3/totalI3;
percent=fract*100;
gffine=10^loggf;
hfgf=fract*gffine;
loghfgf=log10(hfgf);


%% put results together
output=[transitions(1,:); transitions(2,:); wavenr;
   percent; loghfgf];

output=output';
```

B.2 Oscillator strength data

In Table B.1 oscillator strengths for hfs transitions belonging to 44 fine structure transitions are shown.

Table B.1: $\log gf$ values for hfs components belonging to 44 fine structure transitions in neutral scandium. The oscillator strength for the fine structure transition is shown in column $\log gf$. In the next 2 column quantum number F for the hfs levels are given. Column σ_F gives the wavenumber of hfs transitions. The next column shows the relative intensity of each hfs component in percentages. The last column gives the oscillator strength for the hfs transitions.

Upper Configuration	Term	Lower Configuration	Term	σ_J cm^{-1}	$\log gf$	Uncertainty %	F_u	F_l	σ_F cm^{-1}	Percentage %	hfs $\log gf$
3d4s(^{3}D)4p	$^4F_{3/2}$	3d^2(^{3}F)4s	$^4F_{5/2}$	4114.9090	-2.348	27	2	1	4115.0146	6.3	-3.552
							2	2	4115.0043	6.3	-3.552
							2	3	4114.9888	3.1	-3.853
							3	2	4114.9828	4.2	-3.728
							3	3	4114.9673	9.1	-3.388
							3	4	4114.9467	8.6	-3.414
							4	3	4114.9389	2.3	-3.978
							4	4	4114.9184	9.3	-3.380
							4	5	4114.8928	16.5	-3.131
							5	4	4114.8836	0.9	-4.406
							5	5	4114.8580	6.4	-3.541
							5	6	4114.8275	27.1	-2.915
3d4s(^{3}D)4p	$^4F_{5/2}$	3d^2(^{3}F)4s	$^4F_{7/2}$	4146.2750	-2.644	37	1	0	4146.0671	1.6	-4.450
							1	1	4146.0742	3.0	-4.165
							1	2	4146.0884	1.7	-4.420
							2	1	4146.0915	1.7	-4.420
							2	2	4146.1057	4.7	-3.977
							2	3	4146.1269	4.1	-4.032
							3	2	4146.1316	1.5	-4.471
							3	3	4146.1528	5.7	-3.886
							3	4	4146.1811	7.4	-3.777
							4	3	4146.1872	1.1	-4.596

Table B.1: $\log gf$ values of hfs components for 44 fine structure transitions in neutral scandium, continued.

Upper Configuration	Term	Lower Configuration	Term	σ_J cm^{-1}	$\log gf$	Uncertainty %	F_u	F_l	σ_F cm^{-1}	Percentage %	hfs $\log gf$
							4	4	4146.2155	6.0	-3.864
							4	5	4146.2508	11.6	-3.579
							5	4	4146.2583	0.7	-4.818
							5	5	4146.2936	5.3	-3.918
							5	6	4146.3358	16.9	-3.415
							6	5	4146.3447	0.3	-5.228
							6	6	4146.3869	3.4	-4.114
							6	7	4146.4359	23.4	-3.274
3d4s(^{3}D)4p	$^4F_{3/2}$	3d^2(^{3}F)4s	$^4F_{3/2}$	4152.5980	-1.411	23	2	1	4152.5688	6.3	-2.615
							2	2	4152.5794	6.3	-2.615
							2	3	4152.5952	3.1	-2.916
							3	2	4152.5662	4.2	-2.791
							3	3	4152.5821	9.1	-2.451
							3	4	4152.6032	8.6	-2.477
							4	3	4152.5641	2.3	-3.041
							4	4	4152.5852	9.3	-2.443
							4	5	4152.6117	16.5	-2.194
							5	4	4152.5621	0.9	-3.469
							5	5	4152.5885	6.4	-2.604
							5	6	4152.6203	27.1	-1.978
3d4s(^{3}D)4p	$^4F_{5/2}$	3d^2(^{3}F)4s	$^4F_{5/2}$	4198.8770	-1.276	23	1	1	4199.0750	2.2	-2.927
							1	2	4199.0646	4.0	-2.672
							2	1	4199.0500	4.0	-2.672
							2	2	4199.0397	0.1	-4.580
							2	3	4199.0242	6.3	-2.473
							3	2	4199.0022	6.3	-2.473

Table B.1: $\log gf$ values of hfs components for 44 fine structure transitions in neutral scandium, continued.

Upper Configuration	Term	Lower Configuration	Term	σ_J cm^{-1}	$\log gf$	Uncertainty %	F_u	F_l	σ_F cm^{-1}	Percentage %	hfs $\log gf$
							3	3	4198.9867	0.9	-3.337
							3	4	4198.9662	7.4	-2.409
							4	3	4198.9369	7.4	-2.409
							4	4	4198.9163	4.5	-2.620
							4	5	4198.8907	6.9	-2.440
							5	4	4198.8541	6.9	-2.440
							5	5	4198.8285	11.5	-2.214
							5	6	4198.7980	4.5	-2.621
							6	5	4198.7540	4.5	-2.621
							6	6	4198.7235	22.6	-1.922
3d4s(^{3}D)4p	$^4F_{7/2}$	3d^2(^{3}F)4s	$^4F_{9/2}$	4204.4210	-2.660	31	0	1	4204.4153	1.6	-4.466
							1	1	4204.4274	1.8	-4.399
							1	2	4204.4083	2.9	-4.203
							2	1	4204.4517	0.4	-5.098
							2	2	4204.4326	2.9	-4.203
							2	3	4204.4039	4.6	-3.999
							3	2	4204.4688	0.5	-4.943
							3	3	4204.4402	3.6	-4.098
							3	4	4204.4020	6.8	-3.829
							4	3	4204.4884	0.5	-4.943
							4	4	4204.4502	4.1	-4.051
							4	5	4204.4024	9.5	-3.683
							5	4	4204.5102	0.4	-5.040
							5	5	4204.4625	4.0	-4.057
							5	6	4204.4052	12.8	-3.554
							6	5	4204.5341	0.3	-5.244

Table B.1: log gf values of hfs components for 44 fine structure transitions in neutral scandium, continued.

Upper Configuration	Term	Lower Configuration	Term	σ_J cm^{-1}	log gf	Uncertainty %	F_u	F_l	σ_F cm^{-1}	Percentage %	hfs log gf
							6	6	4204.4769	3.4	-4.130
							6	7	4204.4102	16.7	-3.438
							7	6	4204.5600	0.1	-5.642
							7	7	4204.4933	2.1	-4.341
							7	8	4204.4172	21.3	-3.333
3d4s(^{3}D)4p	$^4F_{5/2}$	3d^2(^{3}F)4s	$^4F_{3/2}$	4236.5620	-2.047	24	1	2	4236.4173	6.3	-3.251
							2	2	4236.4368	6.3	-3.251
							2	3	4236.4526	4.2	-3.427
							3	2	4236.4661	3.1	-3.552
							3	3	4236.4819	9.1	-3.087
							3	4	4236.5030	2.3	-3.677
							4	3	4236.5207	8.6	-3.113
							4	4	4236.5418	9.3	-3.079
							4	5	4236.5684	0.9	-4.105
							5	4	4236.5901	16.5	-2.830
							5	5	4236.6166	6.4	-3.240
							6	5	4236.6740	27.1	-2.614
3d4s(^{3}D)4p	$^4F_{7/2}$	3d^2(^{3}F)4s	$^4F_{7/2}$	4271.4760	-1.272	22	0	1	4271.2013	1.6	-3.078
							1	0	4271.2077	1.6	-3.078
							1	1	4271.2134	0.1	-4.099
							1	2	4271.2249	3.0	-2.798
							2	1	4271.2377	3.0	-2.798
							2	2	4271.2492	0.7	-3.400
							2	3	4271.2664	4.1	-2.660
							3	2	4271.2854	4.1	-2.660
							3	3	4271.3027	2.1	-2.953

Table B.1: $\log gf$ values of hfs components for 44 fine structure transitions in neutral scandium, continued.

Upper Configuration	Term	Lower Configuration	Term	σ_J cm^{-1}	$\log gf$	Uncertainty %	F_u	F_l	σ_F cm^{-1}	Percentage %	hfs $\log gf$
							3	4	4271.3258	4.8	-2.594
							4	3	4271.3509	4.8	-2.594
							4	4	4271.3740	4.5	-2.622
							4	5	4271.4029	4.8	-2.587
							5	4	4271.4340	4.8	-2.587
							5	5	4271.4629	8.2	-2.359
							5	6	4271.4978	4.2	-2.652
							6	5	4271.5346	4.2	-2.652
							6	6	4271.5695	13.5	-2.140
							6	7	4271.6104	2.6	-2.856
							7	6	4271.6526	2.6	-2.856
							7	7	4271.6935	20.8	-1.953
3d4s(^{3}D)4p	$^4F_{7/2}$	3d^2(^{3}F)4s	$^4F_{5/2}$	4324.0560	-2.036	23	0	1	4323.9244	1.6	-3.842
							1	1	4323.9366	3.0	-3.557
							1	2	4323.9262	1.7	-3.812
							2	1	4323.9608	1.7	-3.812
							2	2	4323.9504	4.7	-3.369
							2	3	4323.9349	1.5	-3.863
							3	2	4323.9867	4.1	-3.424
							3	3	4323.9712	5.7	-3.278
							3	4	4323.9506	1.1	-3.988
							4	3	4324.0194	7.4	-3.169
							4	4	4323.9989	6.0	-3.256
							4	5	4323.9733	0.7	-4.210
							5	4	4324.0589	11.6	-2.971
							5	5	4324.0333	5.3	-3.310

Table B.1: $\log gf$ values of hfs components for 44 fine structure transitions in neutral scandium, continued.

Upper Configuration	Term	Lower Configuration	Term	σ_J cm^{-1}	$\log gf$	Uncertainty %	F_u	F_l	σ_F cm^{-1}	Percentage %	hfs $\log gf$
							5	6	4324.0028	0.3	-4.620
							6	5	4324.1049	16.9	-2.807
							6	6	4324.0745	3.4	-3.506
							7	6	4324.1575	23.4	-2.666
3d4s(^{3}D)4p	$^4F_{9/2}$	3d^2(^{3}F)4s	$^4F_{9/2}$	4349.2450	-1.137	22	1	1	4349.1769	2.3	-2.777
							1	2	4349.1578	1.5	-2.973
							2	1	4349.2032	1.5	-2.973
							2	2	4349.1841	2.4	-2.763
							2	3	4349.1554	2.4	-2.752
							3	2	4349.2234	2.4	-2.752
							3	3	4349.1948	3.2	-2.625
							3	4	4349.1566	3.1	-2.649
							4	3	4349.2472	3.1	-2.649
							4	4	4349.2090	4.8	-2.458
							4	5	4349.1613	3.4	-2.606
							5	4	4349.2744	3.4	-2.606
							5	5	4349.2267	7.0	-2.289
							5	6	4349.1695	3.3	-2.617
							6	5	4349.3051	3.3	-2.617
							6	6	4349.2478	10.2	-2.130
							6	7	4349.1812	2.8	-2.694
							7	6	4349.3390	2.8	-2.694
							7	7	4349.2724	14.3	-1.982
							7	8	4349.1963	1.7	-2.909
							8	7	4349.3763	1.7	-2.909
							8	8	4349.3002	19.6	-1.846

Table B.1: $\log gf$ values of hfs components for 44 fine structure transitions in neutral scandium, continued.

Upper Configuration	Term	Lower Configuration	Term	σ_J cm^{-1}	$\log gf$	Uncertainty %	F_u	F_l	σ_F cm^{-1}	Percentage %	hfs $\log gf$
3d4s(^{1}D)4p	$^2D_{5/2}$	3d^2(^{3}F)4s	$^4F_{7/2}$	4412.4950	-1.478	24	1	0	4412.3699	1.6	-3.284
							1	1	4412.3616	3.0	-2.999
							1	2	4412.3448	1.7	-3.254
							2	1	4412.4103	1.7	-3.254
							2	2	4412.3935	4.7	-2.811
							2	3	4412.3684	4.1	-2.866
							3	2	4412.4648	1.5	-3.305
							3	3	4412.4397	5.7	-2.720
							3	4	4412.4063	7.4	-2.611
							4	3	4412.5316	1.1	-3.430
							4	4	4412.4981	6.0	-2.698
							4	5	4412.4565	11.6	-2.413
							5	4	4412.6076	0.7	-3.652
							5	5	4412.5660	5.3	-2.752
							5	6	4412.5161	16.9	-2.249
							6	5	4412.6896	0.3	-4.062
							6	6	4412.6397	3.4	-2.948
							6	7	4412.5817	23.4	-2.108
3d4s(^{3}D)4p	$^4F_{9/2}$	3d^2(^{3}F)4s	$^4F_{7/2}$	4416.3080	-2.167	24	1	0	4416.1876	1.6	-3.973
							1	1	4416.1793	1.8	-3.906
							1	2	4416.1627	0.4	-4.605
							2	1	4416.2056	2.9	-3.710
							2	2	4416.1889	2.9	-3.710
							2	3	4416.1640	0.5	-4.450
							3	2	4416.2283	4.6	-3.506
							3	3	4416.2033	3.6	-3.605

Table B.1: $\log gf$ values of hfs components for 44 fine structure transitions in neutral scandium, continued.

Upper Configuration	Term	Lower Configuration	Term	σ_J cm^{-1}	$\log gf$	Uncertainty %	F_u	F_l	σ_F cm^{-1}	Percentage %	hfs $\log gf$
							3	4	4416.1700	0.5	-4.450
							4	3	4416.2558	6.8	-3.336
							4	4	4416.2224	4.1	-3.558
							4	5	4416.1807	0.4	-4.547
							5	4	4416.2879	9.5	-3.190
							5	5	4416.2461	4.0	-3.564
							5	6	4416.1959	0.3	-4.751
							6	5	4416.3245	12.8	-3.061
							6	6	4416.2743	3.4	-3.637
							6	7	4416.2156	0.1	-5.149
							7	6	4416.3655	16.7	-2.945
							7	7	4416.3068	2.1	-3.848
							8	7	4416.4108	21.3	-2.840
3d4s(^{3}D)4p	$^4D_{3/2}$	3d^2(^{3}F)4s	$^4F_{5/2}$	4464.1250	-1.181	23	2	1	4464.2184	6.3	-2.385
							2	2	4464.2081	6.3	-2.385
							2	3	4464.1926	3.1	-2.686
							3	2	4464.1923	4.2	-2.561
							3	3	4464.1768	9.1	-2.221
							3	4	4464.1562	8.6	-2.247
							4	3	4464.1557	2.3	-2.811
							4	4	4464.1351	9.3	-2.213
							4	5	4464.1096	16.5	-1.964
							5	4	4464.1086	0.9	-3.239
							5	5	4464.0830	6.4	-2.374
							5	6	4464.0525	27.1	-1.748
3d4s(^{1}D)4p	$^2D_{5/2}$	3d^2(^{3}F)4s	$^4F_{5/2}$	4465.0760	-2.960	67	1	1	4465.2133	2.2	-4.611

Table B.1: $\log gf$ values of hfs components for 44 fine structure transitions in neutral scandium, continued.

Upper Configuration	Term	Lower Configuration	Term	σ_J cm^{-1}	$\log gf$	Uncertainty %	F_u	F_l	σ_F cm^{-1}	Percentage %	hfs $\log gf$
							1	2	4465.2029	4.0	-4.356
							2	1	4465.1991	4.0	-4.356
							2	2	4465.1887	0.1	-6.264
							2	3	4465.1732	6.3	-4.157
							3	2	4465.1674	6.3	-4.157
							3	3	4465.1519	0.9	-5.021
							3	4	4465.1314	7.4	-4.093
							4	3	4465.1236	7.4	-4.093
							4	4	4465.1031	4.5	-4.304
							4	5	4465.0775	6.9	-4.124
							5	4	4465.0679	6.9	-4.124
							5	5	4465.0423	11.5	-3.898
							5	6	4465.0118	4.5	-4.305
							6	5	4465.0003	4.5	-4.305
							6	6	4464.9698	22.6	-3.606
3d4s(^{3}D)4p	$^4D_{1/2}$	3d^2(^{3}F)4s	$^4F_{3/2}$	4489.7820	-1.276	22	3	2	4489.7849	15.6	-2.082
							3	3	4489.8006	16.4	-2.061
							3	4	4489.8218	11.7	-2.207
							4	3	4489.7322	5.5	-2.538
							4	4	4489.7533	16.4	-2.061
							4	5	4489.7799	34.4	-1.740
3d4s(^{3}D)4p	$^4D_{3/2}$	3d^2(^{3}F)4s	$^4F_{3/2}$	4501.8150	-1.829	23	2	2	4501.7043	6.3	-3.033
							2	3	4501.7200	9.4	-2.857
							3	2	4501.7355	9.4	-2.857
							3	4	4501.7724	12.5	-2.732
							4	3	4501.7959	12.5	-2.732

Table B.1: $\log gf$ values of hfs components for 44 fine structure transitions in neutral scandium, continued.

Upper Configuration	Term	Lower Configuration	Term	σ_J cm^{-1}	$\log gf$	Uncertainty %	F_u	F_l	σ_F cm^{-1}	Percentage %	hfs $\log gf$
							4	4	4501.8170	6.0	-3.051
							4	5	4501.8436	9.6	-2.846
							5	4	4501.8777	9.6	-2.846
							5	5	4501.9042	24.8	-2.435
3d4s(^{3}D)4p	$^4D_{5/2}$	3d^2(^{3}F)4s	$^4F_{7/2}$	4530.7660	-0.833	23	1	0	4530.7825	1.6	-2.639
							1	1	4530.7741	3.0	-2.354
							1	2	4530.7574	1.7	-2.609
							2	1	4530.7946	1.7	-2.609
							2	2	4530.7779	4.7	-2.166
							2	3	4530.7528	4.1	-2.221
							3	2	4530.8086	1.5	-2.660
							3	3	4530.7835	5.7	-2.075
							3	4	4530.7501	7.4	-1.966
							4	3	4530.8244	1.1	-2.785
							4	4	4530.7910	6.0	-2.053
							4	5	4530.7493	11.6	-1.768
							5	4	4530.8419	0.7	-3.007
							5	5	4530.8002	5.3	-2.107
							5	6	4530.7503	16.9	-1.604
							6	5	4530.8612	0.3	-3.417
							6	6	4530.8113	3.4	-2.303
							6	7	4530.7533	23.4	-1.463
3d4s(^{3}D)4p	$^4D_{7/2}$	3d^2(^{3}F)4s	$^4F_{9/2}$	4533.5050	-0.731	22	0	1	4533.4484	1.6	-2.537
							1	1	4533.4637	1.8	-2.470
							1	2	4533.4446	2.9	-2.274
							2	1	4533.4942	0.4	-3.169

Table B.1: log gf values of hfs components for 44 fine structure transitions in neutral scandium, continued.

Upper Configuration	Term	Lower Configuration	Term	σ_J cm^{-1}	log gf	Uncertainty %	F_u	F_l	σ_F cm^{-1}	Percentage %	hfs log gf
							2	2	4533.4751	2.9	-2.274
							2	3	4533.4464	4.6	-2.070
							3	2	4533.5208	0.5	-3.014
							3	3	4533.4921	3.6	-2.169
							3	4	4533.4539	6.8	-1.900
							4	3	4533.5532	0.5	-3.014
							4	4	4533.5150	4.1	-2.122
							4	5	4533.4672	9.5	-1.754
							5	4	4533.5912	0.4	-3.111
							5	5	4533.5435	4.0	-2.128
							5	6	4533.4863	12.8	-1.625
							6	5	4533.6350	0.3	-3.315
							6	6	4533.5778	3.4	-2.201
							6	7	4533.5111	16.7	-1.509
							7	6	4533.6847	0.1	-3.713
							7	7	4533.6180	2.1	-2.412
							7	8	4533.5419	21.3	-1.404
3d4s(^{1}D)4p	$^2D_{3/2}$	3d^2(^{3}F)4s	$^4F_{5/2}$	4539.2310	-1.412	24	2	1	4539.2558	6.3	-2.616
							2	2	4539.2663	6.3	-2.616
							2	3	4539.2821	3.1	-2.917
							3	2	4539.2287	4.2	-2.792
							3	3	4539.2446	9.1	-2.452
							3	4	4539.2657	8.6	-2.478
							4	3	4539.1947	2.3	-3.042
							4	4	4539.2158	9.3	-2.444
							4	5	4539.2423	16.5	-2.195

Table B.1: log gf values of hfs components for 44 fine structure transitions in neutral scandium, continued.

Upper Configuration	Term	Lower Configuration	Term	σ_J cm^{-1}	log gf	Uncertainty %	F_u	F_l	σ_F cm^{-1}	Percentage %	hfs log gf
							5	4	4539.1538	0.9	-3.470
							5	5	4539.1802	6.4	-2.605
							5	6	4539.2120	27.1	-1.979
3d4s(^{1}D)4p	$^2D_{3/2}$	3d^2(^{3}F)4s	$^4F_{3/2}$	4576.9230	-1.756	24	2	2	4576.9716	6.3	-2.960
							2	3	4576.9873	9.4	-2.784
							3	2	4576.9340	9.4	-2.784
							3	4	4576.9709	12.5	-2.659
							4	3	4576.8999	12.5	-2.659
							4	4	4576.9210	6.0	-2.978
							4	5	4576.9475	9.6	-2.773
							5	4	4576.8590	9.6	-2.773
							5	5	4576.8855	24.8	-2.362
3d^2(^{3}P)4s	$^2P_{3/2}$	3d4s(^{3}D)4p	$^4D_{5/2}$	4578.8240	-2.587	36	2	1	4578.9865	6.3	-3.791
							2	2	4578.9662	6.3	-3.791
							2	3	4578.9356	3.1	-4.092
							3	2	4578.9447	4.2	-3.967
							3	3	4578.9141	9.1	-3.627
							3	4	4578.8733	8.6	-3.653
							4	3	4578.8858	2.3	-4.217
							4	4	4578.8450	9.3	-3.619
							4	5	4578.7940	16.5	-3.370
							5	4	4578.8102	0.9	-4.645
							5	5	4578.7591	6.4	-3.780
							5	6	4578.6979	27.1	-3.154
3d4s(^{3}D)4p	$^4D_{5/2}$	3d^2(^{3}F)4s	$^4F_{5/2}$	4583.3450	-1.485	23	1	1	4583.2879	2.2	-3.136
							1	2	4583.2776	4.0	-2.881

Table B.1: $\log gf$ values of hfs components for 44 fine structure transitions in neutral scandium, continued.

Upper Configuration	Term	Lower Configuration	Term	σ_J cm^{-1}	$\log gf$	Uncertainty %	F_u	F_l	σ_F cm^{-1}	Percentage %	hfs $\log gf$
							2	1	4583.3084	4.0	-2.881
							2	2	4583.2981	0.1	-4.789
							2	3	4583.2826	6.3	-2.682
							3	2	4583.3288	6.3	-2.682
							3	3	4583.3133	0.9	-3.546
							3	4	4583.2927	7.4	-2.618
							4	3	4583.3541	7.4	-2.618
							4	4	4583.3336	4.5	-2.829
							4	5	4583.3080	6.9	-2.649
							5	4	4583.3845	6.9	-2.649
							5	5	4583.3589	11.5	-2.423
							5	6	4583.3285	4.5	-2.830
							6	5	4583.4199	4.5	-2.830
							6	6	4583.3894	22.6	-2.131
3d^2(^{3}P)4s	$^2P_{1/2}$	3d4s(^{1}D)4p	$^2D_{3/2}$	4584.5230	-2.372	26	3	2	4584.4114	15.6	-3.178
							3	3	4584.4490	16.4	-3.157
							3	4	4584.4989	11.7	-3.303
							4	3	4584.4977	5.5	-3.634
							4	4	4584.5476	16.4	-3.157
							4	5	4584.6096	34.4	-2.836
3d4s(^{3}D)4p	$^4D_{7/2}$	3d^2(^{3}F)4s	$^4F_{7/2}$	4600.5820	-1.766	23	0	1	4600.4648	1.6	-3.572
							1	0	4600.4884	1.6	-3.572
							1	1	4600.4801	0.1	-4.593
							1	2	4600.4634	3.0	-3.292
							2	1	4600.5106	3.0	-3.292
							2	2	4600.4939	0.7	-3.894

Table B.1: $\log gf$ values of hfs components for 44 fine structure transitions in neutral scandium, continued.

Upper Configuration	Term	Lower Configuration	Term	σ_J cm^{-1}	$\log gf$	Uncertainty %	F_u	F_l	σ_F cm^{-1}	Percentage %	hfs $\log gf$
							2	3	4600.4690	4.1	-3.154
							3	2	4600.5397	4.1	-3.154
							3	3	4600.5147	2.1	-3.447
							3	4	4600.4814	4.8	-3.088
							4	3	4600.5757	4.8	-3.088
							4	4	4600.5424	4.5	-3.116
							4	5	4600.5007	4.8	-3.081
							5	4	4600.6187	4.8	-3.081
							5	5	4600.5769	8.2	-2.853
							5	6	4600.5267	4.2	-3.146
							6	5	4600.6685	4.2	-3.146
							6	6	4600.6183	13.5	-2.634
							6	7	4600.5596	2.6	-3.350
							7	6	4600.7251	2.6	-3.350
							7	7	4600.6664	20.8	-2.447
3d4s(^{3}D)4p	$^4D_{5/2}$	3d^2(^{3}F)4s	$^4F_{3/2}$	4621.0330	-2.753	46	1	2	4620.8827	6.3	-3.957
							2	2	4620.9030	6.3	-3.957
							2	3	4620.9188	4.2	-4.133
							3	2	4620.9336	3.1	-4.258
							3	3	4620.9494	9.1	-3.793
							3	4	4620.9705	2.3	-4.383
							4	3	4620.9902	8.6	-3.819
							4	4	4621.0113	9.3	-3.785
							4	5	4621.0378	0.9	-4.811
							5	4	4621.0623	16.5	-3.536
							5	5	4621.0888	6.4	-3.946

Table B.1: $\log gf$ values of hfs components for 44 fine structure transitions in neutral scandium, continued.

Upper Configuration	Term	Lower Configuration	Term	σ_J cm^{-1}	$\log gf$	Uncertainty %	F_u	F_l	σ_F cm^{-1}	Percentage %	hfs $\log gf$
							6	5	4621.1501	27.1	-3.320
3d^2(^{3}P)4s	$^2P_{3/2}$	3d4s(^{1}D)4p	$^2D_{3/2}$	4622.9450	-2.942	69	2	2	4622.9086	6.3	-4.146
							2	3	4622.9462	9.4	-3.970
							3	2	4622.8871	9.4	-3.970
							3	4	4622.9746	12.5	-3.845
							4	3	4622.8964	12.5	-3.845
							4	4	4622.9462	6.0	-4.164
							4	5	4623.0083	9.6	-3.959
							5	4	4622.9114	9.6	-3.959
							5	5	4622.9734	24.8	-3.548
3d4s(^{3}D)4p	$^4D_{7/2}$	3d^2(^{3}F)4s	$^4F_{5/2}$	4653.1530	-3.105	22	0	1	4652.9714	1.6	-4.911
							1	1	4652.9864	3.0	-4.626
							1	2	4652.9761	1.7	-4.881
							2	1	4653.0166	1.7	-4.881
							2	2	4653.0062	4.7	-4.438
							2	3	4652.9907	1.5	-4.932
							3	2	4653.0515	4.1	-4.493
							3	3	4653.0360	5.7	-4.347
							3	4	4653.0155	1.1	-5.057
							4	3	4653.0967	7.4	-4.238
							4	4	4653.0761	6.0	-4.325
							4	5	4653.0506	0.7	-5.279
							5	4	4653.1523	11.6	-4.040
							5	5	4653.1267	5.3	-4.379
							5	6	4653.0962	0.3	-5.689
							6	5	4653.2186	16.9	-3.876

Table B.1: log gf values of hfs components for 44 fine structure transitions in neutral scandium, continued.

Upper Configuration	Term	Lower Configuration	Term	σ_J cm^{-1}	log gf	Uncertainty %	F_u	F_l	σ_F cm^{-1}	Percentage %	hfs log gf
							6	6	4653.1881	3.4	-4.575
							7	6	4653.2960	23.4	-3.735
3d^2(^{3}P)4s	$^2P_{1/2}$	3d4s(^{3}D)4p	$^4D_{3/2}$	4659.6520	-2.524	29	3	2	4659.6997	15.6	-3.330
							3	3	4659.6685	16.4	-3.309
							3	4	4659.6238	11.7	-3.455
							4	3	4659.7172	5.5	-3.786
							4	4	4659.6725	16.4	-3.309
							4	5	4659.6119	34.4	-2.988
3d^2(^{3}P)4s	$^2P_{3/2}$	3d4s(^{1}D)4p	$^2D_{5/2}$	4697.1300	-1.951	24	2	1	4697.4343	6.3	-3.155
							2	2	4697.3856	6.3	-3.155
							2	3	4697.3142	3.1	-3.456
							3	2	4697.3640	4.2	-3.331
							3	3	4697.2927	9.1	-2.991
							3	4	4697.2009	8.6	-3.017
							4	3	4697.2644	2.3	-3.581
							4	4	4697.1726	9.3	-2.983
							4	5	4697.0631	16.5	-2.734
							5	4	4697.1378	0.9	-4.009
							5	5	4697.0283	6.4	-3.144
							5	6	4696.9046	27.1	-2.518
3d^2(^{3}P)4s	$^2P_{3/2}$	3d4s(^{3}D)4p	$^4F_{5/2}$	4963.3050	-3.043	76	2	1	4963.4619	6.3	-4.247
							2	2	4963.4424	6.3	-4.247
							2	3	4963.4131	3.1	-4.548
							3	2	4963.4209	4.2	-4.423
							3	3	4963.3916	9.1	-4.083
							3	4	4963.3527	8.6	-4.109

Table B.1: log gf values of hfs components for 44 fine structure transitions in neutral scandium, continued.

Upper Configuration	Term	Lower Configuration	Term	σ_J cm^{-1}	log gf	Uncertainty %	F_u	F_l	σ_F cm^{-1}	Percentage %	hfs log gf
							4	3	4963.3633	2.3	-4.673
							4	4	4963.3244	9.3	-4.075
							4	5	4963.2762	16.5	-3.826
							5	4	4963.2896	0.9	-5.101
							5	5	4963.2414	6.4	-4.236
							5	6	4963.1839	27.1	-3.610
3d^2(^{3}P)4s	$^2P_{1/2}$	3d4s(^{3}D)4p	$^4F_{3/2}$	5008.8370	-3.281	61	3	2	5008.7794	15.6	-4.087
							3	3	5008.7925	16.4	-4.066
							3	4	5008.8104	11.7	-4.212
							4	3	5008.8412	5.5	-4.543
							4	4	5008.8591	16.4	-4.066
							4	5	5008.8823	34.4	-3.745
3d^2(^{3}P)4s	$^2P_{3/2}$	3d4s(^{3}D)4p	$^4F_{3/2}$	5047.2610	-3.704	42	2	2	5047.2786	6.3	-4.908
							2	3	5047.2917	9.4	-4.732
							3	2	5047.2571	9.4	-4.732
							3	4	5047.2881	12.5	-4.607
							4	3	5047.2419	12.5	-4.607
							4	4	5047.2598	6.0	-4.926
							4	5	5047.2830	9.6	-4.721
							5	4	5047.2250	9.6	-4.721
							5	5	5047.2481	24.8	-4.310
3d^2(^{1}S)4s	$^2S_{1/2}$	3d4s(^{3}D)4p	$^4P_{3/2}$	8421.2970	-2.872	62	3	2	8421.2756	15.6	-3.678
							3	3	8421.2043	16.4	-3.657
							3	4	8421.1076	11.7	-3.803
							4	3	8421.5321	5.5	-4.134
							4	4	8421.4354	16.4	-3.657

Table B.1: $\log gf$ values of hfs components for 44 fine structure transitions in neutral scandium, continued.

Upper Configuration	Term	Lower Configuration	Term	σ_J cm^{-1}	$\log gf$	Uncertainty %	F_u	F_l	σ_F cm^{-1}	Percentage %	hfs $\log gf$
							4	5	8421.3121	34.4	-3.336
3d4s(^{3}D)4p	$^4F_{3/2}$	3d4s^2	$^2D_{5/2}$	15504.2150	-3.333	25	2	1	15504.2866	6.3	-4.537
							2	2	15504.2795	6.3	-4.537
							2	3	15504.2687	3.1	-4.838
							3	2	15504.2664	4.2	-4.713
							3	3	15504.2556	9.1	-4.373
							3	4	15504.2409	8.6	-4.399
							4	3	15504.2376	2.3	-4.963
							4	4	15504.2230	9.3	-4.365
							4	5	15504.2042	16.5	-4.116
							5	4	15504.1998	0.9	-5.391
							5	5	15504.1811	6.4	-4.526
							5	6	15504.1580	27.1	-3.900
3d4s(^{3}D)4p	$^4F_{5/2}$	3d4s^2	$^2D_{5/2}$	15588.1920	-2.397	23	1	1	15588.1242	2.2	-4.048
							1	2	15588.1171	4.0	-3.793
							2	1	15588.1438	4.0	-3.793
							2	2	15588.1367	0.1	-5.701
							2	3	15588.1259	6.3	-3.594
							3	2	15588.1660	6.3	-3.594
							3	3	15588.1552	0.9	-4.458
							3	4	15588.1405	7.4	-3.530
							4	3	15588.1940	7.4	-3.530
							4	4	15588.1794	4.5	-3.741
							4	5	15588.1606	6.9	-3.561
							5	4	15588.2276	6.9	-3.561
							5	5	15588.2089	11.5	-3.335

Table B.1: $\log gf$ values of hfs components for 44 fine structure transitions in neutral scandium, continued.

Upper Configuration	Term	Lower Configuration	Term	σ_J cm^{-1}	$\log gf$	Uncertainty %	F_u	F_l	σ_F cm^{-1}	Percentage %	hfs $\log gf$
							5	6	15588.1858	4.5	-3.742
							6	5	15588.2663	4.5	-3.742
							6	6	15588.2432	22.6	-3.043
3d4s(^{3}D)4p	$^4F_{3/2}$	3d4s^2	$^2D_{3/2}$	15672.5580	-2.332	23	2	2	15672.6493	6.3	-3.536
							2	3	15672.6219	9.4	-3.360
							3	2	15672.6362	9.4	-3.360
							3	4	15672.5727	12.5	-3.235
							4	3	15672.5909	12.5	-3.235
							4	4	15672.5547	6.0	-3.554
							4	5	15672.5100	9.6	-3.349
							5	4	15672.5316	9.6	-3.349
							5	5	15672.4868	24.8	-2.938
3d4s(^{3}D)4p	$^4F_{5/2}$	3d4s^2	$^2D_{3/2}$	15756.5300	-3.245	24	1	2	15756.4819	6.3	-4.449
							2	2	15756.5015	6.3	-4.449
							2	3	15756.4742	4.2	-4.625
							3	2	15756.5308	3.1	-4.750
							3	3	15756.5034	9.1	-4.285
							3	4	15756.4673	2.3	-4.875
							4	3	15756.5423	8.6	-4.311
							4	4	15756.5061	9.3	-4.277
							4	5	15756.4614	0.9	-5.303
							5	4	15756.5543	16.5	-4.028
							5	5	15756.5096	6.4	-4.438
							6	5	15756.5670	27.1	-3.812
3d4s(^{1}D)4p	$^2D_{5/2}$	3d4s^2	$^2D_{5/2}$	15854.3830	-1.161	22	1	1	15854.1679	2.2	-2.812
							1	2	15854.1608	4.0	-2.557

Table B.1: $\log gf$ values of hfs components for 44 fine structure transitions in neutral scandium, continued.

Upper Configuration	Term	Lower Configuration	Term	σ_J cm^{-1}	$\log gf$	Uncertainty %	F_u	F_l	σ_F cm^{-1}	Percentage %	hfs $\log gf$
							2	1	15854.2166	4.0	-2.557
							2	2	15854.2095	0.1	-4.465
							2	3	15854.1987	6.3	-2.358
							3	2	15854.2808	6.3	-2.358
							3	3	15854.2700	0.9	-3.222
							3	4	15854.2554	7.4	-2.294
							4	3	15854.3618	7.4	-2.294
							4	4	15854.3472	4.5	-2.505
							4	5	15854.3284	6.9	-2.325
							5	4	15854.4567	6.9	-2.325
							5	5	15854.4379	11.5	-2.099
							5	6	15854.4149	4.5	-2.506
							6	5	15854.5616	4.5	-2.506
							6	6	15854.5385	22.6	-1.807
3d4s(^{1}D)4p	$^4D_{3/2}$	3d4s^2	$^2D_{5/2}$	15928.5450	-2.621	22	2	1	15928.6705	6.3	-3.825
							2	2	15928.6634	6.3	-3.825
							2	3	15928.6526	3.1	-4.126
							3	2	15928.6259	4.2	-4.001
							3	3	15928.6151	9.1	-3.661
							3	4	15928.6004	8.6	-3.687
							4	3	15928.5652	2.3	-4.251
							4	4	15928.5505	9.3	-3.653
							4	5	15928.5318	16.5	-3.404
							5	4	15928.4885	0.9	-4.679
							5	5	15928.4698	6.4	-3.814
							5	6	15928.4467	27.1	-3.188

Table B.1: $\log gf$ values of hfs components for 44 fine structure transitions in neutral scandium, continued.

Upper Configuration	Term	Lower Configuration	Term	σ_J cm^{-1}	$\log gf$	Uncertainty %	F_u	F_l	σ_F cm^{-1}	Percentage %	hfs $\log gf$
3d4s(^{3}D)4p	$^4D_{5/2}$	3d4s^2	$^2D_{5/2}$	15972.6630	-1.794	23	1	1	15972.5895	2.2	-3.445
							1	2	15972.5824	4.0	-3.190
							2	1	15972.6100	4.0	-3.190
							2	2	15972.6029	0.1	-5.098
							2	3	15972.5921	6.3	-2.991
							3	2	15972.6336	6.3	-2.991
							3	3	15972.6228	0.9	-3.855
							3	4	15972.6081	7.4	-2.927
							4	3	15972.6636	7.4	-2.927
							4	4	15972.6490	4.5	-3.138
							4	5	15972.6302	6.9	-2.958
							5	4	15972.6999	6.9	-2.958
							5	5	15972.6812	11.5	-2.732
							5	6	15972.6581	4.5	-3.139
							6	5	15972.7421	4.5	-3.139
							6	6	15972.7191	22.6	-2.440
3d4s(^{3}D)4p	$^4D_{3/2}$	3d4s^2	$^2D_{3/2}$	16021.7770	-1.702	22	2	2	16021.7629	6.3	-2.906
							2	3	16021.7356	9.4	-2.730
							3	2	16021.7942	9.4	-2.730
							3	4	16021.7307	12.5	-2.605
							4	3	16021.8115	12.5	-2.605
							4	4	16021.7753	6.0	-2.924
							4	5	16021.7306	9.6	-2.719
							5	4	16021.8360	9.6	-2.719
							5	5	16021.7912	24.8	-2.308
3d4s(^{1}D)4p	$^2D_{5/2}$	3d4s^2	$^2D_{3/2}$	16022.7260	-2.204	22	1	2	16022.5306	6.3	-3.408

Table B.1: $\log gf$ values of hfs components for 44 fine structure transitions in neutral scandium, continued.

Upper Configuration	Term	Lower Configuration	Term	σ_J cm^{-1}	$\log gf$	Uncertainty %	F_u	F_l	σ_F cm^{-1}	Percentage %	hfs $\log gf$
							2	2	16022.5793	6.3	-3.408
							2	3	16022.5520	4.2	-3.584
							3	2	16022.6506	3.1	-3.709
							3	3	16022.6233	9.1	-3.244
							3	4	16022.5871	2.3	-3.834
							4	3	16022.7151	8.6	-3.270
							4	4	16022.6789	9.3	-3.236
							4	5	16022.6342	0.9	-4.262
							5	4	16022.7884	16.5	-2.987
							5	5	16022.7437	6.4	-3.397
							6	5	16022.8673	27.1	-2.771
3d4s(^{1}D)4p	$^2D_{3/2}$	3d4s^2	$^2D_{3/2}$	16096.8830	-1.436	22	2	2	16097.0282	6.3	-2.640
							2	3	16097.0009	9.4	-2.464
							3	2	16096.9907	9.4	-2.464
							3	4	16096.9272	12.5	-2.339
							4	3	16096.9135	12.5	-2.339
							4	4	16096.8773	6.0	-2.658
							4	5	16096.8326	9.6	-2.453
							5	4	16096.8153	9.6	-2.453
							5	5	16096.7705	24.8	-2.042
3d^2(^{3}F)4p	$^4G_{5/2}$	3d^2(^{3}F)4s	$^4F_{5/2}$	17465.2120	-0.773	23	1	1	17465.1572	2.2	-2.424
							1	2	17465.1468	4.0	-2.169
							2	1	17465.1778	4.0	-2.169
							2	2	17465.1674	0.1	-4.077
							2	3	17465.1519	6.3	-1.970
							3	2	17465.1980	6.3	-1.970

Table B.1: log gf values of hfs components for 44 fine structure transitions in neutral scandium, continued.

Upper Configuration	Term	Lower Configuration	Term	σ_J cm^{-1}	log gf	Uncertainty %	F_u	F_l	σ_F cm^{-1}	Percentage %	hfs log gf
							3	3	17465.1825	0.9	-2.834
							3	4	17465.1619	7.4	-1.906
							4	3	17465.2227	7.4	-1.906
							4	4	17465.2021	4.5	-2.117
							4	5	17465.1765	6.9	-1.937
							5	4	17465.2513	6.9	-1.937
							5	5	17465.2258	11.5	-1.711
							5	6	17465.1953	4.5	-2.118
							6	5	17465.2834	4.5	-2.118
							6	6	17465.2529	22.6	-1.419
3d^2(^{3}F)4p	$^4G_{5/2}$	3d^2(^{3}F)4s	$^4F_{3/2}$	17502.9060	0.137	23	1	2	17502.7577	6.3	-1.067
							2	2	17502.7784	6.3	-1.067
							2	3	17502.7941	4.2	-1.243
							3	2	17502.8089	3.1	-1.368
							3	3	17502.8247	9.1	-0.903
							3	4	17502.8458	2.3	-1.493
							4	3	17502.8649	8.6	-0.929
							4	4	17502.8860	9.3	-0.895
							4	5	17502.9125	0.9	-1.921
							5	4	17502.9352	16.5	-0.646
							5	5	17502.9617	6.4	-1.056
							6	5	17503.0194	27.1	-0.430